The Effects of Early-Life Drug and Dietary Interventions on Late-Life Disease Development

By

Theresa Mau

A dissertation submitted in partial fulfillment
of the requirements for the degree of
Doctor of Philosophy
(Immunology)
in the University of Michigan
2019

Doctoral Committee:

Professor Raymond Yung, Chair
Associate Professor Carey Lumeng
Professor Bethany Moore
Professor Amr Sawalha
Assistant Professor Kanakadurga Singer

Theresa Mau

tmau@umich.edu

ORCID ID: 0000-0003-4278-6438

DEDICATION

To my parents who, in their youths, were brave enough to escape war and violence so that I and my sister could enjoy life at greater degrees of freedom.

ACKNOWLEDGEMENTS

The journey of this dissertation sat on roller coaster tracks. Fortunately, my mentor, colleagues, and friends were the safety bar. I thank my mentor, Dr. Raymond Yung, for his sense of practicality in science and dedication to people. I am forever grateful that my mentor practices and teaches empathy as an essential and professional skill. In the early years of my training, I thank committee member Dr. Carey Lumeng and his lab members who became teammates and trained me on various techniques and invited me to participate in their weekly lab meetings. I am especially blessed to have Dr. Kanakadurga Singer on my committee who has not only been the voice of gender disparities in the workplace of science and medicine, but she further improves science through her specific interest in gender differences within her field of study. I thank committee member Dr. Amr Sawalha for his continuous presence at my talks and invaluable discussions at meetings. I would also like to thank Director of Immunology—Dr. Bethany Moore and program coordinators Zarinah Aquil and Dawn Storball who work relentlessly to prevent the carts from falling off the roller coaster tracks.

My gratitude further extends to colleagues in both the Graduate Program in Immunology and the Geriatrics Center. My journey was enriching with the blend of immunology and biogerontology in my projects. My colleagues stood by me when my thesis work suffered from an unexpected outbreak in our lab's mouse colony, and they generously offered expertise that saved me significant quantities of time and troubleshooting in my new projects. I want to specifically thank my lab manager Martin O'Brien for his day-to-day support ranging from experiments to sympathetic listener. I also want to thank all the wonderful collaborators who enabled me to assemble and complete my dissertation despite the outbreak. I am especially grateful for Dr. Ingrid Bergin and Dr. Vincent Young for their expertise that made it possible for me to salvage data for an outbreak report and initiate an entirely new and interesting project.

TABLE OF CONTENTS

LIST OF FIGURES

LIST OF TABLES

ABSTRACT

This dissertation is a culmination of several projects that each explore how early-life diet or drug can impact later-life health outcomes. The first chapter is an introduction to provide important context or supplementary information (in addition to the introduction in each chapter).

Chapter 2 is a collaborative project testing the adipose-tissue specific effect of three Interventions Testing Program (ITP) drugs that extend median lifespan in mice: acarbose (ACA), 17α-estradiol (17aE2), and rapamycin (Rapa). We hypothesized these three ITP drugs may extend life through the reduction of adipose tissue inflammation. We found ACA and 17aE2 do not alter adipose tissue inflammation. Rapa-treated HET3 mice have increased M1 adipose tissue macrophages. We conclude that Rapa's lifespan extension benefits occur in the context of exacerbated adipose tissue inflammation.

Chapter 3 documents the spontaneous outbreak of *C. difficile* infection (CDI) in our mouse colony. During this outbreak, methyl-donor supplementation (MS) diet F1 mice had higher mortality than control diet F1 mice. We hypothesized the MS diet alters F1 gut microbiota in a way that increases CDI susceptibility. In Chapter 4, we tested if MS diet affects gut microbiota, and if so, whether these changes affect colonization resistance. We found the MS diet F1 mice gut microbiota is enriched with *Lactobacillus*, *Porphyromonadaceae*, and *Bacteroides* and decreased abundance of certain types of *Bacteroides*, *Akkermansia*, and *Alistipes*. We show that F0 diet can lead to an altered F1 gut microbiota. Interestingly, the altered gut microbiota does not compromise F1 colonization resistance to the 16N203 *C. difficile* spore dosage we tested.

The MS diet is modeled after the diet, epigenetic, and obesity link established in the agouti viable yellow (A^{vy}) mice. In Chapter 5, we hypothesized the MS diet can protect C57BL/6J F1 mice from diet-induced obesity in adult life through reduction of adipose tissue inflammation. We found that the MS diet generally does not alter obesity susceptibility nor metabolic inflammation outcomes in C57BL/6J F1 mice.

Chapter 1 – Introduction

Portions of this chapter have been published:

Theresa Mau and Raymond Yung. Adipose tissue inflammation in aging. (2017) *Experimental Gerontology*. Review. DOI: 10.1016/j.exger.2017.10.014. PubMed PMID: 29054535.

The introduction contains the background information partitioned into 5 subsections. These 5 subsections will first cover some literature that discusses the relationship between diet and later-life disease using the developmental origins of health and disease (DOHaD) concept. Following this, I will describe the methyl-donor supplementation (MS) diet used in Chapters 3-5, and I highlight a few studies that have tested later-life disease outcomes using a similar peri-/pre-natal methyl-donor diet. Next, I discuss adipose tissue inflammation in the context of diet-induced obesity (DIO) in the young (metaflammation) and age-associated obesity in the old (inflammaging). These details and concepts are useful for understanding the adipose tissue biology for Chapters 2 and 5. In the last subsection, I briefly review the role of fat mass in longevity and provide some history of the National Institute of Aging's Intervention Testing Program (ITP) and the HET3 mice which are 4-strain crossed mice (first generation offspring of CByB6F1/J and C3D2F1/J parents) we use in Chapter 2.

Developmental Origins of Adult Health and Disease

Early-life nutritional programming influences offspring disease susceptibility across generations[1,2], in part through epigenetic mechanisms including DNA methylation, histone modifications, and the gut microbiome. Fetal programming *in utero* is affected by environmental factors, including early-life exposure and adaptation to maternal

nourishment levels[3–5]. The Hales and Barker 'thrifty phenotype hypothesis' is often used to explain the potential mismatch of *in utero* adaptations to *ex utero* conditions, forming the developmental origin of adult metabolic disease [6,7]. This notion is now expanded to broadly include any disease that may result similarly from 'soft inheritance' of epigenetic marks that affect adult life disease in offspring.

A well-known example of diet and later-life disease in humans was the association found between 1st trimester *in utero* exposure to the Dutch famine of 1944-1945 and low birthweights[3], and this association was also then linked to another important observation: a majority of these fetuses in their adult life succumbed to cardiovascular disease. This was not the first case where the correlation between low birthweights and heart disease was noted, an earlier study similarly reported this connection in the Hertfordshire records[8] of Britain in the 1900s. These epidemiological studies form the basis to the developmental origins of health and disease, and in particular, it supports the existence of a relationship between maternal nutrition and fetus later-life disease risk[5].

It is believed that the fetus makes adaptations based on environmental stresses, including nutrition levels, to better cope with anticipated *ex utero* environment. However, if the fetus is born into an environment where there is significantly higher nutrition availability, then this 'mismatch' adaptation can translate into poorer metabolic health[9–12], especially if they experience "catch-up" growth[12]. These fetal intra-womb 'decisions and adaptations' are believed to be penned with epigenetic marks, enabling developmental plasticity.

Prenatal Nutrition and Epigenetics

During development, the integrity of DNA methylation is indispensable for temporal silencing of specific genes to differentiate tissues at the correct stages of growth. Maternal intake of macronutrients and micronutrients play a crucial role in the infant's development, because the availability of resources (metabolites) for DNA methylation can affect this process[13]. DNA methylation and histone modifications were

considered to the two major epigenetic mechanisms. However, within the last decade, DNA methylation, histone modifications, and non-coding RNA (microRNA) regulation are all surfacing as major and highly interconnected epigenetic mechanisms[14].

A group of enzymes, DNA methyltransferases (DNMTs), catalyze the addition of the methyl group to the DNA. The DNMT family includes DNMT1, DNMT3a, DNMT3b, and DNMT3l. During DNA replication, hemimethylated DNA are important intermediates for DNA methylation to be maintained in cell lineages, but during replication and embryogenesis, *de novo* methylation of DNA also occurs[15,16]. DMNTs facilitate the addition of a methyl group at the C5 position of cytosine residues on CpG (cytosine-phosphate-guanine) islands. S-adenosylmethionine (SAM) is as an intermediate methionine metabolism product that acts as a methyl-donor for methylation processes[17].

Methyl-donor supplementation (MS) diets have been used in studies as a prenatal diet and include folate, choline, betaine, and vitamin B12. The MS diet leads to hypermethylation of A^{vy} and $Axin^{Fu}$ alleles in mice. This results in fewer F1 A^{vy} mice born with pseudoagouti (brown) coat color which is associated to decreased obesity[18], and it also leads to reduced severity of tail-kinking in $Axin^{Fu}$ mice[19]. Choline and betaine (metabolite formed from choline) also influence DNA and histone methylation status. Betaine donates a labile methyl group to homocysteine to form methionine and eventually lead to SAM synthesis which is the methylating agent and required cofactor for DMNTs[20].

Methyl-donor diet intervention and later-life diseases (Ch. 3-5)

Viable Agouti mouse model of obesity and epigenetics

A clear demonstration of epigenetic inheritance of metabolic disease is the viable agouti A^{vy} mouse model of obesity[18,21]. The *agouti* gene encodes a paracrine signaling molecule that produces either black eumelanin (a) or yellow phaeomelanin (A) which influences coat color. An endogenous retrovirus-like gene that is known as the intracisternal A particle (IAP) retrotransposon insertion leads to ectopic expression of the

agouti gene, and this leads to the agouti coat color and proneness to developing obesity and tumors, shortening the lifespan of F1 mice. When a methyl-donor supplementation (MS) diet is prescribed to the dams, the F1 mice were protected by methylation on the *agouti* IAP gene promoter site[22], and degree of methylation on the promoter (up to 9) shifts F1 mice towards corresponding pseudoagouti coat colors[23]. These protective marks suppress ectopic expression of the agouti gene and is associated with decreased obesity[18] and tumorigenesis in F1 mice[24], leading to increased lifespan. The observations from the viable agouti mouse model lend insight into the relationship between diet and its effects on later-life disease through epigenetic mechanisms.

Genistein, an isoflavone from soybeans, and bisphenol A (BPA), a chemical used in the manufacturing of polycarbonate plastics, have been shown to affect DNA methylation in the A^{vy} allele. In an interesting expansion of this classic mouse model of later-life disease and epigenetics, it was reported that the MS diet protects against BPA-induced hypomethylation in F1 mice[25]. In this case, the viable agouti mice served as biosensors to environmental stressors that could alter the epigenome[21], and secondly, it demonstrates how early-life diet (in the F0 generation) could impart disease risk or protection in the F1. However, it should be noted that a different group tried repeating this MS diet and BPA study but reported insignificant results[26].

Methyl donor supplementation diet mice model (Ch. 3-5)

Others have ventured to test similar variations of the MS diet in different contexts[27]. The viable agouti mice are unique in that they possess the retrotransposon insertion that leads to ectopic expression of the *agouti* gene. Therefore, these mice are a model of a unique genetic-epigenetic predisposition of obesity. A study that followed the classic agouti mice papers set out to test a high folic acid supplement diet in non-agouti mice in conjunction with diet-induced obesity (DIO) and reported worsened metabolic outcomes in C57BL/6J male mice[28]. There is some evidence this MS diet could also affect neuro-behavioral phenotypes such as its reversal of alcohol-induced DNA methylation changes on *Igf2*[29]. However, high folic acid supplementation in C57BL/6J mice has also been associated with an increase of anxiety-like and hyperactive

behavior[30]. MS diet in rats have been reported to exacerbate aspects of DIO and metabolic function through hypermethylation of the leptin promoter *Ob*, decreasing F1 rat leptin levels[31]. They also revealed that MS diet was associated with impaired post-natal growth, and male rats displayed increased long-term body weight gain—potentially due to the suppression of leptin expression[31].

Our lab has previously shown that a MS diet, closely modeled to the classic agouti mouse studies, is protective in an atherosclerosis mouse model[32]. Apolipoprotein E ApoE(-/-) deficient mice spontaneously develop atherosclerotic lesions, and MS pre- and peri-natal diet exposure decreases T-cell mediated pro-inflammatory cytokine and chemokine responses in F1 mice. *Ccr2* is important for the inflammatory pathogenesis of atherosclerosis. In a subsequent study, MS diet F1 mice have increased global CD3+ T cell methylation and *Ccr2* expression was significantly reduced[33].

The MS diet has also been shown to affect gut microbiota and inflammation in a mouse model of human inflammatory bowel disease[34,35]. In this study, the authors showed that a chemically-induced colitis with dextran sulfate sodium (DSS) is exacerbated in F1 mice whose parents were on the MS diet. In a later experiment, they showed that cage swapping to enable a fecal microbiome transfer between MS diet and germ-free mice was sufficient to worsen colitis, compared to a control diet and germ-free cage swap control group[34]. These studies on MS diet and host gut inflammatory responses differ from the obesity studies in that they show that the MS diet could affect later-life disease in avenues other than DNA methylation and instead, through the gut microbiome.

Diet, the microbiota, and colonization resistance (Ch. 3-4)

Gut microbiota, the gastrointestinal resident microbial community, is important for colonization resistance[36,37] and host immune responses[38]. The primary risk factor *Clostridium difficile* infection (CDI), which is the most common nosocomial pathogen in the United States, is antibiotic-use[39–42]. Non-antibiotic associated CDI is on the rise[43], prompting new studies to search for other major risk factors. In the last few years, the

effect of diet on gut microbiota has been shown to be a potential contributor to the rise of CDI, especially the hypervirulent strains of *C. difficile*[44,45].

Diet as a transient stimulus has shown to induce changes in the microbiota in humans. In mice, an excess of zinc in a diet drastically alters the gut microbiota and with an additional antibiotic challenge, colonization resistance against *C. difficile* was lost[45]. Whereas, control mice on a low-dose zinc diet with the antibiotic challenge maintained colonization resistance, thereby preventing CDI. The zinc diet study demonstrates that metal levels in environment, in this case diet, can directly alter gut microbiota through metal-toxicity reduction of microbial diversity or microbial homeostasis and lead to changes in host health outcomes.

Another recent study revealed that the hypervirulent *C. difficile* strains RT027 and RT078 gain significantly higher fitness in the presence of a sugary substitute in processed foods, trehalose, that likely aided in its successful spread in North American and West Europe[44]. The trehalose study shows that diet could also shift microbial composition through means of increased fitness for specific microorganisms as opposed to reduction of other microbial populations as in the zinc study. The role that diet plays in later life disease through various epigenetic mechanisms currently remain unclear, but the recent studies that demonstrate the significant and differential ways in which diet could alter gut structure and function indicate that diet is no minor player.

Obesity in the Young and Old (Ch. 2 & 5)

Adipose, or fat tissue, is the largest endocrine organ in humans and in other cases, can be the largest organ in an obese individual. Adipose tissue plays a pivotal role in age-related metabolic dysfunction and longevity[46–48]. With old age, fat distribution shifts from subcutaneous to visceral fat depots, while triglycerides ectopically deposit on liver, muscle, bone marrow, and heart[49]. These changes are associated with the development and progression of a variety of age-associated diseases.

Obesity accelerates the onset of these age-associated diseases, further emphasizing the level of impact adipose tissue plays in aging[46,50]. Similar to inflammaging, obesity is linked to a systemic, chronic, low-grade inflammation. Adipose tissue inflammation in obesity is also termed 'metaflammation'[51]. While most recent studies focus on how adipose tissue dysfunction progresses in diet-induced obesity, much less efforts have been devoted to understanding the pathogenic mechanisms of old-age obesity. Whether inflammaging and metaflammation share common inflammatory pathways or have similar sources of inflammation, including the role of different fat depots, are important questions. It is likely there are fundamental differences between diet- versus age-dependent obesity, given the widespread immunological and physiological changes that are known to occur in old age.

The majority of interventions that extend lifespan function through nutrient sensing and processing pathways, and they have important effects on adipose tissue formation and function. Growth hormone deficient mice, in addition to improved lifespan, have less ectopic fat deposition, improved adipocyte progenitor cell function, and reduction in cellular senescence[50]. A number of single-gene mutations are known to extend lifespan in lower organisms, and similar lifespan extension is observed even if the mutations are restricted to adipose tissue[52–54].

Obesity paradox and aging

The obesity paradox refers to a collection of unexpected findings, where several chronic diseases, including cardiovascular, have lower all-cause mortality rates in elevated body mass index (BMI) patients[55]. The "obese healthy" implicates that having a higher BMI can be protective and that the "lean" BMI is in actuality, not the lowest mortality group. For example, obese (BMI >30 kg/m^2) and severely obese (BMI >40 kg/m^2) patients after coronary artery bypass grafting are at lower risk for postoperative complications than patients with a lower but "normal" (18.5 kg/m^2 < BMI <25 kg/m^2) categorization[55]. It has been controversial as to how this can occur—and many of these observations were thought to be particularly true in elderly patients. It is reasonable to

postulate that, in some circumstances, adiposity may confer a degree of biological resiliency that enhances recovery after a stressful life event.

Studies described the mortality risks as a 'U-shaped curve' for the elderly while the younger individuals have a 'check-mark' or 'j' shape mortality curve. Where increased BMI in the overweight and even obesity ranges have exhibited protective effects on patients, although true in the datasets, also held many caveats in the design study. When body composition was measured using a different method, it seems BMI frequently misclassifies body fat status, and it was argued that BMI is a better predictor of lean body mass than of adiposity[55]. Therefore, patients with higher BMI are protected by higher lean body mass and not body fat.

There are many other prominent theories summarized[55,56]—with some arguing that lean individuals plagued with chronic conditions could also be suffering 'malnutrition-inflammation complex syndrome' which would be worse than carrying a high BMI. It was also hypothesized that young obese with abdominal obesity die earlier and those who survive towards higher age categories like those of the obesity paradox studies actually carry greater degree of lower-body obesity. Alternate theories suggest muscle quality determined by muscle mass and grip strength would also be important indicators of health[55,56]. Others suggest genetic predisposition contributes to the formation of these obese healthy[56] or metabolically obese[57] phenotypes observed.

Metaflammation (diet-induced obesity in the young) (Ch. 5)

Adipose Tissue Immunological Profile During Diet-induced Obesity

In obesity, adipose tissue homeostasis is perturbed: the balance between energy intake and expenditure is pushed towards the former. In aging, there is also a reduction in resting metabolic rate and lower total daily energy expenditure, particularly in frail individuals[58]. With excessive accumulation and expansion of adipose tissue in obesity, there is an increased likelihood of metabolic syndrome, cardiovascular disease and type 2 diabetes mellitus[54]. Adipose tissue inflammation, specifically white visceral-gonadal adipose tissue, is a major contributor to metaflammation and insulin resistance.

Compared to lean individuals, white adipose tissue (WAT) from obese adults secretes higher levels of tumor necrosis factor α (TNFα), an inflammatory cytokine capable of interfering insulin signaling. When TNFα is inhibited, glucose tolerance and insulin sensitivity is improved[59]. Pro-inflammatory cytokines and chemokines such as interleukin 1b (IL-1b), monocyte chemoattractant protein (MCP-1), and interleukin 6 (IL-6) are also secreted at elevated levels from obese adipose tissue macrophages[60,61].

Adipose Tissue Macrophages, Inflammation, and Organelle Stress

Aging is associated with important changes in the innate immune system. Macrophages perform important innate immune functions including phagocytic clearance of dying cells. Depending on the stimuli, macrophages can become polarized into "M1" or "M2" subsets. Classically-activated or M1 "killer" macrophages and alternatively activated M2 "healing" macrophages are convenient terms that describe the plasticity of macrophage subsets and function. However, it is important to note that macrophages may not form clear-cut activation subsets nor expand clonally[62]. Studies aimed to elucidate the source of inflammation in obesity have found that macrophages accumulate in WAT[63] and exhibit a predominantly proinflammatory "M1" profile, as compared to the less or anti-inflammatory "M2" in lean healthy control adipose tissue[60,61]. Hypertrophy and hypoxia also leads to the formation of crown-like structures where macrophages surround a dead or dying adipocyte[64]. This very characteristic crown-like structure is used as one means of quantifying levels of inflammation in adipose tissue and has been shown to persist in the tissue even with weight loss in mice[65].

In obesity, adipose tissue macrophages are burdened with an increase in adipocyte death, leading to inflammasome activation, and formation of crown-like structures in the adipose. Diet-induced obesity has also been shown to increase endoplasmic reticulum (ER) stress in mice, involving all 3 major branches of the unfolded protein response (UPR)—BIP, CHOP, and ATF4[66,67]. The higher ER stress responses involving IRE1α and CHOP has recently been shown to directly lead to stress-induced polarization of macrophages[68,69] away from the M2 state, contributing to the domination of M1 polarization in adipose tissue.

Outside of macrophages, the immune cell profile of obese WAT undergoes a multitude of other changes. CD4+ and CD8+ effector T cell ratios also shift towards CD8+ T cells—a significant number of CD8+ T cells infiltrate the adipose tissue while CD4+ T cell numbers remain low[70] during diet-induced obesity. It is also suggested that this is how T cells can initiate adipose tissue inflammation via recruitment and stimulation of resident ATMs[70]. Of note, regulatory T cells (Tregs) in the adipose tissue are also reported to be diminished in lean animals when compared to obese[71]. Other studies have also reported on how eosinophils promote adipose tissue inflammation via supplying ATMs with a steady source of IL-4 in the tissue[72]. While similar to CD8+ T cells, B cells during obesity can accumulate in the adipose tissue and secrete pathogenic IgG, spurring further inflammation, insulin resistance, and glucose intolerance[73]. Mast cells have been shown to also contribute to inflammation and insulin resistance via production of IL-6 and IFNγ[74]. The immune profile of obese WAT all contribute to adipose tissue inflammation and sustenance of proinflammatory polarization of ATMs.

Non-immune Players in Adipose Tissue Inflammation

As previously mentioned, adipose tissue is an endocrine organ. Adipocytes can by themselves secrete adipokines which are chemokines and cytokines, some more unique to the adipose tissue and metabolism (e.g., leptin, adiponectin) while others are familiar to the immune system (IL-6, TNFα)[75]. During obesity, adipocytes increase proinflammatory cytokine and chemokine secretion of IL-6 and TNFα, where TNFα has been shown to increase insulin resistance in diet-induced obese mice[51]. Apart from immune cell infiltration, adipose tissue dysfunction in obesity is complicated by abnormalities of lipid metabolism[76,77].

While adipose dysfunction is not solely reliant on immune cell-driven inflammation, adipocyte function also cross-talks with immune cells and independently contributes inflammatory signals. For instance, higher levels of circulating free fatty acids in obese conditions that undergo lipolysis generate saturated fatty acids (SFAs), proinflammatory lipid compounds that stimulate macrophage[78], adipocyte[79], myocyte[80]

and hepatocyte[81] inflammation, leading to insulin resistance[82–84]. SFAs activate macrophages via Toll-like receptor 4 (TLR4), but they are also precursors for ceramide biosynthesis which can directly decrease insulin sensitivity or indirectly affect insulin signaling through the production of Fetuin-A (FetA)[85]. Interestingly, FetA null mice have protection against insulin resistance in an obesity and aging model as well[86], and we recently report that TLR4 KO mice have a reduction in adipose tissue inflammation in aging[87]. These findings indicate that while adipose tissue inflammation is primarily attributed to ATMs in literature, there are other non-immune players that similarly contribute and overlap in perpetuation of the inflammatory cycle in the adipose tissue.

Inflammaging (age-associated obesity) (Ch.2)

Loss of Basic Adipose Function

With old age, adipose tissue distribution shifts towards visceral fat storage[49]. Patients with human immunodeficiency virus (HIV) also suffer loss of subcutaneous fat with an increase in visceral fat. (HIV)-associated lipodystrophy leads to increased risk of CVD and diabetes, stressing the importance of subcutaneous-visceral adipose tissue distribution and metabolic health[88]. Ectopic deposition of triglycerides also occurs on other organs such as liver, skeletal muscle, and even bone marrow[49]. This trend is associated with higher risk of cardiovascular and metabolic disorders.

Aging Adipose Tissue and Immunological Profile

We have previously examined and characterized immune changes in WAT in old mice and found that in aging adipose tissue, similar to obesity, macrophages exhibit a shift away from M2 and towards double negative (CD206-CD11c-) expression[89]. In this study, young and old mice adipose tissue was fractioned into ATMs (CD11b+), adipose tissue stromal cells (ATSCs) (CD11b-), and adipocytes. These fractions were then individually analyzed for cytokine and chemokine production. While all 3 fractions excreted IL-6 and MCP-1 *in vitro*, ATSCs and ATMs produced substantially higher levels, implicating that the major contributors to adipose tissue inflammation in aging are the resident fat immune cells and not adipocytes.

In a separate study, we investigated the role endoplasmic reticulum (ER) stress plays on macrophage inflammation in old adipose tissue. Similar to obese ATMs, old ATMs also display elevated ER stress and inflammation[90]. Alleviating the ER stress in old murine ATMs *in vitro* and *in vivo* via a chemical chaperone decreases the production of inflammatory cytokines and chemokines[90]. Another study similarly employed chemical chaperones to reduce ER stress in the adipose tissue of diet-induced obese mice and succeeded decreasing adipose tissue inflammation[91]. In a later investigation, we observed that old mice also possess perturbed autophagy function within their SVF, contributing to adipose tissue ER stress and inflammation. Furthermore, blocking autophagy function in the SVF increased ER stress marker CHOP and pro-inflammatory markers IL-6 and MCP-1[92]. These results emphasize the importance of adipose tissue homeostasis and metabolism, particularly at how large of a role non-adipocytes can play.

In old adipose tissue, there was also a higher total stromal vascular cells (SVF) per gram of WAT, showing that adipose tissue accumulates resident cells over time. The increase in SVF was observed in T cells (CD3+), particularly CD4+ T cells and a minor increase in CD8+ T cells. A three-fold increase of regulatory T cells (Tregs) was present in old WAT[89]. Aging has been reported to be associated with increased Treg function secondary to age-related epigenetic drift and T cell DNA hypomethylation[93]. Excessive Tregs activity may contribute to age-related susceptibility to infection, neurodegeneration, and cancer[94–96]. The origin of the Tregs in aging adipose tissue is not defined but is presumably derived from peripheral naïve CD4 T cells responding to the local aging microenvironment. Nevertheless, the results were unexpected as others have shown that visceral adipose tissue of lean animals have higher number of Tregs compared to their obese cohort. The adipose tissue Tregs presumably playing a protective role in metabolic disorder, suppresses the production of local inflammatory mediators and improves insulin resistance[71,97]. Importantly, a recent study also showed that the depletion of these fat-specific Tregs prevent age-associated insulin resistance in mice[98], supporting the notion that distinct immune cell subpopulations all play an inter-connecting role in age-associated inflammation and diseases.

Human aging is in part, characterized by a chronic, low-grade inflammation that develops in various aging tissues. This phenomenon is termed 'inflammaging'[99,100]. The health detriments and benefits of inflammaging are inconclusive. While super centenarians boast a higher inflammatory cytokine profile[101], inflammatory mediators are critical to the pathogenesis of age-related diseases such as arthritis, diabetes, sarcopenia, cardiovascular disease (CVD), cancer, and dementia[102,103]. While sources of inflammaging remain under investigation, some prominent conversations include immunosenescence[99,104], self-debris[105], senescent cells[106], mitochondria dysfunction[107,108], microbiome[109], and adipose tissue[47,50,110].

The Role of Fat Mass in Longevity (Ch. 2)

Caloric restriction and the role of fat mass in lifespan

In mammals, caloric restriction is the classic method of lifespan extension, and given that caloric restriction (CR) results in smaller growth and therefore reduced fat mass gain, it was believed that CR benefits stem from having less fat mass[111]. In the last two decades, the growing literature on the wide range of functions of adipose tissue has become supportive evidence of fat mass's influence on health[48,112]. As previously discussed in the metaflammation and inflammaging sections of this chapter, the detrimental changes to adipose tissue in obesity have been likened to a state of accelerated aging[47]. Whereas, inflammation in aging has been, in part, attributed to lipid redistribution[49,113–116], ectopic fat deposition on various organs[49,116,117], and immune changes to gonadal white adipose tissue[89,90,93]. These collectively build into the notion that adipose tissue health, though not the sole factor, can determine an organism's lifespan.

Senescent cells in aging adipose tissue

Senescence serves as the brakes to tissue renewal and cancer cell development in organisms. More specifically, senescence is a process where cells become irreversibly arrested in cell-cycle to prevent further replication in response to stress[118]. In aging, environmental stresses compound overtime: DNA damage, telomere attrition, mitogenic signals, and chromatin dysfunction lead to the accumulation of senescent cells in various

tissues[118]. While senescent cells become non-replicative, they also undergo phenotypic changes, including tumor-suppressor and secretome switches[119], that enable them to affect the tissue microenvironment, influencing neighboring cell structure and function.

Two primary tumor-suppressor pathways, involving p53 and pRB, are attributed with regulating the senescent states of cells. These transcriptional regulators are nestled in the center of the pathways, with stress response proteins upstream and downstream effectors that promote and maintain senescent states. Loss of p53 function in studies have shown to diminish replicative senescence in human cells[120] while inactivation of p21, a cell cycle inhibitor that is also a p53 target, allows cells to bypass telomere attrition-dependent senescence[121]. The pRB pathway contains p16, a cell cycle inhibitor that responds to stress. Senescence occurs with either pathway or both; however, downstream of these pathways, upregulated genes include secreted proteins that include cytokines and chemokines[122].

Senescent cells have been reported to secrete various proinflammatory cytokines such as IL-6, IL-8, and TNF-a, collectively known as the senescence-associated secretory phenotype (SASP)[106]. These proinflammatory factors accumulate with aging, as the old immune system becomes less efficient with the clearance of senescent cells[118,122]. They become a potential source of inflammation in inflammaging. Recently, studies indicate that visceral and inguinal adipose tissue in mice harbor large quantities of senescent cells that are $p16^{Ink4a}$ positive[123]. Tissue accumulation of p16, p21, and β-galactosidase are markers of senescence, and senolytics are designed for the clearance of senescent cells that fail to be naturally cleared by the host immune system. Recent senolytics studies successfully depleted $p16^{Ink4a}$ via a novel transgene, INK-ATTAC, and it was demonstrated that age-related disorders can be attenuated in the BubR1 progeroid mouse model[123,124].

ITP Drug Interventions and Lifespan Extension (Ch. 2)

The Interventions Testing Program is an endeavor sponsored by the NIA to evaluate potential interventions in various forms (pharmaceuticals, nutraceuticals, foods, diets, dietary supplements, plant extracts, hormones, peptides, amino acids, chelators, redox agents, and other agents / mixtures of agents) that could extend lifespan, delay disease and dysfunction in mice (https://www.nia.nih.gov/research/dab/interventions-testing-program-itp).

Up until the year 2000, the National Institute of Aging (NIA) had been providing predominantly genetically homogenous aging mice either from inbred lines or F1 hybrid stocks. Genetically heterogeneous mice were then generated via a four-way cross breeding scheme[125,126] that generate "HET" mice from mating between (Balb/cJNia x C57BL/6JNia) F1 mothers and (C3H/JNia x DBA/2JNia) F1 fathers. This results in no two mice that are genetically identical. The goal behind the HET strain of mice is to enable the use of a mouse model where strain-specific idiosyncrasies can be untangled where experimental design allows for the use of heterogenous animals (for example, tissue transplantation would be infeasible in this mouse model).

Chapter 2 – Lifespan extension drug interventions affect adipose tissue inflammation in aging

This chapter is in preparation for submission as a manuscript.

Theresa Mau, Martin O'Brien, Amiya K. Ghosh, Richard A. Miller, and Raymond Yung.

Abstract

The National Institute on Aging-sponsored Interventions Testing Program (ITP) has identified a number of dietary drug interventions that significantly extend median lifespan, including rapamycin, acarbose, and 17-α estradiol. However, these drugs have diverse downstream targets, and their effects on age-associated organ-specific changes are unclear [127]. Potential mechanisms by which these drugs may be extending life could be through their effect on inflammatory processes often noted in tissues of aging mice and humans. Our study focuses on the effects of three lifespan extension drugs in the ITP on inflammation in gonadal white adipose tissue (gWAT) of female and male HET3 mice. gWAT was harvested to study the drugs' impact on adipose tissue inflammation—including age-related fat mass gain, adipose tissue macrophage (ATM) M1/M2 polarization, markers of cellular senescence and endoplasmic reticulum stress. We observe that rapamycin led to a 56% increase of CD45+ leukocytes in gWAT, where the majority of these are ATMs. Specifically, rapamycin led to a 217% and 106% increase of M1 (CD45+CD64+CD206-) ATMs in females and males, respectively. We found that HET3 mice exhibit a spectrum of age-associated changes in the gWAT, but acarbose and 17-α estradiol did not strongly alter these phenotypes. Our data suggest that rapamycin may achieve lifespan extension in part through adipose tissue inflammation. Our results also suggest that acarbose and 17-α estradiol may not influence lifespan through mechanisms involving adipose tissue inflammation.

Introduction

Human aging is, in part, characterized by the tendency of the body to develop a proinflammatory status with advancing age [128–134]. Chronic inflammation plays an important role in the pathogenesis of many age-associated diseases [103,135,136], such as Alzheimer's disease, atherosclerosis, cardiovascular disease, type II diabetes, and invasive cancer. Adipose tissue inflammation is believed to be a major contributor to a range of age-related functional declines [47,48,112]. Effects of abnormalities in adipose tissue could in principle be mediated by changes in energy storage, lipid metabolism, or production and secretion of adipokines and hormones.

With advancing age in humans and rodents, adipose tissue mass increases through middle and early-old age, and white adipose tissue (WAT) redistributes from subcutaneous to intra-abdominal visceral depots[49,113–116]. WAT also exhibits ectopic lipid infiltration in liver, muscle, and bone[49,116,117]—though rodent models of lipodystrophy are still being developed and lack female data [137–139]. In gonadal white adipose tissue (gWAT), the distribution of adipose tissue macrophage (ATM) subsets shift toward pro-inflammatory phenotypes with age[89,90,93]. We have previously shown that in gWAT of old (22 mo.) C57BL/6J male mice, ATMs shifted from an anti-inflammatory "M2" phenotype (CD206+) towards the pro-inflammatory "M1" (CD206-) phenotype when compared to young (6 mo.) controls [89]. This upward shift in M1:M2 ATMs ratio was associated with increased levels of pro-inflammatory chemokines and cytokines. Although the M1/M2 distinction over-simplifies a network of inter-related cell types of overlapping function, we will, for the purpose of discussion, refer to $CD45^{+}CD64^{+}CD206^{-}$ macrophages as "M1s" and $CD45^{+}CD64^{+}CD206^{+}$ macrophages as "M2s" in this report.

Our subsequent studies revealed that endoplasmic reticulum (ER) stress plays a significant role in ATM inflammation in aging-associated obesity. Alleviation of ER stress in old murine-derived ATMs blocked secretion of interleukin-6 (IL-6), tumor necrosis factor-alpha (TNF-α), and monocyte chemoattractant protein-1 (MCP-1), restoring a phenotype to that of young ATMs [90,92]. Another notable source of

inflammation in aging adipose tissue is production of inflammatory cytokines by senescent cells, termed senescence-associated secretory phenotype (SASP). Relative to other tissues (brain, liver, colon, lung, pancreas, and heart), white adipose tissue, along with skeletal muscle and the eyes, is a major reservoir for $p16^{Ink4a}$ and senescence-associated β-galactosidase (SA-β-Gal) senescent cell accumulation. There is some evidence that reduction of $p16^{Ink4a}$ senescent cells may attenuate the onset of age-related disorders, at least in a mouse model of progeria [123,124]. However, the inflammatory status of the specific aging tissues that seem to benefit from the senolytics were unexplored—necessitating future work to question whether or not the reduction of senescent cells directly diminishes adipose tissue inflammation.

Previous studies [140–146] of the ITP drugs have reported on the sex differences, extent of lifespan extension, and dose-dependent response using genetically heterogeneous HET3 mice. In this system, 30% caloric or dietary restriction can extend life in female and male mice by 36% [147]. ACA, which blunts post-prandial glucose spikes, extends male lifespan by 22% and leads to an increase of only 5% in females [145]. 17aE2 does not extend lifespan of females but extends male lifespan by 19% [145]. Rapa, which inhibits the mechanistic target of rapamycin (mTOR) kinase, can extend lifespan in females by 26% and in males by 23% at the highest doses tested [140,141,143,148]. Further details on the NIA Interventions Testing Program are summarized[127] (https://www.nia.nih.gov/research/dab/interventions-testing-program-itp).

These changes in aging adipose tissue collectively contribute to age-associated adipose tissue dysfunction which affects health and lifespan [149]. Interventions for lifespan extension target nutrient-sensing pathways that also have significant effects on adipose tissue in lower organisms[50,52,111,150,151]. In a few cases, mutations that extend lifespan in lower organisms such as flies or worms, also lead to lifespan extension when the mutation is limited to adipose tissue [152,153]. Fat-specific insulin receptor knockout (FIRKO) mice have reduced fat mass, protection from age-associated obesity, and mean lifespan extended by 18% [154]. In the current study, we hypothesized that ITP pharmacological interventions, specifically acarbose (ACA), 17-α estradiol (17aE2), and

rapamycin (Rapa), may extend life by slowing or preventing age-related increases in adipose tissue inflammation. We measure aspects of adipose tissue composition and function in six groups of HET3 mice (young, old, calorie restriction (CR), ACA, 17aE2, and Rapa), with emphasis on the levels of adipose tissue ER stress and the relative proportions of ATM subsets. Additionally, we evaluate the effects of age on HET3 mouse adipose tissue and whether any of the ITP drugs influence these age-related phenotypes.

Materials and Methods

Animals: Breeding & Husbandry Protocol

Genetically heterogeneous UM-HET3 mice were produced via a four way cross between CbyB6F1/J mothers (BALB/cJ x C57Bl/6J, JAX #100009) and C3D2F1/J fathers (C3H/J x DBA/2J, JAX #100004) at University of Michigan (UM) as previously described [125]. The mice were housed in pairs per cage from weaning, cages were inspected daily, and mice that died were not replaced. At 4 months of age, F1 mice from different breeding pairs were randomly allocated to 2 control and 4 treatment groups: young and old controls; calorie-restriction (CR), Acarbose (Aca), 17-α-estradiol (17aE2 or Est), and Rapamycin (Rapa) treatment groups.

Control and Experimental Diets

Breeding pairs were fed Purina 5008 chow. Young (4 mo.) and old (22 mo.) control mice were fed the Purina 5LG6 chow post-weaning and throughout. Control and treatment diets were prepared by TestDiet, Inc., Purina Mills (Richmond, IN, USA). For calorie-restriction mice: 22 months of age, 30% CR from 4 months of age.CR group were given an amount of food equal to 90% of the amount consumed by mice in the *ad libitum* control group ("AL" group) for 2 weeks. They were then shifted to 75% food availability for 2 weeks and then shifted to 60% food intake for the remainder of the experiment [155]. Acarbose 1000ppm: purchased from Spectrum Chemical Mfg. Corp. Gardena, CA, USA; 22 months of age, Acarbose from 4 months of age. 17-a-Estradiol 14 ppm: purchased from Steraloids Inc. (Newport, RI, USA) 22 months of age, estradiol

from 9 months of age. Rapamycin: at 4 months of age were given a diet containing encapsulated rapamycin at 14.7 ppm (mg of drug per kg of food).

Tissue extraction: gWAT stromal vascular fraction

Gonadal white adipose tissue (gWAT) is removed with minimal cuts, weighed, and placed into a sterile petri-dish containing ice cold dye-free Dulbecco's Modified Eagle Medium (DMEM) containing 10% FBS (Gibco 21063-029) and 1% Penicillin Streptomycin (Gibco 15140-122). Collagenase (Sigma Life Science, #C6885-1G) is prepared in DMEM buffer with a final 10mg/mL concentration. gWAT fat pads were minced, gently passed through 100 μm filter, centrifuged (1500 RPM), and collagenase-digested in an 37° C incubator for 45 min with rotation. A second rinse-filter step follows. ACK lysis (Lonza, #10-548E) is mixed into cell pellets and neutralized at 5 minutes with ice cold PBS. A third rinse-filter step occurs with cold PBS. SVF cell fractions are resuspended in 1 mL of cold PBS and 10 μl is saved for trypan blue (Invitrogen) cell counting using the Cell Countess (Invitrogen).

Flow cytometry stains

SVF cells extracted from gWAT are washed and resuspended in sterile filtered FACs buffer (PBS, 0.5% BSA, 0.1% NaN3) and cells per sample are pooled together to form the control cells for Single Positive Controls (SPCs), Full-minus-one Controls (FMOs), and the negative cells. Samples are blocked with anti-mouse CD16/CD32 (eBioscienceaffymetrix #14-0161) for 1 hr on ice. After rinsing, cells are incubated with anti-mouse CD45 (eBioscienceaffymetrix #48-0451), CD64 (BD Pharmingen 558455), CD11c (eBioscienceaffymetrix #47-0114), CD11b (eBioscienceaffymetrix #11-0112), CD206 (eBioscienceaffymetrix #17-2061), & CD31 (eBioscienceaffymetrix #46-0311) for 1 hr on ice, in foil. Cells were fixed with 2% paraformaldehyde (PFA) for 20 min on ice prior to washing and storing in FACs buffer until analysis. Samples were run on a LSRFortessa (University of Michigan Flow Cytometry Core) and analyzed on FlowJo version 10.0.0.1.

mRNA isolation and RT-qPCR

Total RNA was isolated from whole adipose tissue (gonadal / inguinal depots), homogenized in Qiazol lysis reagent (Qiagen, #1023537), and processed through a QIAshredder (Qiagen, #79656) prior to using the RNeasy Lipid Tissue Mini Kit (Qiagen, #1023539) in conjunction with a RNase-Free DNase (Qiagen, #79254) digestion step. Reverse transcription and cDNA amplification was performed with QuantiTect SYBR Green RT-PCR Kit (Qiagen, #1054498) on a real-time R6-6006 Corbett Thermalcycler. All primers were obtained from IDT and specific primer sequences are listed (Table 1.1).

Western blot

Briefly, whole gWAT protein lysates were mixed with 4x Laemmli (Biorad #161-0737), denatured, loaded at 40 μg per well into 15-well 4-20% gel casts (Biorad Mini-PROTEAN TGX Precast Gels, #456-1096) and ran at 90V in a Tris/Glycine/SDS buffer. It was transferred to a PVDF membrane (BioradImmun-Blot, #1620177) in a Tris/Glycine/20% MeOH buffer at 100V. Then, it is rinsed with TBS / 0.1% tween and blocked (Thermo Scientific Superblock T20, #37536) for 1 hr at RT on rotator. Primary antibody (CHOP (anti-DDIT3 Abcam ab179823), P62 (Abcam ab9691526), or IgG (goat anti-mouse IgG-HRP Santa Cruz sc-2031), a-tubulin (Abcam ab18251)) is administered overnight in a 4°C cold room. Blots were washed 3x 10 min with TBS / 0.1% tween prior to incubation with secondary antibody (in 5% non-fat milk powder in TBS/tween) for 30 min at RT on rotator. Chemiluminescence is captured via Pierce ECL Western Blotting Substrate (Thermo Scientific, #32106) on Image Quant LAS 4000 (GE Healthcare) machine. Densitometry is calculated with ImageJ software.

Statistical Analyses

2way-ANOVA analyses were performed, setting factor 1 = sex [female; male], factor 2 = [old controls; one of the following groups: young controls, CR-, ACA-, 17aE2-, or Rapa-treated mice. Interaction term = sex term x treatment term, each reported (* $p<0.05$, ** $p<0.01$, *** $p<0.001$, **** $p<0.0001$). A post-hoc test used as a follow-up was Sidak's multiple comparisons, reporting average difference in mean for each sex (* $p<0.05$, ** $p<0.01$, *** $p<0.001$, **** $p<0.0001$). If interaction or sex effect were

insignificant, sexes were pooled and submitted to normality tests D'Agostino & Pearson and Shapiro-Wilks (alpha=0.05). If normality test passes ($p \geq 0.05$), then a Student's unpaired T-test is run and if significant (^ $p<0.05$, ^^ $p<0.01$, ^^^ $p<0.001$, ^^^^ $p<0.0001$), reported degree of significance and average difference in mean. If normality test fails ($p \leq 0.05$), then a Mann-Whitney test is run, and if significant ($^{\#}p<0.05$, $^{\#\#}p<0.01$, $^{\#\#\#}p<0.001$, $^{\#\#\#\#}p<0.0001$), degree of significance and average difference in median were reported. Values reported within text are mean ± SEM. Where there are significant sex effects, percent change is reported within the text. Occasionally, the follow-up Sidak's comparisons test (for individual sexes) do not reach statistical significance and are denoted as not significant (N.S.), and these trends may be reported to highlight the sex effects and will be further explored in discussion. *P*-values reported for interaction (sex*treatment), sex, or treatment represent 2way-ANOVA results which is comprehensively reported with the submitted manuscript, and further details on this table is within the statistical methods section. In cases where the sex and/or interaction term in the 2way-ANOVA is insignificant, the mean ± SEM reported represent pooled sex data. **Table 1** contains a concise summary of statistically significant findings.

Results

Genetically heterogeneous HET3 mice were assigned to either young or old controls. CR, ACA, 17aE2, and Rapa treatment began at 4 months of age with the exception of 17aE2 mice which were placed on 17aE2-treatment diet at 9 months of age (**Figure 2-1A**).

Lifespan extension drugs and adiposity

With age, the changes in rodent and human adipose tissue distribution and mass lead to an age-associated form of obesity [49,112,115,116]. HET3 mice steadily gain weight with advancing age, and we had previously observed that HET3 mice undergo age-related weight decline beginning at approximately 18 months of age [143,148]. Similar to reports in human aging [115,116,156], advanced stages of aging in HET3 mice are characterized by a decline in body weight, and this was clearly present in males and to a lesser extent in females [145]. In this current study, we report HET3 mice weights at 22 months of age, a time point that likely reflects a 4-month period of age-related decline in

body mass. Consistent with previous studies, old control females (34.7 ± 1.71 g) weigh more than young control females (24.1 ± 0.6 g; $p<0.001$), while there are no significant differences in average body mass between old (36.0 ± 2.1 g) and young (37.1 ± 1.1 g) control males (**Figure 2-1B**).

In CR mice, interaction between sex and treatment on body mass is significant ($p<0.01$). Old CR females have body masses (22.9 ± 0.4 g) similar to their young counterparts and weigh less than old control females (34.7 ± 1.7 g; $p<0.0001$) (**Figure 2-1B**). The age-associated loss of fat in old control males (36.0 ± 2.1 g) may be why these mice are statistically indistinct from old CR males (33.2 ± 1.5 g) in body mass. Consistent with our previous study [145], 17aE2-treated HET3 mice of both sexes have no significant body mass differences at 22 months of age. ACA-treated mice also do not have changes to body mass when compared to old controls. However, we have previously observed that ACA-treated females developed smaller body masses than old control females [145], therefore interpretation of this data should take this into account. In another study, when Rapa treatment was administered beginning at 9 months of age, we observed trends of smaller body weights at the highest dosage (42 ppm) while moderate dosage (14 ppm) induced no significant body weight changes in either sex [143]. In this current study, we observe that when Rapa treatment is prescribed at 4 months of age at the moderate dosage, by 22 months, total body mass of Rapa-treated female and male mice (39.1 ± 1.1 g) is significantly higher than old controls (35.2 ± 1.3 g; $p<0.05$).

We next compared the masses of gonadal white adipose tissue (gWAT) from each mouse (**Figure 2-1B**). The interaction between age and gender is significant for gWAT mass ($p<0.01$), indicating that at 22 months, gWAT fat pads are different between the two sexes. Consistent with reported aging trends on visceral fat mass gain in humans [49,116] and rodents [113,157], old female mice (2.4 ± 0.4 g) have larger gWAT pads than young females (0.7 ± 0.1 g; $p<0.0001$). We observe no significant mass difference between young (1.4 ± 0.1 g) and old (1.3 ± 0.2 g) male fat pads. Without gWAT measurements at 12 and 18 months of age, we are unable to conclude whether male gWATs amassed differently with age than females or if their age-related decline in total body weight

A

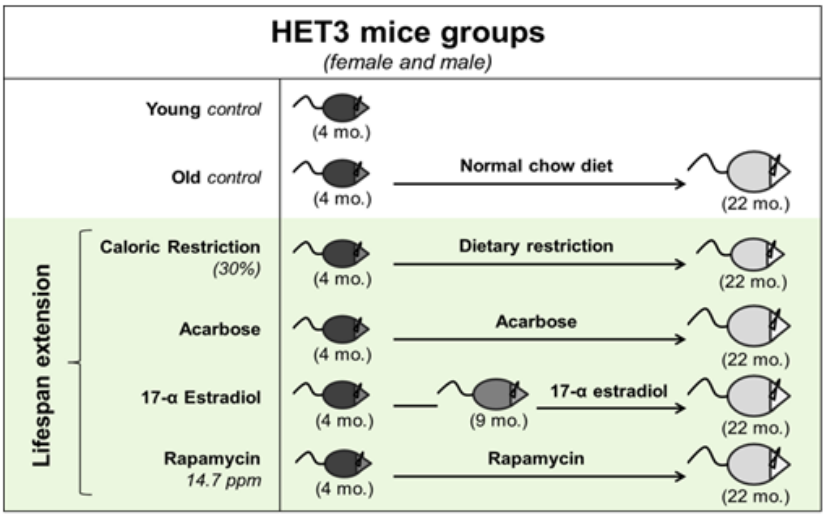

B

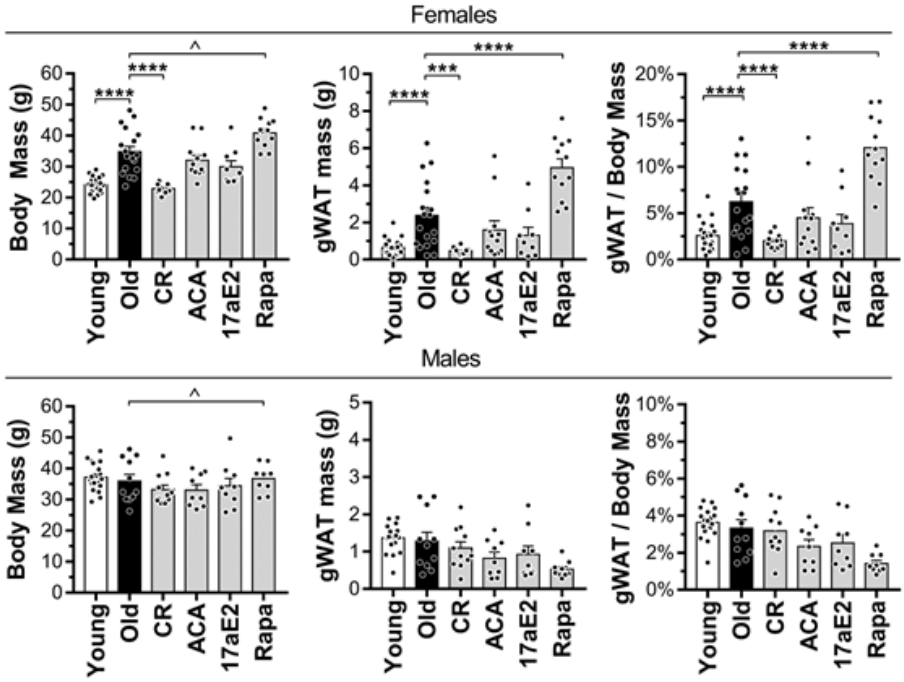

Figure 2-1 – ITP drug interventions differentially influence gWAT and body mass ratio of HET3 mice. A) HET3 mice in drug-intervention timeline. All mice were analyzed at 22 months of age except for young controls which were 4 months of age. **B**) Total body mass and gWAT mass (1 fat pad per mouse) were measured, and gWAT to body mass ratios were calculated. n=9-19 per group of mice. Error bars are SEM. 2-way-ANOVA, Sidak's multiple comparison's post hoc test (* p<0.05, ** p<0.01, *** p<0.001, **** p<0.0001). If no sex effect was significant, sexes were pooled for analyses with either Student's unpaired T-test (^ p<0.05, ^^ p<0.01, ^^^ p<0.001, ^^^^ p<0.0001) or by Mann-Whitney if normality tests failed, ($^{\#}$ p<0.05, $^{\#\#}$ p<0.01, $^{\#\#\#}$ p<0.001, $^{\#\#\#\#}$ p<0.0001).

heavily stems from gWAT mass loss. There is a significant interaction between sex and CR in gWAT mass ($p<0.05$). CR female mice (0.5 ± 0.1 g) develop smaller fat pads than old non-CR females (2.4 ± 0.4 g; $p<0.0001$), shifting them towards sizes similar to young females (0.7 ± 0.1 g). ACA- and 17aE2-treated mice have a modest decline in fat pad sizes that did not reach statistical significance (**Appendix 1**). In contrast, Rapa-treated female mice (5.0 ± 0.5 g) have a substantial increase in their fat pad masses compared to controls (2.4 ± 0.4 g; $p<0.001$), while Rapa-treated male mice (0.5 ± 0.1 g) are on average lower than controls (1.3 ± 0.2 g, N.S.). Given this difference, interaction between sex and Rapa-treatment is highly significant ($p<0.0001$).

To account for body mass differences, we also calculated the fat pad to body mass ratio for each mouse (**Figure 2-1B**). In congruence with the fat pad and body mass analysis, this ratio is significantly increased between young (2.6 ± 0.4 %) and old (6.2 ± 0.9 %; $p<0.0001$) females and not between young (3.6 ± 0.2 %) and old (3.3 ± 0.5 %) males. CR treatment in female mice (2.0 ± 0.2 %) lead to smaller fat pad to body ratio than controls (6.2 ± 0.9 %; $p<0.001$), while ITP drugs ACA and 17aE2 do not affect either sex. In contrast, Rapa-treated female mice (12.1 ± 1.0 %) have an increase to their gWAT to body-mass ratio compared to controls (6.2 ± 0.9 %; $p<0.0001$). This indicates in females, Rapa-treatment leads to gonadal fat pad expansion well-beyond the age-related fat mass gain observed in old female controls. Interestingly, while Rapa-treated female mice have a ~95% increase in gWAT to body mass ratio, Rapa-treated male mice (1.4 ± 0.2 %) have a ~58% decrease from old control males' gWAT to body mass ratio (3.3 ± 0.5 %, N.S.).

SVF density in gWAT is altered by certain ITP drugs

To study the immune composition of the gWAT, we first separated the stromal vascular fraction (SVF) cells of the gWAT from the adipocyte fraction. We have previously reported in C57BL/6J mice, there were increased gWAT SVF cells in old males (22 mo.) compared to young males (6 mo.) [89]. Here, we observe a significant effect of age in the gWAT SVF cell numbers of female HET3 mice ($p<0.05$). Old females ($4.0 \times 10^6 \pm 0.6 \times 10^6$ cells) have significantly higher total SVF count than young

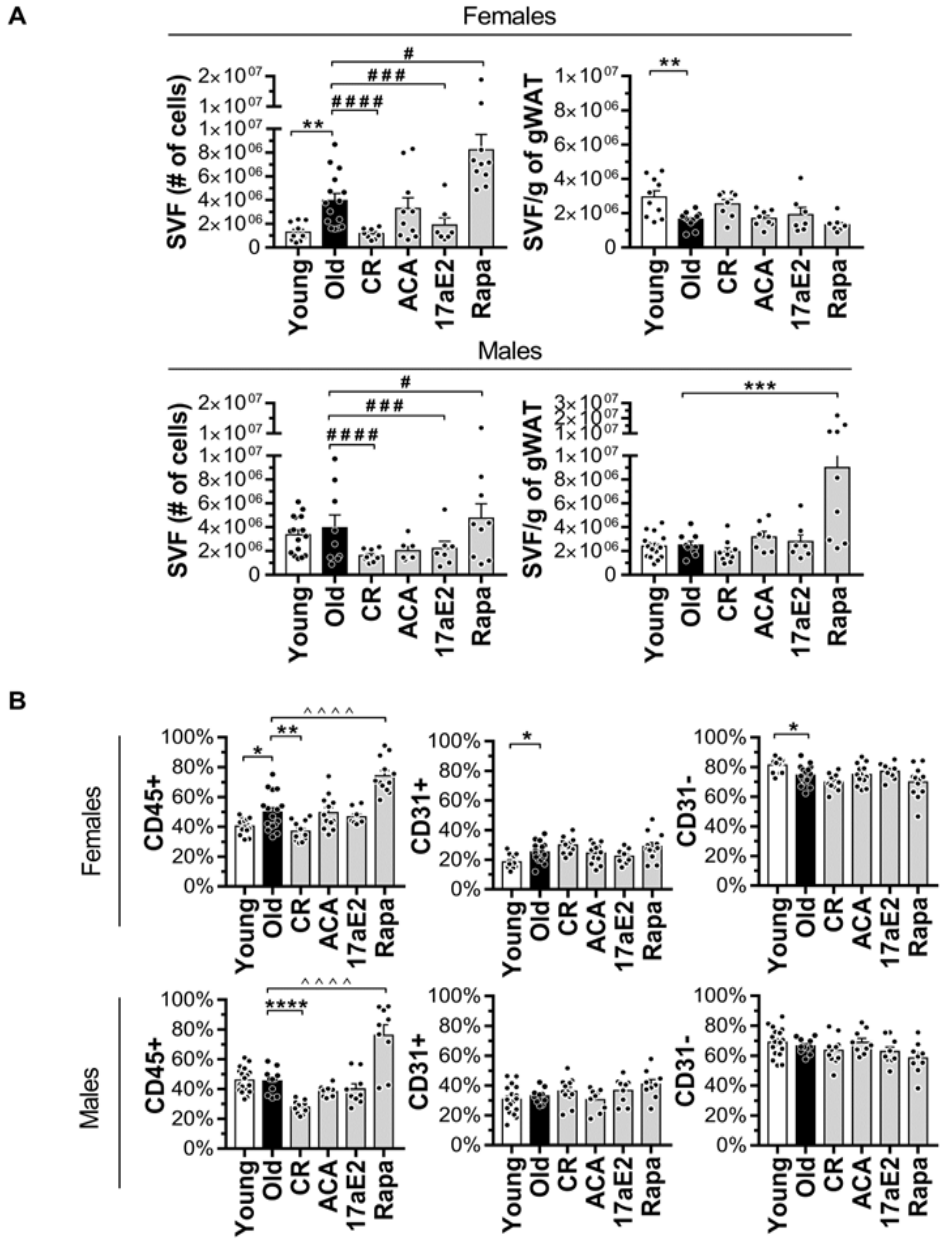

Figure 2-2 – CR and Rapamycin alter gWAT cell density and CD45+ leukocyte frequencies differently. A) Stromal vascular fraction (SVF) total cell numbers are reported for each mouse, separated by sex. n=9-19 per group of mice. On the right, SVF cell counts are normalized to each mouse's gWAT mass which provides a cell density value as number of cells per 1 gram of gWAT. **B**) Flow cytometry of gWAT leukocytes, endothelial cells, and cells enriched for ATSCs. n=9-19 per group of mice. CD45+ leukocyte frequency is reported as a percentage of the singlets gate, CD31+ endothelial cells and CD31- ATSC-enriched cells are reported as a percentage of the parent population CD45- cells. Error bars are SEM. 2-way-ANOVA, Sidak's multiple comparison's post hoc test (* p<0.05, ** p<0.01, *** p<0.001, **** p<0.0001). If no sex effect was significant, sexes were pooled for analyses with either Student's unpaired T-test (^ p<0.05, ^^ p<0.01, ^^^ p<0.001, ^^^^ p<0.0001) or by Mann-Whitney if normality test failed, ($^{\#}$ p<0.05, $^{\#\#}$ p<0.01, $^{\#\#\#}$ p<0.001, $^{\#\#\#\#}$ p<0.0001).

females ($1.3 \times 10^6 \pm 0.4 \times 10^6$ cells /mouse; $p<0.001$) (**Figure 2-2A**). CR mice ($1.4 \times 10^6 \pm 0.1 \times 10^6$ cells) and 17aE2-treated mice ($1.6 \times 10^6 \pm 0.4 \times 10^6$ cells) have lower SVF count than old controls ($4.0 \times 10^6 \pm 0.5 \times 10^6$ cells; CR: $p<0.0001$, 17aE2: $p<0.001$). Rapa-treatment significantly increases total SVF in both sexes ($6.6 \times 10^6 \pm 1.0 \times 10^6$ cells; $p<0.05$) (**Figure 2-2A**). Interestingly, CR- and 17aE2-treated mice have trends of shifting the SVF count down while Rapa-treatment appears to increase these cells in both sexes.

To ask whether the density of SVF cells changes with age or ITP drug treatment, we normalized the total SVF cells per gram of gWAT mass in individual mice (**Figure 2-2A**). The density of gWAT SVF cells is sex- and age-dependent (interaction, $p<0.05$). Old females ($1.6 \times 10^6 \pm 0.1 \times 10^6$ cells/g gWAT) have a significant decrease of gWAT SVF cell density compared to young females ($2.9 \times 10^6 \pm 0.4 \times 10^6$ cells/g gWAT; $p<0.01$). CR and ITP drugs ACA and 17aE2 do not alter SVF density. Rapa-treated males ($4.8 \times 10^6 \pm 1.2 \times 10^6$ cells/g gWAT) have significantly increased SVF density compared to control males ($3.9 \times 10^6 \pm 1.1 \times 10^6$ cells/g gWAT; $p<0.001$).

gWAT SVF Immune Compartment

The gWAT SVF cells that remain post-collagenase digestion contain preadipocytes, endothelial cells, immune cells, and other non-fat cells [72,89]. In humans and rodents, there is some evidence supporting the notion that SVF produces more proinflammatory mediators than adipocytes [89], which are known to also secrete adipokines and also contribute to inflammation [72]. In this study, we observe an increase of CD45+ leukocytes in the gWAT of old females (49.8 ± 3.0 %) compared to young females (40.4 ± 1.7 %; $p<0.05$), and no changes were noted between old (45.4 ± 2.5 %) and young (46.1 ± 2.0 %) males (**Figure 2-2B**). CR affects leukocyte frequency in a sex-dependent manner ($p<0.05$) and leads to 26% and 38% decreased leukocyte frequencies in females (37.1 ± 2.0 %; $p<0.01$) and males (28.0 ± 1.3 %; $p<0.0001$) respectively. ACA and 17aE2 do not alter leukocyte frequencies in either sex. When compared to old control mice (48.1 ± 2.1 %), Rapa-treated mice of both sexes have a substantial increase in CD45+ leukocytes (75.1 ± 3.5 %; $p<0.0001$). We next analyze CD45- CD31+ endothelial cell numbers and find no overall differences, although old females (25.3 ± 1.6

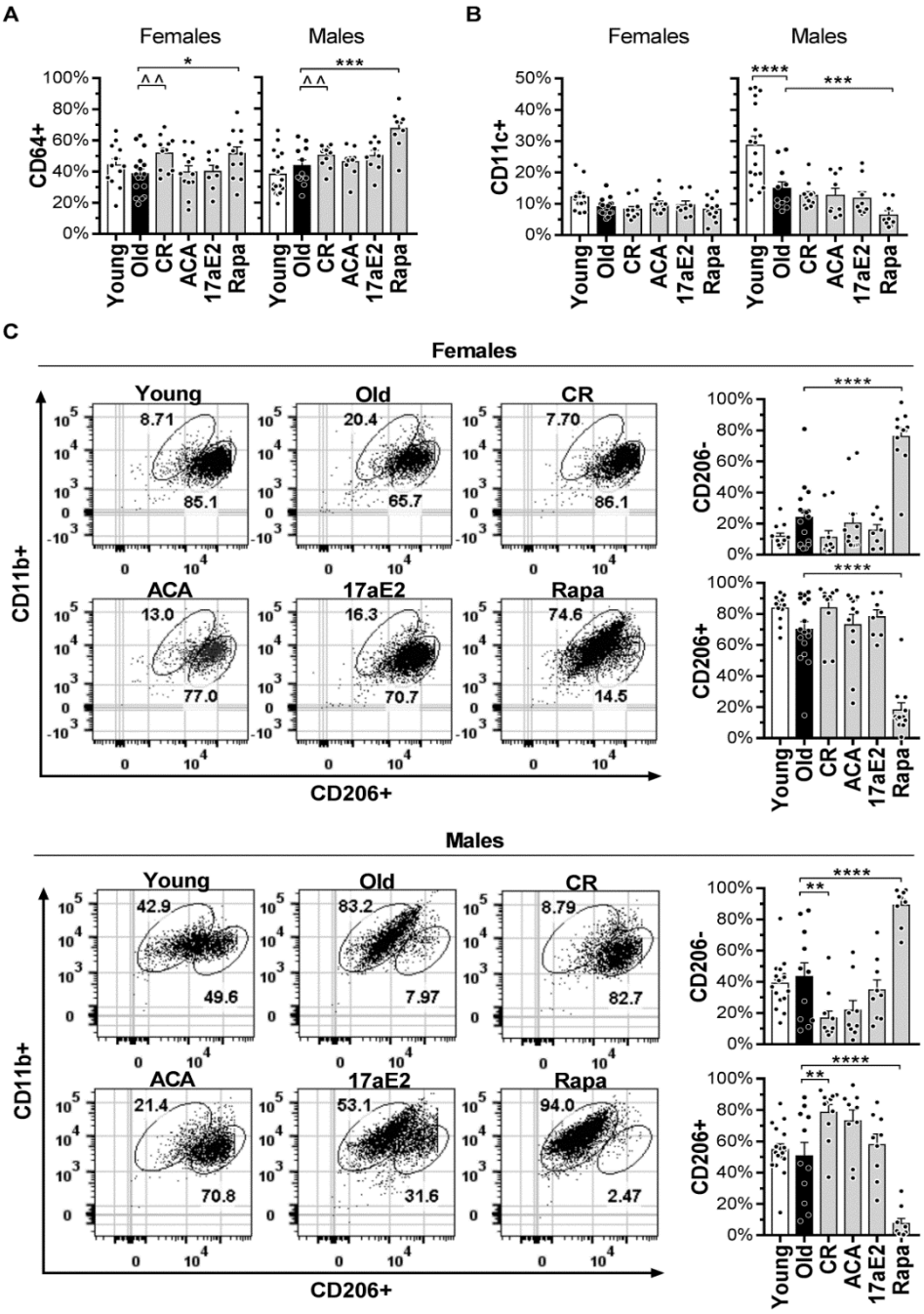

Figure 2-3 – Lifespan extension drugs affect adipose tissue macrophage polarization. Flow cytometry of gWAT **A**) macrophages (CD45+CD64+) reported and **B**) dendritic cells (CD45+CD64-CD11c+). n=9-19 per group and sex. **C**) Representative flow panel, n=2 per group and sex. Gates: (y-axis) singlets > CD45+ > CD64+ > CD11b+ and CD206+ (x-axis). "M1" (CD45+CD64+CD11b+CD206-) and "M2" (CD45+ CD64+ CD11b+ CD206+) macrophages reported as a % of CD45+ CD64+ cells. Error bars are SEM. 2-way-ANOVA, Sidak's multiple comparison's post hoc test (* p<0.05, ** p<0.01, *** p<0.001, **** p<0.0001). If no sex effect was significant, sexes were pooled for analyses with either Student's unpaired T-test (^ p<0.05, ^^ p<0.01, ^^^ p<0.001, ^^^^ p<0.0001) or by Mann-Whitney if normality test failed, ($^{\#}$ p<0.05, $^{\#\#}$ p<0.01, $^{\#\#\#}$ p<0.001, $^{\#\#\#\#}$ p<0.0001).

%) have a modest increase compared to young cohorts (18.4 ± 1.4 %; $p<0.05$). CD45-CD31- cells are analyzed as cells enriched for adipose tissue stem cells (ATSCs), but it appears none of the ITP drugs alter this compartment significantly.

ITP drugs' effect on adipose tissue macrophages

Adipose tissue macrophages (ATMs) play a considerable role in adipose tissue inflammation [89]. Many studies of ATMs in mice have used markers such as CD11b and F4/80, which also identifies subsets of dendritic cells and eosinophils. In an effort to disentangle these overlaps, the Immunological Genome Project identified a core murine macrophage marker, FcγR1 (CD64) [158]. It has been shown that $CD45^+CD64^+$ is specific for ATMs not only in C57Bl/6J male mice gWAT but also in human omental and subcutaneous adipose tissues [159]. In our data, there is no effect of aging on $CD45^+CD64^+$ ATM frequencies in either sex (**Figure 2-3A**)—similar to what we have previously reported in young (6 mo.) and old (22 mo.) C57BL/6J male mice [89]. CR mice of both sexes (51.0 ± 1.9 %) have a significant increase in ATM frequency compared to controls (40.5 ± 2.4 %; $p<0.01$). Neither ACA nor 17aE2 alters the frequency of total ATMs. There is a sex difference with Rapa-treatment effects on total ATM frequency ($p<0.05$). Rapa-treated females (51.4 ± 4.4 %) have a 33% increase in ATM frequency compared to old females (38.6 ± 3.2 %; $p<0.05$), whereas Rapa-treated males (67.3 ± 4.3 %) have a 55% increase compared to old males (43.5 ± 3.8 %; $p<0.001$). Rapamycin significantly increases the proportion of CD64+ cells sufficient to account for the increase in total CD45+ cells in mice treated with this drug (**Figure 2-3A, 2-4A**). We observe a sex- and age-dependent (interaction $p<0.05$) decrease of $CD45^+CD64^-CD11c^+$ dendritic cells (DCs) in old males (14.9 ± 0.6 %) compared to young males (28.6 ± 2.9 %; $p<0.0001$) (**Figure 2-3B**). Of the three ITP drugs we test, only Rapa (6.4 ± 1.3 %) alters these DCs in males—shrinking this population by 57% when compared with old controls ($p<0.001$).

In aged mice, ATMs shift towards M1-polarized "pro-inflammatory" macrophages, away from M2-polarized "anti-inflammatory" macrophages [89]. We observe a significant sex difference in age-associated ATM phenotypic switch in HET3 mice (**Figure 2-3C, Appendix 1**). These sex effects are present in both

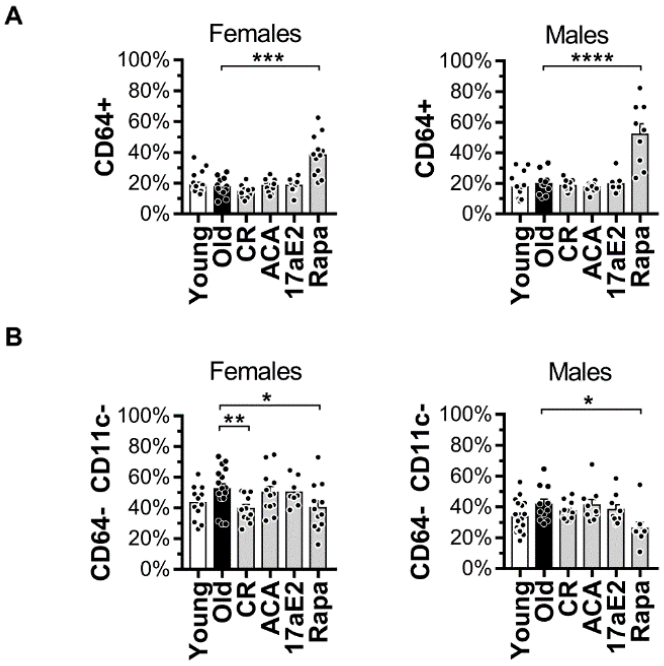

Figure 2-4 –A) Flow cytometry frequency of gWAT CD64+ cells expressed as a percentage of singlets in HET3 female and male mice, n=9-19 per group and sex. **B**) Flow cytometry frequency of gWAT non-macrophage, non-DC leukocytes (CD64-CD11c-) as a percentage of total CD45+ cells. Error bars are SEM. 2-way-ANOVA, Sidak's multiple comparison's post hoc test (* $p<0.05$, ** $p<0.01$, *** $p<0.001$, **** $p<0.0001$).

$CD45^+CD64^+CD206^-$ "M1" ATM frequencies ($p<0.0001$) and $CD45^+CD64^+CD206^+$ "M2" ATM frequencies ($p<0.0001$). CR yield significant and modest sex effects on M1 and M2 ATM frequencies ($p<0.05$ and $p<0.05$) as well.

M1 Adipose tissue macrophages

Old females (24.0 ± 4.8 %) have a 103% increase in M1 ATMs compared to young females (11.8 ± 2.1 %, N.S.), and old males (43.4 ± 8.8 %) have an 11% increase of M1 ATMs compared to young males (39.0 ± 3.5%, N.S.) (**Figure 2-3C**). M1 ATMs in CR females (11.2 ± 4.2 %) decreases by 53% compared to old females (N.S.), and CR-male mice (16.7 ± 4.5 %) have a 62% decrease in M1 ATMs compared to old males ($p<0.01$). ACA and 17aE2 treated mice have M1/M2 shifts similar to CR, though Sidak's multiple comparisons do not identify any significant changes in either sex. In contrast, Rapa treatment leads to substantial increases to M1 macrophages in both

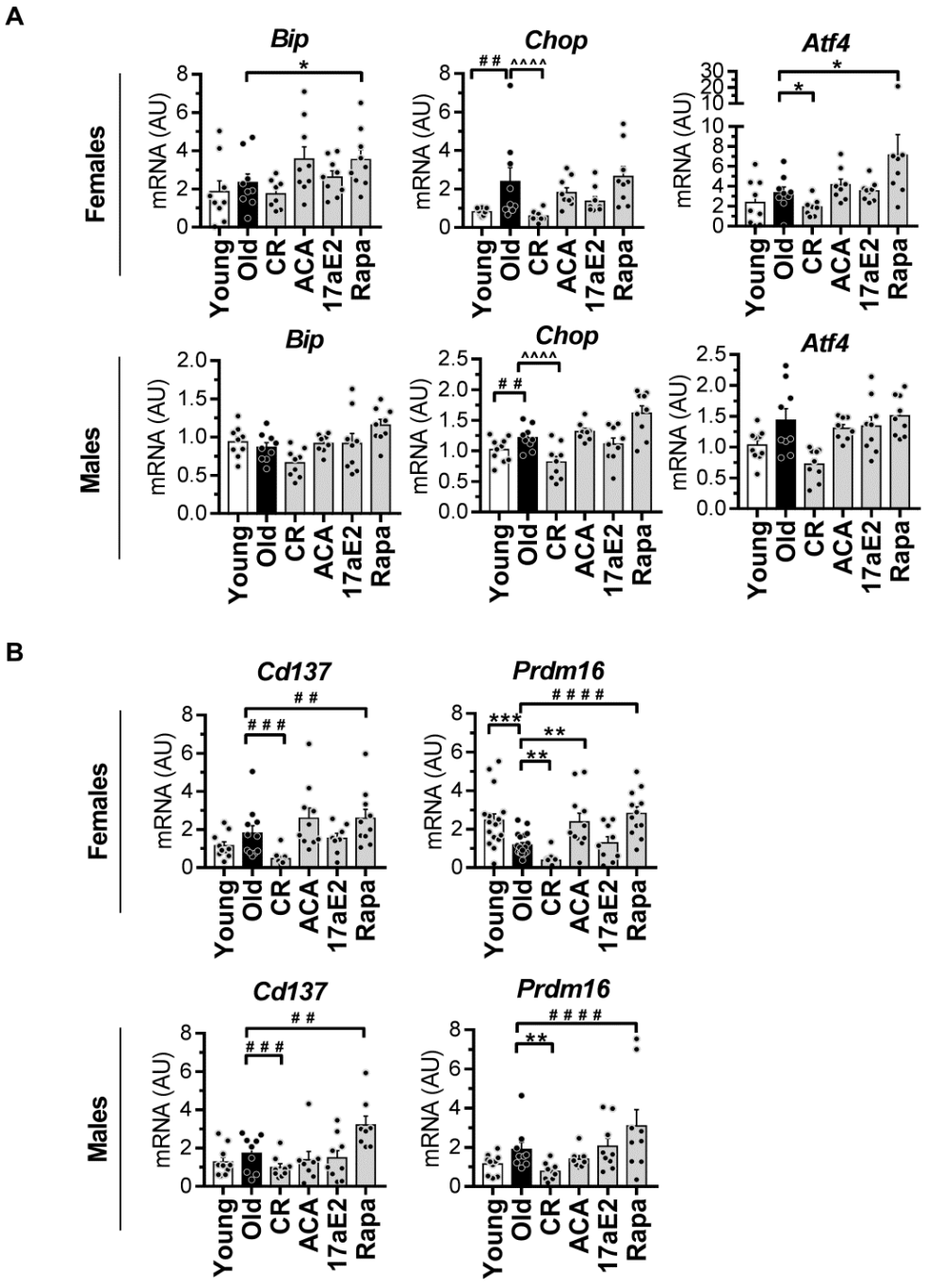

Figure 2-5 – Expression of **A**) ER stress genes (*Bip, Chop, Atf4*) and **B**) brite markers (*Cd137* and *Prdm16*) in gWAT, Error bars are SEM. 2-way-ANOVA, Sidak's multiple comparison's post hoc test (* p<0.05, ** p<0.01, *** p<0.001, **** p<0.0001). If no sex effect was significant, sexes were pooled. Student's unpaired T-test (^ p<0.05, ^^ p<0.01, ^^^ p<0.001, ^^^^ p<0.0001) or by Mann-Whitney if normality test failed, ($^{\#}$ p<0.05, $^{\#\#}$ p<0.01, $^{\#\#\#}$ p<0.001, $^{\#\#\#\#}$ p<0.0001). n=9-19 per group and sex and each sample was normalized to *Gapdh*.

sexes (**Figure 2-3C**) and modest sex differences in M1/M2 ATMs ($p<0.05$, **Appendix 1**). Rapa-treated females (76.1 ± 5.3 %) have a 217% increase of M1-polarized ATMs compared to old controls ($p<0.0001$), and similarly but to a lesser extent, Rapa-treated males (89.2 ± 3.9 %) have a 106% increase to their M1 ATM population ($p<0.0001$).

M2 Adipose tissue macrophages

Naturally, the shifts in M1-polarization ($CD206^-$ ATMs) have a proportional switch in M2-polarization ($CD206^+$ ATMs) in these mice (**Figure 2-3C**). Old females (70.0 ± 5.0 %) have a 17% decrease of M2 ATMs compared to young females (83.8 ± 2.5 %; N.S.), whereas old males (50.5 ± 8.8 %) have an 8% decrease of M2 ATMs compared to young males (54.7 ± 3.6%; N.S.). CR increases M2 ATMs 20% compared to old females (83.8 ± 5.3 %; N.S.) and 55% M2 ATMs compared to old males (78.4 ± 5.0 %; $p<0.01$). Compared to old controls, Rapa-treated females (18.1 ± 4.6 %) have a 74% decrease of M2-polarized ATMs ($p<0.0001$), and Rapa-treated males (7.5 ± 3.2 %) have an 85% decrease to their M1 ATM population ($p<0.0001$). In addition, Rapa-treated mice have a 24% and 37% decrease in frequency of non-macrophage and non-dendritic cell leukocytes (T and B lymphocytes, eosinophils, etc.) that were $CD45^+CD64^-CD11c^-$ in females ($p<0.05$) and males ($p<0.05$) respectively (**Figure 2-4B**).

ER stress responses in gWAT contribute to adipose tissue inflammation in aging. To determine if ITP drugs modify adipose tissue ER stress, we evaluate mRNA for *Bip, Atf4,* and *Chop* (**Figure 2-5A**). Old control mice of both sexes (1.8 ± 0.4 AU) have increased *Chop* compared to young controls (1.2 ± 0.3 AU; $p<0.01$). CR improves ER stress responses in old HET3 mice: *Chop* is significantly reduced in both sexes (0.7 ± 0.1 AU; $p<0.0001$). CR females (1.9 ± 0.3 AU) also have significantly decreased *Atf4* compared to old controls (3.3 ± 0.6 AU; $p<0.05$). ITP drugs ACA and 17aE2 do not appear to affect lifespan extension through ER-stress in the adipose tissue. Whereas, Rapa-treated females (3.5 ± 0.5 AU) have an increase in *Bip* compared to old females (2.3 ± 0.5 AU; $p<0.05$), and Rapa-treated females (9.6 ± 3.0 AU) also have an increase in *Atf4* compared to old females ($p<0.05$). Overall, we conclude ITP drugs we tested do not alter ER stress in gWAT, with the possible exception of Rapa treatment in females.

It has been postulated that age-related declines in browning and beiging adipose tissue activity in humans [160] and rodents [161,162] are contributing factors to age-related adiposity. To test if 1) old HET3 mice have an effect of age on gWAT thermogenic factors and whether or not 2) any ITP drugs modulated them, we measured mRNA of beige or "brite" (browning of WAT) markers in unstimulated whole gWAT (**Figure 2-5B**). We measure *CD137*, a beige-selective marker [162] and zinc finger protein PR domain containing 16 (*Prdm16*) which is crucial for browning of WAT [163]. CR leads to decreased *CD137* in both females and males (0.7 ± 0.1 AU) compared to old controls (1.8 ± 0.3 AU; $p<0.001$). Rapa leads to increased *CD137* expression (Rapa: 2.9 ± 0.3 AU, old: 1.8 ± 0.3 AU; $p<0.01$). Old females (1.2 ± 0.1 AU) have lower *Prdm16* than young females (2.5 ± 0.3 AU; $p<0.001$). CR decreases *Prdm16* in females (CR: 0.4 ± 0.1 AU, old: 1.2 ± 0.1 AU; $p<0.01$) and males (CR: 0.8 ± 0.1 AU, old: 1.9 ± 0.4; $p<0.01$). ACA-treated females (2.4 ± 0.4 AU) have a modest increase of *Prdm16* compared to old females (1.2 ± 0.1 AU; $p<0.01$). Rapa-treated mice increases *Prdm16* in both females and males (Rapa: 2.9 ± 0.4 AU, old: 1.4 ± 0.2 AU; $p<0.0001$). The ITP drugs we tested appear to moderately affect the basal levels of thermogenic markers in gWAT, though it is likely the lifespan extension from these drugs are independent of these factors.

Accumulation of senescent cells in iWAT

Senescent cells accumulate in aging adipose tissue, particularly in the inguinal white adipose tissue (iWAT), and they play a role in determining lifespan and healthspan [123,124]. We measure *p16*, *p21*, and *p53* in the iWATs of HET3 mice (**Figure 2-6**) to assess if there is an effect of age on the accumulation of these senescent cells in these genetically heterogeneous mice. Both p16 and p21 are cell cycle inhibitors, and p53 is a primary tumor-suppressor pathway; these are important for the regulation of certain senescent states of cells [118,120,121,164]. Consistent with literature [123,124,165], we observe an age effect on senescent cell accumulation in iWAT (**Figure 2-6**). Old female mice have age-dependent increases of *p16* (young: 0.5 ± 0.1 AU, old: 2.5 ± 0.2 AU; $p<0.0001$) and

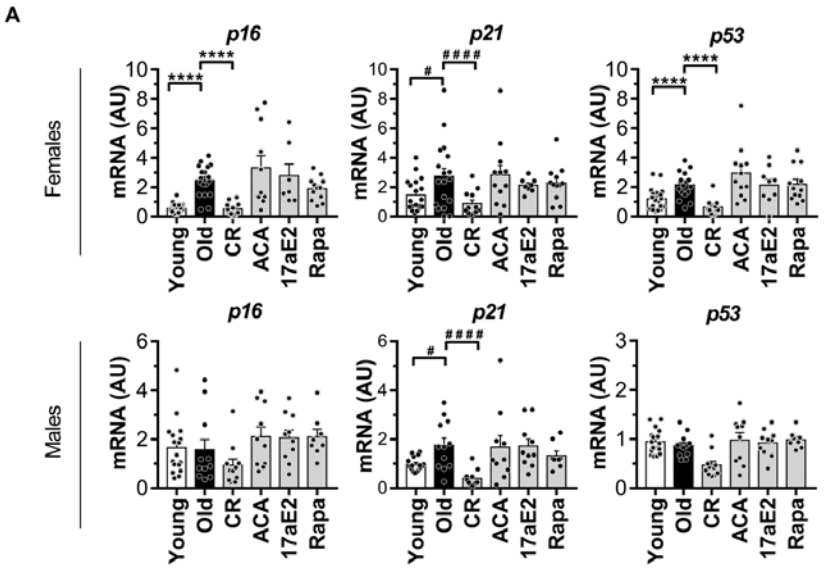

Figure 2-6 – Effect of aging on iWAT expression of senescent markers. Expression of senescence marker genes (*p16*, *p21*, and *p53*) in iWAT of HET3 mice. n=9-19 per group per sex. Each sample was normalized to *Gapdh*. Error bars are SEM. 2-way-ANOVA, Sidak's multiple comparison's post-hoc test (* $p<0.05$, ** $p<0.01$, *** $p<0.001$, **** $p<0.0001$). If no sex effect was significant, sexes were pooled for analyses with Mann-Whitney if normality test failed, ($^{\#}$ $p<0.05$, $^{\#\#}$ $p<0.01$, $^{\#\#\#}$ $p<0.001$, $^{\#\#\#\#}$ $p<0.0001$).

p53 (young: 1.2 ± 0.2 AU, old: 2.2 ± 0.2 AU; $p<0.0001$). Both old females and males (2.3 ± 0.4 AU) have an age-dependent increase of *p21* when compared to young controls (1.3 ± 0.1 AU; $p<0.05$). CR female mice (0.5 ± 0.1 AU) have significantly decreased *p16* compared to old females ($p<0.0001$), and CR females also have decreased *p53* (CR: 0.6 ± 0.2 AU, old: 2.2 ± 0.2 AU; $p<0.0001$), and CR mice of both sexes (0.7 ± 0.1 AU) also have decreased *p21* compared to old controls (2.3 ± 0.4 AU; $p<0.0001$) (**Figure 2-6**).

Discussion

The Interventions Testing Program within the National Institute of Aging is designed to identify treatments with the potential of lifespan extension and delaying disease and dysfunction in mice. The 3 drugs we elected to test in this study, rapamycin (Rapa), Acarbose (ACA), and 17α-estradiol (17aE2) have all been shown to extend lifespan in mice. ACA and 17aE2 primarily benefit males, whereas Rapa extends lifespan in both sexes. These 3 drugs have been shown to affect a multitude of health outcomes in HET3 mice [142,143,145,146,148,166–168]. However, the underlying mechanisms and organ-specific effects remain to be fully explored. How ITP drugs influence the aging processes and whether the different drugs influence lifespan through the same or different mechanisms are unclear.

Caloric restriction (CR) is the classic approach that increases lifespan in healthy mice and has been regarded as the standard intervention for mammalian lifespan extension. CR increases lifespan of HET3 mice by 32-47% [147]. Though not sufficient to completely explain CR-associated lifespan extension, it has been posited that CR may influence lifespan through the loss of fat mass[111]. Of note, the three ITP drugs we tested, Rapa, ACA, and 17aE2, have been associated with different metabolic outcomes in HET3 mice[143,169]. However, very little is known about the effects of these drugs on adipose tissue. Given the important role of adipose tissue inflammation on age-related diseases, we hypothesized that these drugs' effect on adipose tissue inflammation could be an important mechanism in lifespan extension.

Adipose tissue macrophages (ATMs) are the major contributors to inflammation and metabolic dysfunction in diet-induced obesity [51,61,63]. In age-related adiposity and metabolic syndrome, gWAT undergoes phenotypic switching from anti-inflammatory "M2" towards pro-inflammatory "M1" macrophage polarization [89]. Interestingly, our data demonstrate old control HET3 mice have the greatest variability in the immune profile. In particular, old control female mice separate into two groups—those with high- (~90%) and low- (50-70%) $CD206^+$ frequencies. Our data also suggest that only ~65% of old females develop a phenotypic switch from M2 to M1 with age. Therefore, even

though a majority (~65%) of old control females have a lower average M2 macrophage frequency than 4 other female groups in the study (young control, CR, ACA, and 17aE2), the average of old females include the minority high expressers, masking important interpretations to this data. We further postulate that CR and two ITP drugs, ACA and 17aE2, skew macrophage polarization towards M2 by preferentially targeting old mice that express low $CD206^+$ frequency. Similarly, old control male mice show a significant variation in ATM polarization.

In this study, we show that long-term dietary rapamycin fed to HET3 mice leads to significant M1 ATM polarization in the gWAT. Along these lines, we also observe that the increase in $CD45^+$ leukocytes in the adipose tissue of Rapa-treated mice is due to an increase in total macrophages ($CD45^+CD64^+$). Given the role of M1 ATMs in metabolic inflammation and diabetes, the observation is consistent with studies that have shown rapamycin induces glucose intolerance in old rats, old C57BL6/J mice, as well as old and young HET3 mice [143]. Additionally, female and male HET3 mice developed hypoglycemia with both short- and long-term dietary rapamycin, but insulin sensitivity remained intact in both young and old mice [142]. This is unexpected, given the known association drawn between the proinflammatory "M1" macrophage and insulin resistance in the young, diet-induced obesity context [170]. *In vitro*, Rapa-treatment induces a phenotype switch in macrophage cell-lines from M2- to M1-polarized and nearly eliminates CD206+ expression in primary human macrophages [171]. Our data is consistent with these studies—Rapa-treatment in HET3 mice strongly polarizes ATMs toward M1, significantly reducing the M2 macrophage compartment. Both ACA and 17aE2 treatments cause a trend of M2 polarization increase in old male mice, although the results do not reach statistical significance. This resonates with studies that have shown improved metabolic responses in male HET3 mice treated with ACA and 17aE2 [169]. In CR males, there is significantly higher M2 polarization than non-CR old males, and while this trend was also present in females, it did not reach statistical significance. Again, this aligns with the association of CR to improved metabolic responses [143].

When we assayed white adipose tissues for ER stress response genes (*Bip, Chop, Atf4*), beige/browning markers (*Cd137, Prdm16*), and senescent cell markers (*p16, p21, p53*), we find that the three ITP drugs we tested (Rapa, ACA, and 17aE2) did not substantially affect these aging adipose tissue phenotypes. As expected, CR mice strongly resist the effect of normal aging on these markers in adipose tissue. We previously reported old BL/6J male mice have increased gWAT ER stress responses when challenged with thapsigargin *ex vivo*, leading to enhanced release of pro-inflammatory cytokines and chemokines in SVF cells and ATMs. *In vivo,* we reduced the secretion of these pro-inflammatory factors from the gWAT SVF with a chemical chaperone [90,92]. In this current study, we find that *Chop* mRNA levels are increased in old controls while CR mice have reduced *Chop*. In contrast to the CR mice, Rapa-treated females have an increase in *Bip* and *Atf4* mRNA. Our data suggest that the three ITP drugs we tested do not facilitate lifespan extension through alterations on ER stress responses in aging adipose tissue. Although there are sex differences in gWAT browning and beiging marker expression, we did not detect a strong effect of age in the HET3 mice. We find that consistent with published literature [123,124], we detected higher number of senescent cells *p16, p21,* or *p53* in old HET mice inguinal WAT (iWAT). As expected, CR mice of both sexes have significantly lower senescent cell accumulation in iWAT. The three ITP drugs we tested did not alter the expression of senescent markers in the HET3 mice. Based on this data, we conclude that lifespan extending effect of the ITP drugs, Rapa, ACA, and 17aE2, is likely to be independent of senescent cells' accumulation in white adipose tissue.

An important limitation of our study is that we were only able to assay the HET3 mice at the 22-month time point. Male HET3 mice are shorter lived than their female counterparts, and weight loss has been a common phenomenon in male HET3 mice beginning at approximately 18 months of age [143,144,148]. Whereas, old female HET3 mice had displayed a much lesser extent of weight loss or weight loss appears to occur in the final few weeks of life [143,144,148]. Consistent with published data, we found that aging has an important effect on HET3 female mice adipose tissue inflammation. In contrast, the changes in the old male mice were less pronounced. The sex difference in old control

males in our study may therefore represent survival effects of the cohort. This may explain how old control males also have similar body weights as old CR males and young control males.

In summary, we found that CR and Rapa treatments influence aging adipose tissue inflammation differently. These observations add support to the notion that CR and Rapa treatments confer lifespan extension in distinct ways [143]. Our data also show ACA and 17aE2 generally did not influence any aspects of adipose tissue biology that we examined. Overall, this study indicates out of the 3 ITP drugs selected, only Rapa treatment affects adipose tissue inflammation, possibly exacerbating it, in both sexes of HET3 mice. Additional studies will need to be done to determine whether or not these Rapa-associated ATM changes directly contribute to lifespan extension. Future studies of adipose tissue biology of aging should take into account sex differences in age-related adiposity changes.

Table 1 – Summary of dietary-drug interventions effect on aging adipose tissue

Phenotype	Age Effect		CR		ACA		17aE2		Rapa	
	♀	♂	♀	♂	♀	♂	♀	♂	♀	♂
Body mass	↑	↔	↓	↔	↔	↔	↔	↔	↑	↑
gWAT mass	↑	↔	↓	↔	↔	↔	↔	↔	↑	↔
gWAT/body %	↑	↔	↓	↔	↔	↔	↔	↔	↑	↔
SVF cells	↑	↔	↓	↓	↔	↔	↓	↓	↑	↑
SVF/ 1 g gWAT	↓	↔	↔	↔	↔	↔	↔	↔	↔	↑
CD45+	↑	↔	↓	↓	↔	↔	↔	↔	↑	↑
CD45- CD31+	↑	↔	↔	↔	↔	↔	↔	↔	↔	↔
CD45- CD31-	↓	↔	↔	↔	↔	↔	↔	↔	↔	↔
CD45+ CD64+	↔	↔	↑	↑	↔	↔	↔	↔	↑	↑
CD45+ CD64- CD11c+	↔	↓	↔	↔	↔	↔	↔	↔	↔	↓
CD64+ CD206-	↔	↔	↔	↓	↔	↔	↔	↔	↑	↑
CD64+ CD206+	↔	↔	↔	↑	↔	↔	↔	↔	↓	↓
CD64- CD11c-	↔	↔	↓	↔	↔	↔	↔	↔	↓	↓
Bip	↔	↔	↔	↔	↔	↔	↔	↔	↑	↔
Chop	↑	↑	↓	↓	↔	↔	↔	↔	↔	↔
Atf4	↔	↔	↓	↔	↔	↔	↔	↔	↑	↔
Cd137	↔	↔	↓	↓	↔	↔	↔	↔	↑	↑
Prdm16	↓	↔	↓	↓	↑	↔	↔	↔	↑	↑
p16	↑	↔	↓	↔	↔	↔	↔	↔	↔	↔
p21	↑	↑	↓	↓	↔	↔	↔	↔	↔	↔
p53	↑	↔	↓	↔	↔	↔	↔	↔	↔	↔

Table 2 – Sequences for RT-PCR primers used in this chapter

Gene of Interest	Forward 5' → 3'	Reverse 5' → 3'
Bip	GAGACTGCTGAGGCGTATTT	CAGCATCTTTGGTTGCTTGTC
Chop	TCACACGCACATCCCAAA	CCTAGTTCTTCCTTGCTCTTCC
Atf4	CCACTCCAGAGCATTCCTTTAG	CTCCTTTACACATGGAGGGATTAG
p16	CATGTTGTTGAGGCTAGAGAGG	CACCGTAGTTGAGCAGAAGAG
p21	AAGTGTGCCGTTGTCTCTTC	AGTCAAAGTTCCACCGTTCTC
p53	GCCATGGCCATCTACAAGAA	AATTTCCTTCCACCCGGATAAG
Prdm16	GGGCCCTTGTAAACAACAAA	GTCGGTCCTTCCTTGGTGTA
Cd137	GCAGCCTGCAGGAACTTATC	CCATTTCTGTCCCTTTTCCA
Gapdh	AACAGCAACTCCCACTCTTC	CCTGTTGCTGTAGCCGTATT

Chapter 3 – Outbreak of murine infection with *Clostridium difficile* associated with the administration of a pre- and peri- natal methyl-donor diet

This chapter has been submitted and is under review for publication.

Theresa Mau, Samantha S. Eckley, Ingrid L. Bergin, Katie Saund, Jason S. Villano, Kimberly C. Vendrov, Evan S. Snitkin, Vincent B. Young, and Raymond Yung.

Abstract

Between October 2016 and June 2017, a C57BL6/J mouse colony that was undergoing a pre- and peri-natal methyl-donor supplementation diet intervention to study the impact of parental nutrition on offspring susceptibility to disease was found to suffer from an epizootic of unexpected deaths. Necropsy revealed the presence of severe colitis, and further investigation linked these outbreak deaths to a *Clostridium difficile* strain of ribotype 027 we term 16N203. *C. difficile* infection (CDI) is associated with antibiotic use in humans. Current murine models of CDI rely on antibiotic pretreatment to establish clinical phenotypes. In this report, the *C. difficile* outbreak occurs in F1 mice linked to alterations in the parental diet. The diagnosis of CDI in the affected mice was confirmed by cecal/colonic histopathology, presence of *C. difficile* bacteria in fecal/colonic culture, and detection of *C. difficile* toxins. F1 mice from parents fed the methyl-supplementation diet also had significantly reduced survival ($p<0.0001$) than F1 mice from parents fed the control diet. When we tested the 16N203 outbreak strain in an established mouse model of antibiotic-induced CDI, we confirmed that this strain is pathogenic. Our serendipitous observations from this spontaneous outbreak of *C. difficile* in association with a pre- and peri-natal methyl-donor diet suggest the important role diet may play in host defense and CDI risk factors.

Importance

Clostridium difficile infection (CDI) has become the leading cause of infectious diarrhea in hospitals worldwide, owing its preeminence to the emergence of hyperendemic strains, such as ribotype 027 (RT027). A major CDI risk factor is antibiotic exposure which alters gut microbiota, resulting in the loss of colonization resistance. Current murine models of CDI also depend on pretreatment of antibiotics of animals to establish disease. The outbreak we report here is unique in that the CDI occurred in mice with no antibiotic exposure and is associated with a pre- and peri-natal methyl-supplementation donor diet intervention study. Our investigation subsequently reveals that the outbreak strain we term 16N203 is an RT027 strain, and this isolated strain is also pathogenic in an established murine model of CDI (with antibiotics). Our report of this spontaneous outbreak offers additional insight into the importance of environmental factors, such as diet, and CDI susceptibility.

Introduction

Clostridium difficile is a spore-forming, gram positive obligate anaerobe that has become the leading cause of infectious diarrhea in hospitals worldwide. On a yearly basis, nearly half a million cases of *Clostridium difficile* infection (CDI) are reported in the United States (US), with an approximated 29,000 CDI-related deaths [172]. Exposure to *C. difficile* can have varied outcomes ranging from asymptomatic intestinal colonization, to severe diarrhea, development of pseudomembranous colitis, and death [40]. CDI risk is associated with disruption of the gut microbiota, for example following antibiotic administration [39–41], that leads to a loss of resistance towards *C. difficile* colonization.

Following spore germination and establishment of the vegetative form of *C. difficile,* disease results from the production of the large clostridial toxins TcdA and TcdB [173]. These enterotoxins inactivate small GTPases [174–177] (e.g. Rho, Rac, Cdc42) and lead to the rearrangement of the actin cytoskeleton of intestinal epithelial cells. Consequently, mucosal epithelium damage ensues from cellular apoptosis [178] and the induction of colitis via toxin-mediated inflammation. In humans, the increasing clinical

presence of *C. difficile* epidemic strains in the US and West Europe [179] is attributed to antibiotic-use and the rise of endemic strains such as NAP1/027/BI. Ribotype 027 (RT027) strains produce higher quantities of TcdA and TcdB [180] and express an additional *C. difficile* transferase (CDT) binary toxin encoded by *cdtA/cdtB* [181]. The binary toxin also disrupts the cytoskeleton and increases bacterial adhesion to intestinal epithelial cells [182]. The exact role of CDT in *C. difficile* virulence remains undefined, but it has been suggested that CDT plays a significant role in worsened clinical patient outcomes [183] and increases of CDI recurrence [184].

Mouse models have been developed to study the pathogenesis of CDI. These models generally require administration of antibiotics to disrupt the microbiota prior to *C. difficile* exposure. A number of antibiotic regimens have been employed to render animals susceptible to CDI [185–187]. The importance of the indigenous microbiota in mediating colonization resistance against CDI is highlighted by the fact that germ free animals are inherently sensitive to colonization and disease when exposed to *C. difficile* [188].

Here, we report a spontaneous outbreak of *C. difficile* due to a strain of RT027 that occurred in a mouse colony that was associated with the administration of a specific pre- and peri-natal diet. Given that CDI mouse models typically rely on prior gut microbiota disruption via antibiotics to establish disease [189], this outbreak is unique in that it occurred in the absence of antibiotic use and instead, in association with an altered diet.

Materials and Methods

Animals

The animal care and use program at the University of Michigan is AAALAC-accredited. All procedures involving the animals and their care were approved by the University of Michigan Institutional Animal Care and Use Committee. Mice were housed in autoclaved positive-pressure individually-ventilated cages (P/NV IVC, Allentown, Allentown, NJ) with corncob bedding (The Andersons, Frontier) and provided with

reverse osmosis-deionized (RO/DI) water through automated water systems (Edstrom; Waterford, WI). Animal housing rooms were maintained on a 12:12-h light:dark cycle, relative humidity of 30-70%, and temperature of 72 ± 2°F (22.2 ± 1.1°C). For specific-pathogen free (SPF) rooms, cage changing and experimental procedures were performed under a laminar flow cage change station (AniGARD® VF, Baker Company, Sanford, ME) or in laminar flow benches, using a cold sterilant (Spor-Klenz®, Steris, St Loius, MO) for disinfecting gloved hands or transfer forceps. For biocontainment rooms (animal biosafety level 2), procedures were performed under a biosafety cabinet (SterilGARD®, Baker Company, Sanford, ME) using a sporicidal disinfectant cleaner (Perisept, Triple S 48027). Health surveillance program for SPF colonies included quarterly testing of dedicated soiled-bedding sentinel animals via fecal and perianal swab PCR or serology, and PCR of exhaust plenum swabs for fur mites. Health surveillance results indicated that the mice were negative for mouse rotavirus, mouse hepatitis virus, minute virus of mice, ectromelia virus, Theiler mouse encephalomyelitis virus, lymphocytic choriomeningitis virus, mouse adenovirus, mouse parvovirus, mouse polyoma virus, pneumonia virus of mice, reovirus, Sendai virus, *Mycoplasma pulmonis*, pinworms (*Syphacia* spp. and *Aspicularis* spp.) and fur mites (*Myobia musculi*, *Myocoptes musculinis*, and *Radfordia affinis*).

Dietary Study

In the initial dietary study, young adult (8 wk) C57Bl/6 mice were purchased from Jackson Laboratories. All custom diets "TD" are produced and distributed by Harlan-Teklad (Madison, WI). Mice were acclimated for 2 weeks before feeding either control (TD.06689) or methyl-donor supplementation (MS) diet (TD.110144). The MS diet contained 12g/kg methionine, 16.5 g/kg choline, 15 g/kg betaine, 16.5 mg/kg folic acid, 1.56 mg/kg vitamin B12, and 200 mg/kg Zn. Two weeks after starting diet, female and male mice were paired for mating. Mated F0 mice were fed the diet throughout pregnancy and lactation. F1 mice were weaned at 28 days. The F1 mice were then placed on a standard chow diet (PicoLab Laboratory Rodent Diet 5L0D, LabDiet, St. Louis, MO) or a 42% high-fat diet (HFD) (TD.88137).

Outbreak necropsy and assessment

Dead or clinically affected animals were detected during routine daily health checks. Veterinary staff assessed for any clinical sign of gastrointestinal or systemic disease, such as diarrhea, lethargy or unkempt appearance, and euthanized animals via CO_2 inhalation followed by induction of bilateral pneumothorax. Complete necropsy was performed with select tissues processed for histologic examination.

Fecal PCR of selected mice in the colony was performed by a commercial laboratory (Charles River Laboratories, Wilmington, MA) to confirm SPF status. Fecal and/or cecum and colonic samples were submitted for ELISA for *C. perfringens* type A toxin and *C. difficile* toxins A and B (Veterinary Diagnostic Laboratory, Michigan State University, Lansing, MI) or for real-time fluorogenic PCR for *C. difficile* targeting the 23S rRNA gene (Charles River Laboratories, Wilmington, MA). Cecum and colon tissues as well as tissues from other organs were fixed in 10% neutral buffered formalin for a minimum of 24 hours and then routinely processed to paraffin, sectioned, and stained with hematoxylin and eosin by the University of Michigan In Vivo Animal Core (IVAC) histology laboratory. A board-certified veterinary pathologist blinded to the diet groups evaluated the tissues descriptively in the initial outbreak and subsequently performed severity scoring of cecal and colonic tissues according to our previously published scoring system for experimentally-induced *C. difficile*-associated typhlitis and colitis [189]. In brief, slides were evaluated on a 0-4 scale for the individual parameters of edema, inflammation, and epithelial damage and an overall severity score was generated by summing these parameters (scale 0-12).

To investigate the outbreak source and the extent of contamination, environmental and fecal pellet PCR was performed as described above. Swabs were taken from various areas including cardboard rolls collected for mouse enrichment and the interior of the respective collection bins and supply and exhaust plenums of four autoclaved racks. Within the ABSL2 room, door knobs, biosafety cabinet used for changing cages, clean lixits, and rack supply ducts connected to the building ventilation system were sampled. Each PCR sample tested for the affected mouse colony comprised of pooled fecal pellets

(a fecal pellet collected from a representative mouse in each cage in each rack row) combined with the associated rack row's exhaust plenum swab.

C. difficile strain isolation, growth conditions, and colony identification

C. difficile strain 16N203 was isolated from feces frozen at -80°C after collection from a spontaneously affected animal in the dietary study mouse colony. 1.5 fecal pellets were thawed, passed into an anaerobic chamber, and diluted in 200µL sterile anaerobic PBS. 20µL was placed into 3mL of taurocholate cefoxitin cycloserine fructose broth (TCCFB) and incubated at 37°C overnight. A 10µL loop of the TCCFB enrichment culture was streaked onto taurocholate cefoxitin cycloserine fructose agar (TCCFA) to get an isolated colony of *C. difficile*. The isolated colony was used for downstream applications.

For colony identification, a 16N203 *C. difficile* colony was diluted in 15µL UltraPure Water (Invitrogen 10977-015), heated to 95°C for 20 min and then used for colony PCR to determine identity and toxin type of the isolated organism [190,191]. PCR was performed using the following primers for the *C. difficile* specific band F: 5'-TTGAGCGATTTACTTCGGTAAAGA-3' and R: 5'-CCATCCTGTACTGGCTCACCT-3' along with the universal 16S primers 515F: 5'-GTGCCAGCMGCCGCGGTAA-3' and E939R: 5'-CTTGTGCGGGCCCCCGTCAATTC-3' [190]. Toxin specific PCR followed previously published primers omitting the 16s rDNA primers [191]. The PCRs were run in a total volume of 25uL containing GoTaq Green Master Mix (Promega M712), primers, and nuclease free water.

C. difficile cytotoxin assay

Cytotoxicity assay was performed as previously described with the following modifications [189]. Briefly, ATCC CCL-81 Vero cells were grown to confluence in Dulbecco modified Eagle medium (Gibco 11965) supplemented with 10% fetal bovine serum (16140) and 1% Penicillin streptomycin (Gibco 15070). Cells were plated to a density of 10^5 cells/well. Mouse cecal content was diluted 1:10 in sterile PBS, passed

through a 0.22µm filter, and serially diluted to 10^{-6}. Filtered samples were tested in duplicate with a corresponding control which both antitoxin (Techlab T5000) and sample were added. A positive control of *C. difficile* TcdA (List Biologicals 152C) was used. Samples were incubated overnight at 37°C and the cytotoxic titer was determined as the reciprocal of the highest dilution that produced 80% cell rounding.

Genome sequencing, variant identification, and comparative genomics

A colony of *C. difficile* 16N203 was cultured 18 hours anaerobically at 37°C in 13mL Brain Heart Infusion Broth (BD 211059) + 0.01% L-cysteine (Sigma C6852). The culture was spun at 4500g for 12min, washed one time with sterile PBS, spun at 4500g for 12 min and the pellet was re-suspended in 300uL of Dneasy UltraClean Microbial kit Microbead solution (Qiagen 12224-50). The extracted DNA was then prepared for sequencing on an Illumina MiSeq instrument using the NexteraXT kit and sample-specific barcoding. Library preparation and sequencing were performed at the Center for Microbial Systems at the University of Michigan. Quality of reads was assessed with Fastqc [192], and Trimmomatic [193] was used for trimming adapter sequences and low quality bases. Genome assemblies were performed using Spades [194]. Variants were identified by: 1) mapping filtered reads to the assembled *C. difficile* strain 630 reference sequence (NC_009089.1) using the Burrows–Wheeler short-read aligner (BWA), 2) discarding PCR duplicates with Picard, and 3) calling variants with SAMtools and bcftools. Variants were filtered from raw results using GATK's VariantFiltration (QUAL > 100, MQ > 50, > 10 reads supporting variant, FQ <0.025). In addition, a custom python script was used to filter out single nucleotide variants that were: 1) <5 bp in proximity to indels 2) <10 bp in proximity to another variant or 3) not present in the core genome. Maximum likelihood trees were constructed using core genome variants among the outbreak strain and a representative set of previously sequenced *C. difficile* genomes in FastTree [195]. MLST predictions were made by BLASTing genome assemblies against the PubMLST database for *C. difficile* (downloaded on January 3rd, 2017).

Experimental C. difficile infection

8-wk old C57BL/6 wild-type (WT) mice (6 males and 3 females) were obtained from an in-house breeding colony that was established originally with animals from Jackson Laboratories (Bar Harbor, ME). Mice were treated 10 days with 0.5g/L cefoperazone (MP Biomedicals 219969505) in sterile distilled water (Gibco 15230-147) as previously described [189]. Briefly, animals were allowed to drink antibiotic amended water *ad libitum* and the antibiotic water was changed every other day. After 10 days, antibiotic water was switched to sterile distilled water. After 2 days on water without antibiotics, 3 male and 3 female mice (total treated n=6) were challenged via oral gavage with 500 spores of *C. difficile* strain 16N203. Spores (preparation described below) were suspended in 50µl Gibco sterile distilled water and 3 male mice (total mock n=3) were treated with 50µl of Gibco water only. Mice were monitored 16 hours post infection and feces were collected and plated to confirm spore inoculation. Mice were observed every 3 hours for 36 hours for clinical signs of disease until clinical signs appeared. Mice were euthanized by CO_2 inhalation when clinical signs appeared or at study endpoint. Mice were then evaluated at 48 hours after *C. difficile* infection for weight loss, activity, posture, coat, diarrhea and nose/eyes appearance [196]. Animals were euthanized and cecal contents and tissues from the animals were collected for culture and ELISA.

C. difficile spore preparation

16N203 was streaked onto TCCFA and an isolated colony was incubated overnight anaerobically at 37°C in 2mL Columbia broth (BD 294420). The next day the culture was placed into 40mL of Clospore [197] and incubated anaerobically at 37°C for 8 days. The culture was spun at 3200rpm for 20min at 4°C. The pellet was washed two times with sterile water (Gibco 15230-147), once with sterile 0.05% Tween 20 (Fisher BP337), and then once with sterile water. The final pellet was resuspended in 1mL sterile water. The spore stock was stored at 4°C in sterile water. Prior to gavage, spores were heated to 65°C for 20min. Spores were plated on TCCFA to determine dose administered to animals.

Results

Recognition of an outbreak of severe typhlocolitis in a cohort of mice undergoing pre- and peri-natal diet manipulation

Typhlocolitis was observed in a cohort of F1 mice from a study involving parental (F0) pre- and peri-natal methyl-donor supplementation (MS) and post-weaning intake of normal diet (ND) or 42% high-fat diet (HFD) chow. The purpose of the original study was to evaluate MS diet epigenetic effects on obesity development in later-life and at various life stages of the F1 mice.

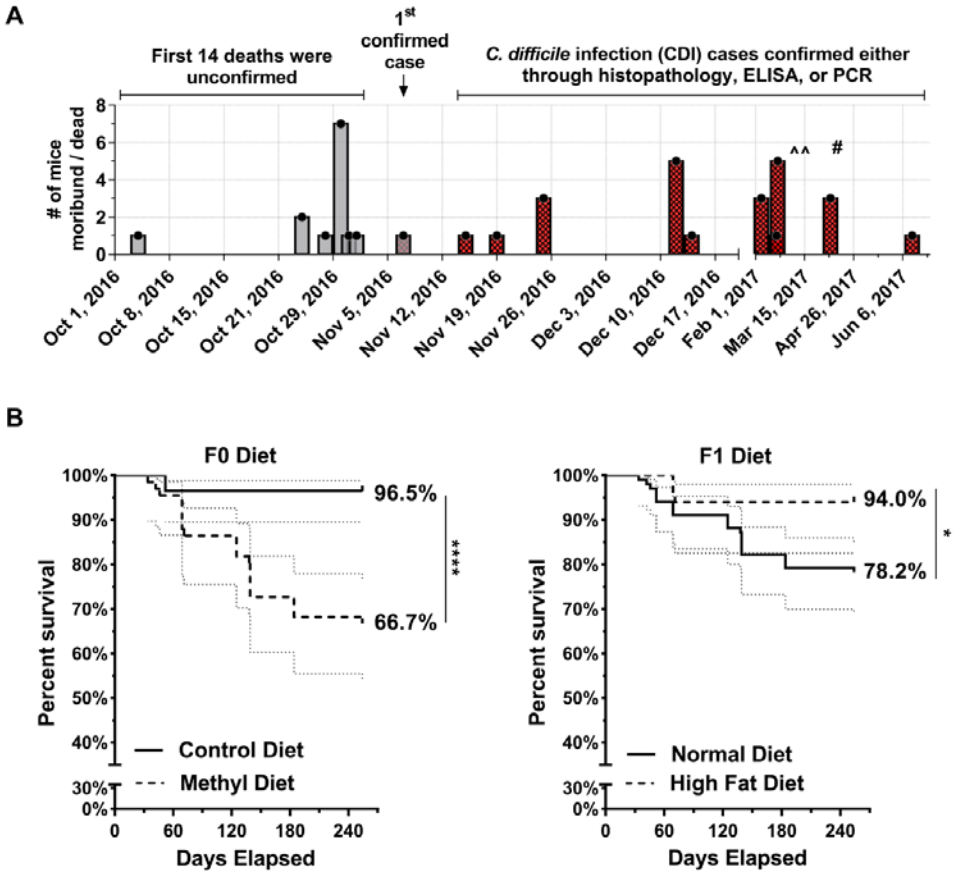

Figure 3-1 – Methyl-donor diet and advanced age mice had higher total mortality during outbreak. A) Epidemic curve depicting the first set of unconfirmed cases that triggered the outbreak investigation and the subsequent cases determined to be consistent with *C. difficile* infection. ^ - *denotes environmental swab tests on 3/9/17, 3/15/17, 10/24/17 (not shown). # - denotes plenum + fecal pellet testing on 4/14/17.* **B**) Kaplan-Meier survival curves of mouse colony comparing the percent survival of the pre-/peri- natal control diet (n=85) versus pre-/peri-natal methyl-supplementation diet (n=66) mice; F1 normal chow diet (n=101) versus 42% high fat diet (n=50) mice over the course of 8.5 months. 95% CI are graphed (gray dotted lines). * $p<0.05$, **** $p<0.0001$, Mantel-Cox log-rank test.

Over the course of 254 days from October 4th, 2016—June 15th, 2017, 57 out of 207 mice in the MS diet study were found dead with no premonitory signs (n=39) or were euthanized for moribund condition (n=18), including hunched posture, lethargy, dyspnea, and mucoid stool with perineal staining. Severe necrotizing typhlocolitis with pseudomembrane formation and severe submucosal edema was observed at necropsy in early cases and was suggestive of *C. difficile* colitis [189]. This led to screening of affected animals for *C. difficile*, which was subsequently identified in a number of these mice, suggesting a potential outbreak. To facilitate investigation of this outbreak, we developed the following case definition: confirmed cases had 1) presentation of a compatible clinical syndrome and either, 2) histopathologic cecal/colonic lesions consistent with *C. difficile* infection or, 3) tested positive for *C. difficile* bacteria or *C. difficile* toxin. Of the 57 animals that died during the study period, we were able to complete analysis on 36 mice and determined 25 of these mice fit our case definition. We excluded the 11 mice that were examined but found to have causes of death unrelated to the outbreak.

We constructed an epidemic curve to follow the course of this outbreak. The initial 14 deaths in the colony that led to the outbreak investigation were included in this epidemic curve (**Figure 3-1A**), but as most of these animals were found dead, or intestinal tissue was not examined, case definitions could not be assigned to these mice. Over the course of the outbreak study, there were 86 MS diet and 97 control diet F1 mice. A Kaplan-Meier survival curve analysis on *only the confirmed cases* of CDI shows lower survival in the MS diet mice (n=66) compared to control diet mice (n=85) (**Figure 3-1B**). Curve analysis indicates that on day 254, which is the day on which the last outbreak case was identified, 96.5% of the control mice survived while only 66.7% of the MS mice remained ($p < 0.0001$). A curve comparison of the confirmed CDI cases based on F1 diets—HFD (n=50) versus ND (n=101) group suggests that HFD fed mice had higher survival percentages ($p < 0.02$), **(Figure 3-1B)**; however, there were 65 F1 mice on HFD mice while 118 F1 mice were on ND in the initial colony.

To try and control this outbreak, breeders on the MS diet and control diet were transferred to a separate room in January 2017 based on negative fecal ELISA results. The remainder of the colony was ultimately transferred to containment housing. On 4/14/17, PCR of pooled plenum and fecal pellets revealed 8/8 rows on one rack and 1/2 rows on a second rack were positive for *C. difficile*. Environmental samples on 3 separate dates (3/9/17, 3/15/17, and 10/24/17) tested negative for *C. difficile.* The timeline of the plenum swabs, fecal sampling, and environmental tests is also included on the epidemic curve (**Figure 3-1A**).

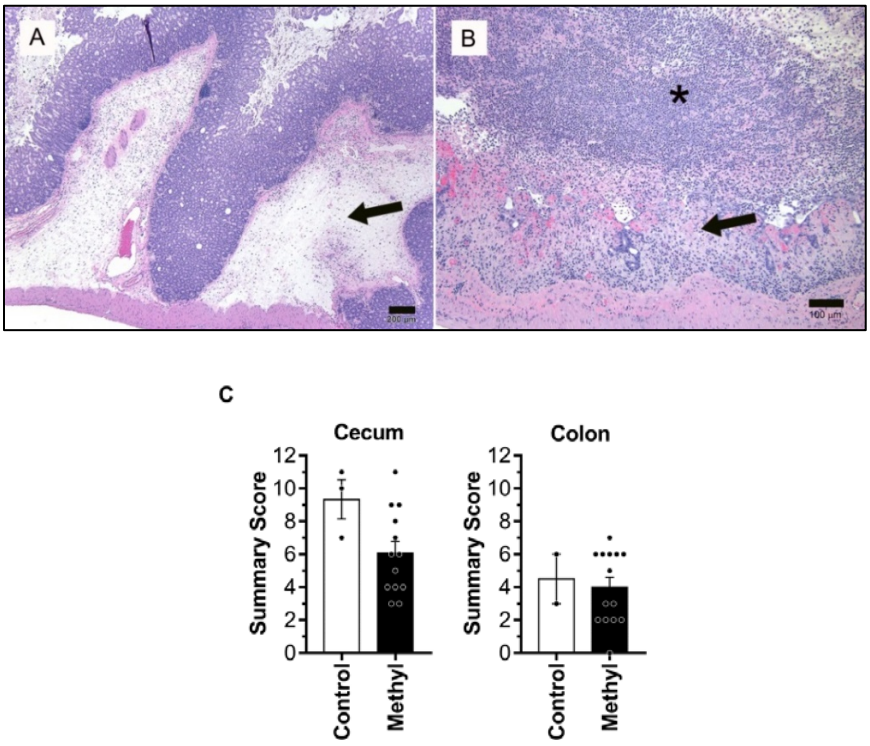

Figure 3-2 – Necropsies and histopathology indicate typhlocolitis as primary diagnosis of affected animals. A) Representative histology of mouse cecum in a *C. difficile* culture-positive case exhibiting severe submucosal edema and inflammation (arrow). H&E stain, Bar=200 µm. **B**) Representative histology of an area of cecum in the same case displaying mucosal necrosis (arrow) and extensive pseudomembrane formation (asterisk), consisting of neutrophils and sloughed enterocytes in a fibrinous matrix. H&E stain, Bar=100 µm. **C**) Histological severity scores for the 17 mice showing typhlocolitis, out of 24 clinically affected mice for which tissues were available. Severity was scored by a board-certified veterinary pathologist using an established murine *C. difficile* scoring system. Each category—edema, inflammation, or epithelial damage was individually scored 0-4 and a summary score was generated (range 0-12). Of the 17 mice, 1 mouse had no cecum score and 1 mouse had no colon score due to tissue autolysis of those samples. As such, for cecum scores, control diet F1 mice n=3 and methyl-supplementation diet (MS) F1 mice n= 13. For colon scores, control diet n=2 and MS diet n=14.

Identification of C. difficile in animals with typhlocolitis

Gastrointestinal (cecum and colon) tissues were available for histologic evaluation in 24 of the total 57 animals found dead or euthanized during the outbreak (**Figure 3-2**). 17 of 24 animals were found to have necrotizing and pseudomembranous typhlocolitis consistent with CDI as seen in experimental murine models [189]. Histological findings included striking submucosal edema of the cecum and colon, accompanied by marked neutrophilic inflammation and necrosis and sloughing of the superficial to mid-portions of the mucosa, often with pseudomembrane formation (**Figure 3-2A-B**). Of the 17 animals with histologically evident typhlocolitis, we were also able to collect and submit fecal and/or cecum and colonic samples from 14 animals for testing. 12 of the 14 animals tested positive for *C. difficile* TcdA and TcdB via ELISA and 2 tested positive for *C. difficile* bacteria via PCR. 14 were F1 mice from the MS diet and 3 were from the control diet groups (**Figure 3-2C**). The cecum summary scores (**Figure 3-2C**) in the MS diet (n=13) was 6.1 ± 2.6 and 9.3 ± 2.1 in the control diet (n=3). The colon summary scores (**Figure 3-2C**) shows that MS diet (n=14) was 4.0 ± 2.2 and control diet (n=2) was 4.5 ± 2.1. One MS-diet F1 mouse had missing colon scores and one control diet F1 mouse had missing cecum scores due to tissue autolysis. Given that significantly fewer control diet F1 mice ($p<0.0001$) were affected in the outbreak (**Figure 3-1B**), we collected fewer control samples and thus cannot draw conclusions on the effect of the F0 diet on disease severity between the two groups of F1 mice.

Overall, we observed that the histology score was higher in cecum than colon in most animals, consistent with experimental murine *C. difficile* models [189]. Of the remaining 7 out of 24 histologically evaluated animals that did not have evidence of typhlocolitis, alternate causes of death/morbidity were identified, including tumors (n=2), bacterial enteritis (n=2), or undetermined by histology (n=3). Finally, there were 12 out of 36 analyzed animals that had no gastrointestinal tissue available to be histologically evaluated, and 8 of these animals tested positive for *C. difficile* bacteria (n=2) and *C. difficile* toxins A and B (n=6) which then allows us to include these 8 as confirmed cases of *C. difficile*-related deaths. The 4 animals that tested negative for *C. difficile* toxin were

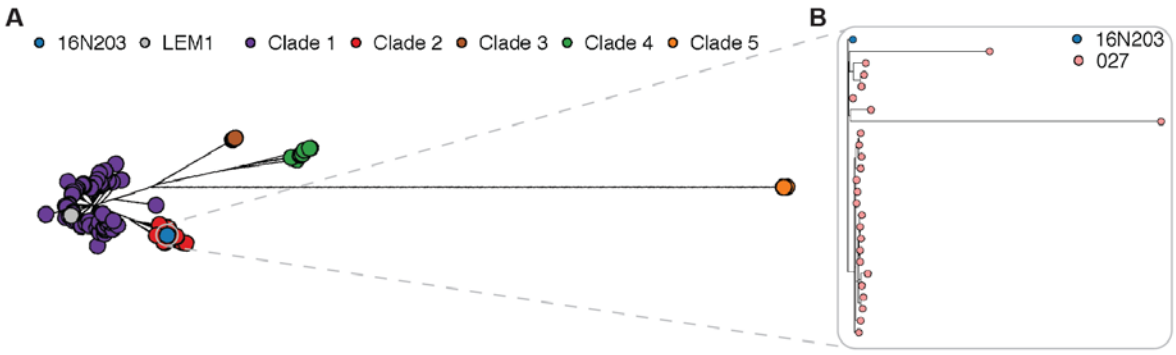

Figure 3-3 – Isolation and genomic sequencing confirms NAP1/027/BI *Clostridium difficile* strain. A) Phylogenetic relationship between the mouse outbreak strain and representative *C. difficile* isolates. Isolates include publicly available clinical genomes, clinical isolates collected at the University of Michigan, and two mouse strains (16N203 and LEM1). A maximum likelihood tree was generated from the recombination filtered, polymorphic core genome positions in all isolates (N = 438). Clade 1 (purple) includes reference strain CD630 and mouse strain LEM1 (gray); clade 2 (red) includes epidemic RT 027. Clades 1-5 are as previously defined[198–200]. **B**) Tree in (A) was subset to include only 027 isolates. The mouse outbreak "16N203" strain (blue) clusters with the RT 027 isolates (pink), a RT in Clade 2 (red).

found to have an alternative cause of death (endometritis n=1) or undetermined (n=3), and naturally, these were not included in the confirmed cases of *C. difficile*.

Isolation of *C. difficile* was performed by the use of selective culture. A *C. difficile* strain (designated 16N203 for the animal from which it was initially isolated) was obtained in pure culture. A PCR [190] confirmed the *C. difficile* bacteria was present in fecal sample (**Figure 3-5A**), and this strain was also positive for the toxin genes *tcdA/tcdB* and *cdtA/cdtB* by PCR [191] (**Figure 3-5B**). Whole genome sequencing of strain 16N203 was undertaken, and a whole genome phylogeny was constructed (**Figure 3-3A**), including a representative set of previously sequenced *C. difficile* isolates. These isolates contain publicly available clinical genomes [198,201,202], clinical isolates collected at the University of Michigan, and two mouse strains (16N203 and LEM1). LEM1 is an indigenous murine spore-forming *C. difficile* strain identified and isolated from mice acquired from common mouse vendors, Jackson Laboratories and Charles River Laboratories [203]. LEM1 appears to not be highly virulent and can protect against the closely related but more virulent strain VPI10463, at least in mice with C57BL/6J or Balb/c background [203]. In our data, the murine strain LEM1 clusters with Clade 1, which

contains reference strain CD630, while the outbreak strain fell within the diversity of Clade 2, which contains RT027 isolates (**Figure 3-3A**). When a phylogenetic tree was constructed with only RT027 isolates, the outbreak 16N203 strain clustered with isolates derived from human patients with clinical CDI [204] (**Figure 3-3B**).

C. difficile strain 16N203 is fully virulent in a mouse model of antibiotic-induced CDI

We had previously demonstrated that *C. difficile* strains have variable virulence in an established mouse model where CDI susceptibility is conveyed by treatment with the antibiotic cefoperazone [189]. To determine whether the pathogenicity of the outbreak strain 16N203 was unique to the dietary model, we assessed whether the outbreak strain 16N203 was virulent in this established model of CDI (**Figure 3-4A**). C57BL/6 mice on a standard diet and without previous dietary manipulations were treated with cefoperazone in drinking water for 10 days and then switched back to plain water. Two days after stopping antibiotics, mice were challenged with either 500 spores of the 16N203 outbreak strain or vehicle via oral gavage. Significant weight loss ($p<0.05$) was observed in mice challenged with 16N203 spores during the 48-hour study time course while mock-treated mice maintained weight (**Figure 3-4B**). Mice challenged with *C. difficile* 16N203 had higher levels of cecal colonization ($p<0.03$) with detectable toxin in intestinal contents ($p<0.05$) and developed clinical signs compatible with severe CDI (**Figure 3-4C**).

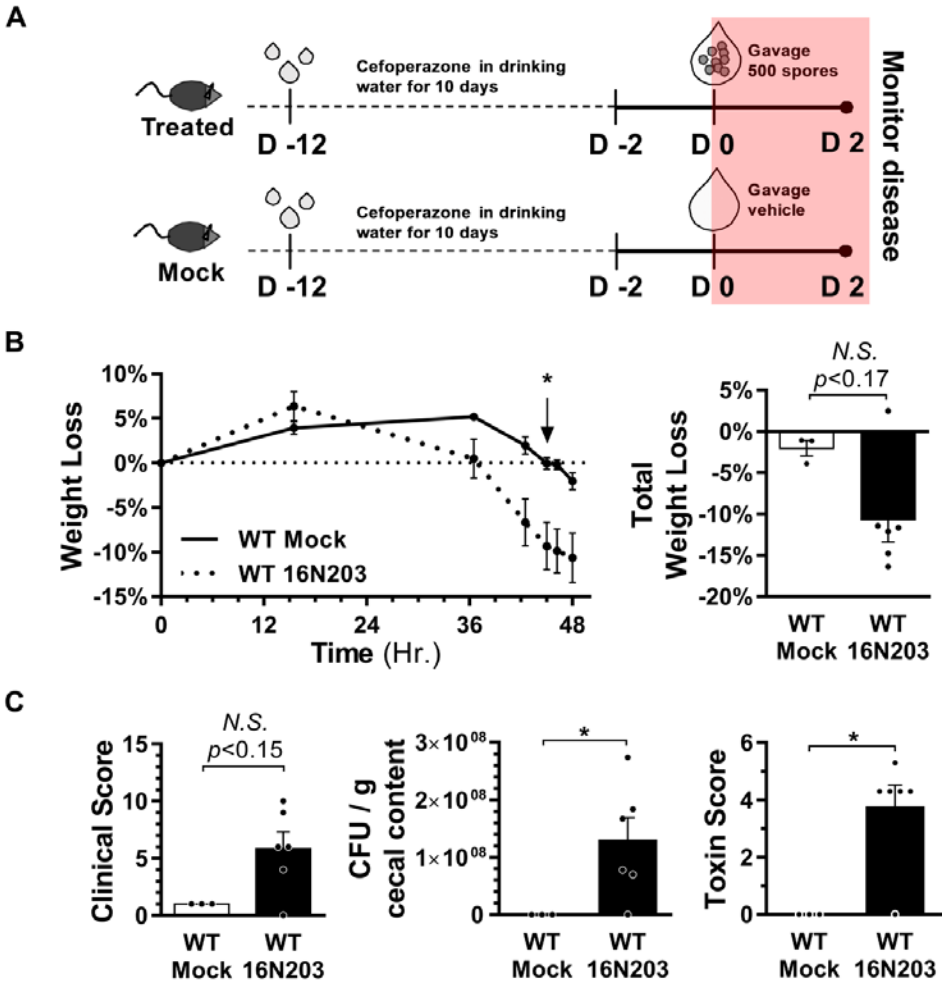

Figure 3-4 – *C. difficile* 'outbreak' strain induces CDI in a standard mouse model with antibiotics. A) CDI mouse model with cefoperazone in drinking water used to assess virulence of the outbreak 16N203 strain. Wild-type (WT) mice were administered cefoperazone in drinking water for 10 days on day -12 (D -12) and then orally gavaged either 16N203 spores (n=6) or the vehicle (distilled water) for mock (n=3) controls on day 0 (D0). Mice were monitored for disease between D0 and D2. **B**) Body weight loss over the course of 48 hours; total percentage of body weight loss shown in column graph. **C**) Clinical score, colonization, and toxin scores at 48 hours. For weight loss, clinical, colonization, and toxin scores, Mann-Whitney test was used for statistical analyses, * $p<0.05$.

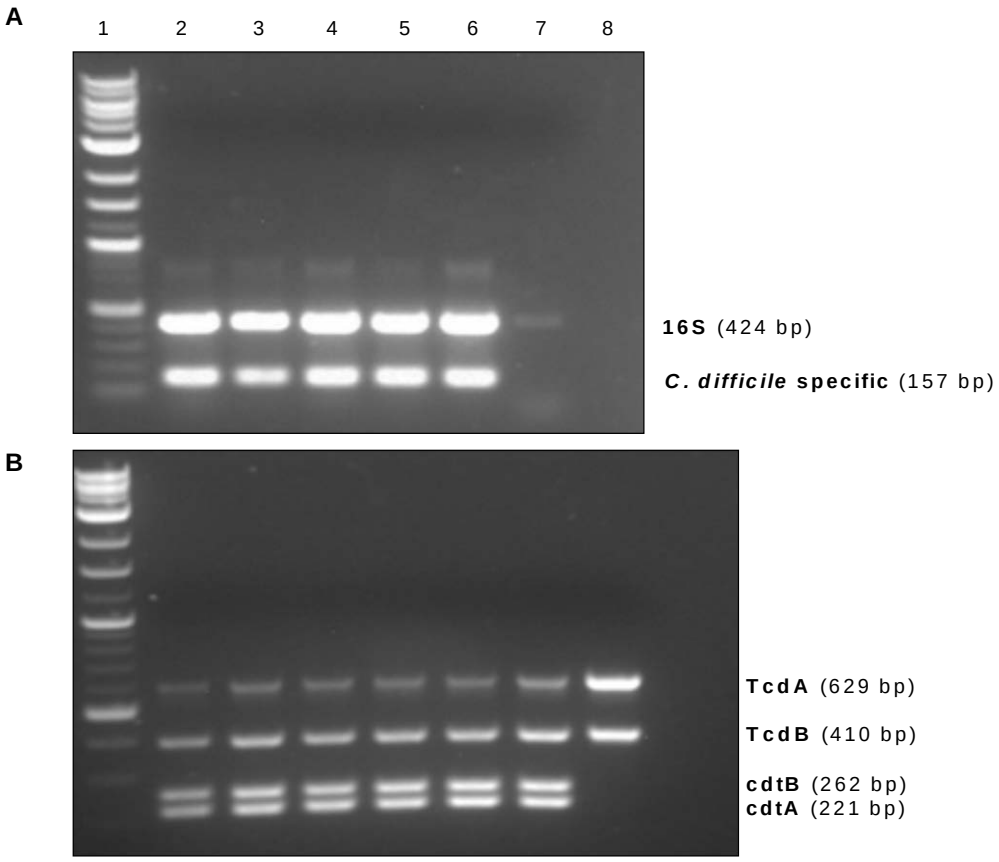

Figure 3-5 – PCR identification of Clostridium difficile and its associated toxins (TcdA, TcdB, and the binary cdtA/cdtB toxin) A) PCR[190] confirming *C. difficile* specific identification. Lane 1 = 100bp ladder, Lane 2 = 16N203-1, Lane 3 = 16N203-2, Lane 4 = 16N203-3, Lane 5 = 16N203-4, Lane 6 = *C. difficile* 630, Lane 7 = water. **B**) PCR[191] confirming presence of CDI toxins: Toxin A (TcdA), Toxin B (TcdB), and binary toxin (cdtA/cdtB). Lane 1 = 100bp ladder, Lane 2 = 16N203-1, Lane 3 = 16N203-1, Lane 4 = 16N203-2, Lane 5 = 16N203-3, Lane 6 = 16N203-4, Lane 7 = *C. difficile* R20291, Lane 8 = *C. difficile* 630.

Discussion

In this report, we describe an outbreak of *C. difficile* infection (CDI) and colitis in laboratory mice associated with diet manipulation. This outbreak is interesting because spontaneous, symptomatic CDI is unusual in laboratory mice, and symptomatic colitis due to experimental CDI generally requires pretreatment with antibiotics [203,205]. Subclinical colonization of mice has been reported previously. In one study it was noted that mice could be colonized with *C. difficile* with or without prior antibiotic treatment but this colonization was at a very low level and not associated with any clinical disease [187]. Administration of the antibiotic clindamycin was associated with increases in the levels of colonization but again without development of clinical colitis. It has been also reported that wild rodents can harbor toxigenic *C. difficile* strains, again without any overt disease [206].

One group reported that laboratory mice obtained from multiple sources appear to harbor LEM1, an indigenous *C. difficile* strain [203]. Colonization with LEM1 in the same study did not result in disease and in fact was associated with protection from disease following challenge with another strain of *C. difficile* that generally produces severe colitis in experimental models of CDI. In contrast, while LEM1 clusters with Clade 1 (containing reference strain CD630 (RT 12)), the outbreak strain in our study clustered in Clade 2 with patient-derived RT 027 isolates and was associated with clinical disease in both spontaneously infected and experimentally infected mice. The source of this strain remains unclear, and our attempt at revealing a source with environmental sampling did not yield conclusive results. Ribotyping and genetic analyses suggest a potential source was through fomites or human carriers, but the source may have been gone by the time of environmental investigation.

The mechanism underlying the unexpected increased susceptibility of these mice is also not entirely clear. Small animal models to recapitulate CDI pathogenesis generally rely on antibiotic pretreatment prior to experimental challenge with *C. difficile*, even with virulent strains [205]. As noted, the current outbreak is unusual in that there were no antibiotics administered to the animals and instead susceptibility to colonization and

colitis was associated with dietary (peri- and pre-natal) manipulation. Our current understanding of the pathogenesis of CDI attributes loss of colonization resistance to altered structure and function of the indigenous intestinal microbiota [207]. However, given the unexpected nature of the outbreak, we were not positioned to determine if there were changes in the microbiota associated to the increased susceptibility we observed in MS F1 mice. Antibiotics, which can cause widespread changes in the indigenous microbiota, are associated with the development of clinical CDI in humans, but other factors that alter microbial populations may also convey susceptibility.

In our study, increased *C. difficile*-associated deaths were seen in the offspring of mice receiving the methyl-supplementation (MS) diet. Diet may be a factor that can alter the community structure and function of the intestinal microbiota, and diet-related susceptibility to CDI has been evaluated in some studies [44,208]. Patients receiving enteral tube feeding had increased risk of developing CDI [209]. Tube feeds given in the form of an elemental diet (i.e. a diet that is entirely absorbed within the small bowel) are thought to deprive the colonic bacteria of nutrition in the form of fiber and resistant starch, increasing the risk of CDI [210]. Microbiota accessible starches may protect against CDI as in murine studies where feeding such carbohydrates can suppress experimental CDI [211]. This protection was associated with an increase in short chain fatty acids which are the metabolic products of microbial fermentation of non-digestible carbohydrates. Another study showed that a low protein diet (which had reciprocal increases in carbohydrate composition) could be protective in a mouse model of CDI [212]. In addition to macronutrients, it was recently demonstrated that zinc deficiency could alter the microbiota and increase susceptibility to experimental CDI [45].

It should be noted that, in contrast to our study, the diet-related susceptibility or amelioration of experimental CDI discussed above occurred in models where the microbiota was still altered via antibiotic administration. An earlier study in hamsters fed an atherogenic diet in the absence of antibiotic administration, unexpected diarrhea and death due to colitis was observed in animals starting 45 days after diet manipulation [213]. Similar to our study, toxigenic *C. difficile* was isolated from affected animals, although

typing of the strain was not performed. It is interesting to note that in these hamsters, the atherogenic diet increased susceptibility to CDI, but in our study, F1 mice that were on a 42% high fat diet (HFD) exhibited increased survival—though it should be noted that this observation was limited by the fact that there were significantly more normal diet mice than HFD mice in the mouse colony at the time.

While hamsters are exquisitely susceptible to *C. difficile*, symptomatic murine *C. difficile* colitis outbreaks in the absence of antibiotic administration are very rare. There is precedence for disease outbreaks in mice associated with *C. difficile*, but the affected mice have had significant immune alterations that increased their susceptibility [214,215]. One such outbreak occurred in a murine experimental autoimmune encephalomyelitis model generated via the administration of pertussis toxin and a myelin oligodendrocyte glycoprotein fragment [215]. These authors speculated that the stress of this experimental manipulation or the development of the autoimmune disease altered the microbiota in a manner that leads to susceptibility to CDI, but they did not profile the microbiota in these animals. Although we were unable to characterize the microbiota in our study due to the unexpected nature of the outbreak, a future avenue to explore would be diet-associated microbial community alterations that may convey susceptibility.

Specific mechanisms by which our methyl-donor diet alters susceptibility to CDI are unclear. A similar methyl-supplementation maternal diet was shown to increase colitis risk in a chemically-induced inflammatory bowel disease (IBD) using dextran sulfate sodium (DSS) [34,216]. F1 mice from methyl-fed dams had worsened colitis and significantly higher mortality than control F1 mice [34]. Colonic mucosal bacterial diversity analyses indicated striking composition variation, including significantly higher prevalence of *Clostridia* in methyl diet F1 mice. In addition, there was an increase in *Firmicutes* (*Lachnospira, Oscillospira, Ruminococcus* and *Catonella*) and a decrease in *Parabacteroides* and *Eubacterium* in methyl F1 mice compared to controls. This suggests that dysbiosis between colitogenic (*Firmicutes*) and anti-inflammatory bacteria (*Parabacteroides*) following prenatal methyl supplementation may have led to the colitis prone phenotype [34]. A fecal microbiome transfer (FMT) via cage swapping (between

methyl F1 mice and germ-free mice) was sufficient to worsen DSS-induced colitis in germ free mice, indicating that the maternal methyl-donor diet alone may enhance a colitis-prone microbiota profile. While this study cannot be directly compared to *C. difficile* colitis, it strongly suggests that a prenatal methyl-donor diet is sufficient in generating a pro-colitic F1 microbiota. In the context of CDI, it remains to be determined whether susceptibility is due strictly to altered community composition, creating a niche for *C. difficile* colonization, or whether microbial changes directly promote colitis-enhancing inflammatory responses. While unexpected, the current spontaneous outbreak of CDI in the absence of antibiotics in mice with parents fed an altered pre- and peri-natal diet may ultimately provide additional insight into the interplay of diet, host responses, and the microbiota that mediates CDI and colitis susceptibility.

Chapter 4 – Methyl-donor diet alters the murine gut microbiota but does not influence colonization resistance

Manuscript in preparation.

Theresa Mau*, Josie Libertucci*, Kimberly Vendrov, Martin O'Brien, Ingrid Bergin, Raymond Yung, and Vincent B. Young. *Denotes equal contribution.

Abstract

Clostridium difficile infection (CDI) has become the most common nosocomial pathogen in North America and West Europe[39–41]. CDI is typically associated to antibiotic-use, but cases of non-antibiotic associated CDI are similarly on the rise[43]. Recent studies have shown that diet plays a considerable role in the gut microbiome and its colonization resistance against CDI[44,45]. In this current study, a methyl-supplementation donor (MS) diet is administered as a pre- and peri-natal diet to C57BL6/J mice, and fecal sampling is performed before and throughout to map the changes that occur between F0 and F1 mice, before and after MS diet intake, and F1 mice microbiota community structure during CDI (using a murine outbreak strain '16N203'). We found the MS diet F1 mice have an increase in the relative abundance of *Lactobacillus*, *Porphyromonadaceae* and decreased abundance of *Bacteroides*, *Akkermansia* and *Alistipes* in F1 microbiota. These changes were not associated to a loss of CDI colonization resistance. Additionally, our data indicate that the use of clindamycin erases the differences between control and methyl F1 diet mice, causing equivalent susceptibility to 16N203 *C. difficile* infection as assessed by colonization and clinical scoring, gastrointestinal (cecum and colon) histopathology, and toxin quantification.

Introduction

Clostridium difficile is a toxin-producing, spore-forming bacillus. *Clostridium difficile* infection (CDI) has become one of the most frequent nosocomial infections, and it has dramatically increased its presence in both North America and West Europe over the past few decades[217,218]. In humans, the major CDI risk factor is antibiotic-use which leads to the loss of colonization resistance, likely through its alteration of the gut microbiota. While the major risk factor for developing CDI in humans is still primarily antibiotic exposure, the rise of non-antibiotic associated CDI[43] has led to studies on other environmental factors, including diet, that are also able to influence structure and function of the gut microbiota[44,45].

Dietary composition can also influence microbial community composition within the gut. In human diet, a sugary substitute used in many processed foods, trehalose, has been shown to increase the fitness and virulence of the two major epidemic strains of *C. difficile*[44]. In murine models of CDI, antibiotic pretreatment is typically required to induce susceptibility. Even in an experiment that showed a high-zinc diet exacerbates CDI colitis in mice, antibiotic-exposure remained necessary for colonization and disease manifestation[45]. Therefore, it was unexpected that an outbreak of *C. difficile* can occur in a mouse colony that uses no antibiotics and is only associated to dietary manipulation (unpublished, Chapter 3 under review). We previously reported a spontaneous murine outbreak of 16N203 *C. difficile*, an RT027 strain, in F1 mice whose parents received pre- and peri-natal dietary manipulation. This was interesting because mice without exposure to antibiotic pre-treatment typically do not become sick with CDI[42,189,203,205]. Due to the spontaneous nature of the outbreak, diet effect on microbial communities could not be assessed in that outbreak study.

The outbreak's association to diet manipulation led us to speculate that the methyl-supplementation donor (MS) diet used in the study may play a role in CDI susceptibility. Studies using mouse models have shown that early nutrition intervention rich in methyl-donors (L-methionine, folic acid, choline, betaine, zinc, and vitamin B-12) can influence F1 mice health in later life[21,23–25,27,28,32,33]. The MS diet has been shown to

worsen chemically-induced dextran sulfate sodium (DSS) colitis in a mouse model of inflammatory bowel disease[34,35]. Importantly, these studies show that the exacerbated outcomes of DSS-induced colitis can be achieved with a fecal microbiota transfer (FMT) between germ-free mice and MS diet F1 mice[34]. This suggests that early nutritional programming can influence the structure and possibly the function of the fecal microbiota in a way that conferred colitis susceptibility.

To date, no studies have investigated changes in diet and its relationship to increased CDI susceptibility, without antibiotic exposure. We aim to investigate CDI susceptibility in F1 mice whose parents received pre- and peri-natal MS diet, without antibiotic exposure. We hypothesize that the MS diet leads to microbiota community structure changes that may increase CDI susceptibility in F1 mice. In this current study, we test the MS and control diets' effect on fecal microbial community, and if so, whether these diet-induced changes associate with alterations to CDI susceptibility.

Materials and Methods

Animals and housing

C57BL/6J 8-week old mice were purchased from Jackson Laboratories (Jackson West RB08; Sacramento, CA). During the breeding and dietary intervention phase, all mice were housed under specific-pathogen free conditions in biosafety level 1 rooms maintained by the Unit for Laboratory Animal Medicine. During the experimental infection phase, mice were transferred to animal biosafety level 2 rooms where procedures were performed under a biosafety cabinet using a sporicidal disinfectant cleaner (Perisept, Triple S 48027). All procedures with animals and their care are approved by the University of Michigan Institutional Animal Care and Use Committee.

F0 mice dietary protocol

C57BL/6J 8-week old female and male mice were placed on custom "TD" diets produced and distributed by Harlan-Teklad (Madison, WI). Mice were acclimated for 2 weeks upon arrival and then placed on either control (TD.06689) or methyl-donor supplementation (MS) diet (TD.110144) for 2 weeks. Mice were then paired for mating

and fed the diet throughout pregnancy and lactation. As previously described[33], the MS diet (TD.110144) is comprised of 12g/kg methionine, 16.5 g/kg choline, 15 g/kg betaine, 16.5 mg/kg folic acid, 1.56 mg/kg vitamin B12, and 200 mg/kg Zn. The MS diet has 18.8% protein, 62.1% carbohydrate, and 19.1% fat (% kcal from). The control diet (TD.06689) is comprised of 4.3 g/kg methionine, 1.35 g/kg choline, 0 g/kg betaine, 0.003 mg/kg folic acid, 0.06 mg/kg vitamin B12, and 0.05 mg/kg Zn. The control diet has 17.6% protein, 64.0% carbohydrate, and 18.4% fat (% kcal from). F1 mice were weaned at 28 days and then placed onto a standard chow diet (PicoLab Laboratory Rodent Diet 5L0D, LabDiet, St. Louis, MO).

Fecal microbiome sample collection

Fresh fecal microbiome samples (MBS) were collected from each F0 mouse prior to diet-exposure, prior to pairing for mating, and twice after paired. MBS was also collected from F1 mice beginning at post-weaning until 3 months of age. All MBS prior to spore-gavage were collected fresh and snap frozen in liquid nitrogen in twist-cap tubes. MBS were also similarly collected throughout experimental-infection phase.

Isolation of lymphocytes and cell counting

Peyer's patches (PP) and mesenteric lymph nodes (mes LN) were excised, collected through a 70 µm filter, and washed with ice cold buffer (5% fetal bovine serum (FBS), 0.4% EDTA in PBS) prior to centrifugation (3000 RPM, 5 min.) to form a cell pellet. The supernatant was discarded and RBC depletion was performed with ACK (Lonza, #10-548E) and washed through a 70 µm filter to neutralize ACK. After rinse and resuspension in cold sterile PBS buffer, 10 µl aliquots of each sample was used for a cell count using Trypan blue paired with an automated cell counter (Invitrogen Countess 1754B).

T cell cytokine stimulation

PP and mes LN cells were cultured in 6-well plates for 4 hours at 36°C in a 5% CO2 incubator in T-cell media (RPMI medium supplemented with 1% penicillin and streptomycin, 1% L-glutamine, 10µM β-mercaptoethanol and 5% heat-inactivated FBS)

in the presence of Monensin (Biolegend 420701) and Cell Activation Cocktail (Biolegend 423303) containing phorbol 12-myristate-13-acetate (PMA), ionomycin, and Brefeldin A. Treatment concentrations were used as per manufacturer suggestions. At 4 hours, cells were gently removed with pipette and washed with PBS and spun down to form cell pellet.

Flow cytometry staining

Single cell suspensions of PP and mes LN were resuspended in PBS in conical pyrostyrene tubes. Small cell samples from each mouse are pooled to form control cells for single positive controls (SPCs), full-minus-one controls (FMOs), and the unstained cells. Sample cells were stained for 30 min (on ice and in the dark, for all stain steps) with a Live/Dead Fixable Dead Cell Stain Kit (Invitrogen L34959). Cells were blocked for 1 hr on ice with anti-mouse CD16/CD32 Purified (eBioscience Affymetrix #14-0161). Following 2 cold PBS rinses, cells were stained with surface markers, anti-mouse CD3 Percp-eF710 (eBioscience 46-0033-80), CD4 PeCy7 (eBioscience 25-0041-81), and CD8 FITC (eBioscience 11-0081) for 45 min. Following 2 washes, the cells were processed with a Fix/Perm Intracellular Staining Buffer Set (eBioscience 00-5523) and then stained with a master mix containing intracellular markers anti-mouse IL-17 APC-Cy7 (BD Pharmingen 560821), IL-22 APC (eBioscience 17-7222-80), Foxp3 PE (eBioscience 12-4774), IL-10 V450 (BD Horizon 561429), and IFN-γ Alexa 700 (557998) for 45 min. Cells were washed and maintained in sterile-flitered FACS buffer (PBS, 0.5% BSA and 0.1% NaN3) until flow cytometry analysis was performed on a LSR Fortessa (University of Michigan Flow Cytometry Core) and analyzed on FlowJo v. 10.2.

Genomic DNA extraction, amplification and sequencing

For microbial community analysis, the V4 region of the 16S rRNA gene was sequenced. Genomic DNA was extracted from fecal pellets using a PowerMagSoil DNA isolation Kit (Mo Bio Laboratories, Inc) using an epMotion 5075 liquid handling system (Eppendorf). The V4 region of the 16S rRNA gene was PCR-amplified prior to sequencing using a MiSeq (Illumina) sequencer as previously described[219,220].

Sequence processing and analysis

16S rRNA gene sequences were analyzed using mothur (v.1.39.5) and MiSeq SOP (accessed January 2018)[219,221]. Sequences aligned to the SILVA reference database were organized into operational taxonomic units (OTUs) at a 97% sequence similarity using the OptiClust algorithm[222–224]. To compare fecal community composition between control and MS diet F1 mice, relative abundances of the highest abundance OTUs (>1% of all sequences) were visualized using the R package "pheatmap" (https://cran.r-project.org/web/packages/pheatmap/index.html) and clustered using an Euclidian algorithm. To determine similarities between different samples, θYC distances were calculated using mothur followed by an analysis of similarity (ANOSIM). A biplot was generated to determine which OTUs explained the variance of the community structure between diet groups using significantly correlated OTUs to principle coordinate axes 1 and 2. This was calculated using a Spearman correlation ($P < 0.001$).

Results

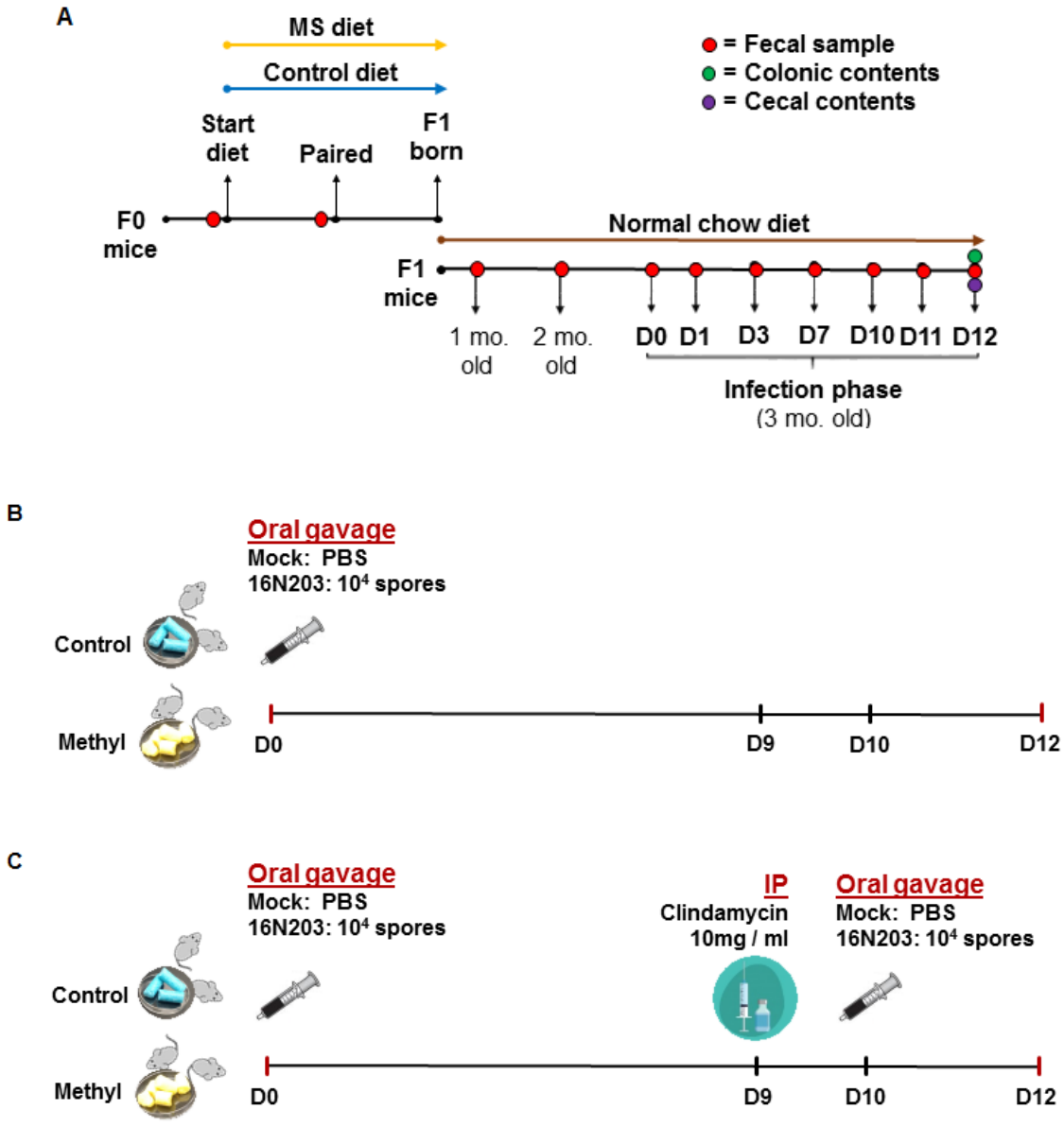

Figure 4-1 – Dietary protocol, microbiota sample collection, and infection model.
A) Dietary protocol and fecal sample collection in F0 and F1 mice. Methyl-donor supplementation (MS) diet (yellow) and control diet (blue) F0 mice were paired and post-weaning, F1 from each group were placed on normal chow diet (brown). **B**) Infection model with no antibiotic use. Control and MS diet F1 mice were partitioned into either mock-treated or 16N203 *C. difficile* infection groups and gavaged on D0 with PBS or 10^4 16N203 *C. difficile* spores. **C**) Infection model in "B" with an IP-injection of 10mg/ml clindamycin on D9 in all mice followed by an additional gavage of 10^4 spores on D10 to *C. difficile*-infection group and PBS to mock controls.

Fecal samples were collected from both F0 and F1 mice to test for diet effects on fecal microbiota composition. In F0 mice, fecal samples were collected before and after pre- and peri-natal diet administration for both control and methyl-donor supplementation (MS) diet (**Figure 4-1A**). In F1 mice, fecal samples were collected at 1- and 2-months of age prior to experimental *C. difficile* infection (CDI). Throughout the infection phase, fecal samples were collected and on day 12 (D12), colonic and cecal contents were also collected at time of tissue harvest.

At 3-months of age, the F1 mice are gavaged with 16N203 *C. difficile* 10^4 spores or PBS on D0 (**Figure 4-1B**, **Figure 4-1C**) and monitored for signs of clinical presentation of CDI. To determine MS diet effects on F1 microbial community structure, the richest abundances (>1% of all sequences) of operational taxonomic units (OTUs) in F1 fecal microbiota samples (uninfected) are determined with our 16S rRNA gene sequencing results clustered at 97% sequence similarity (**Figure 4-2**).

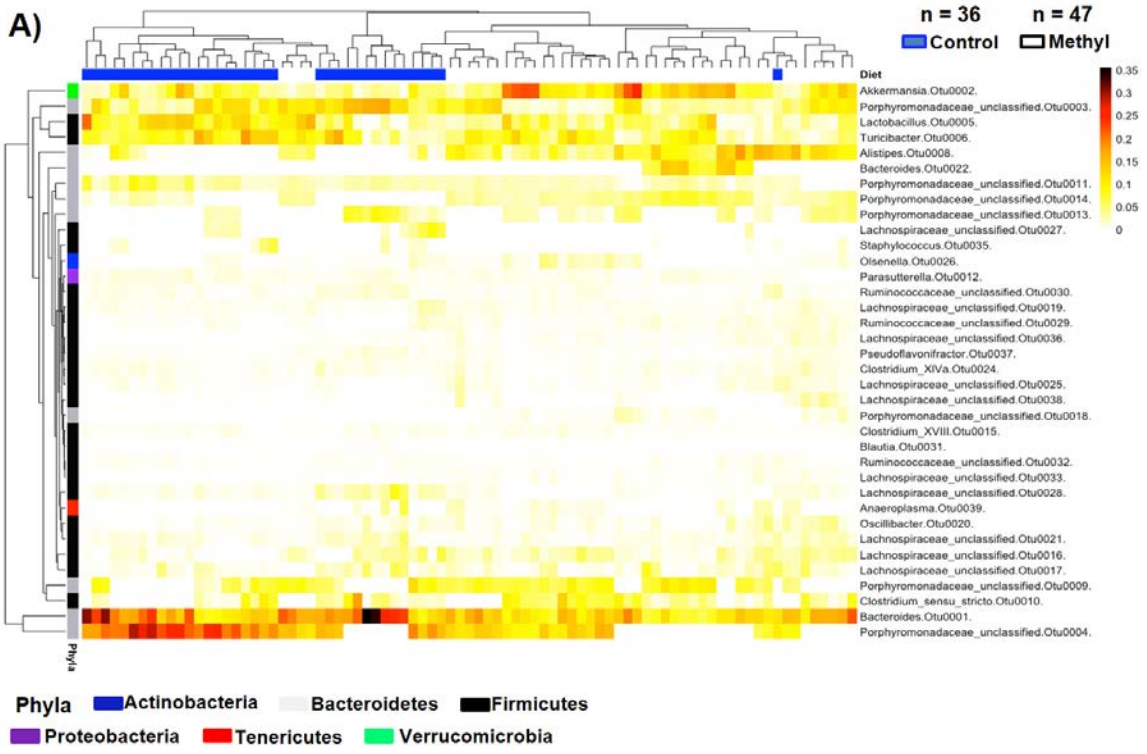

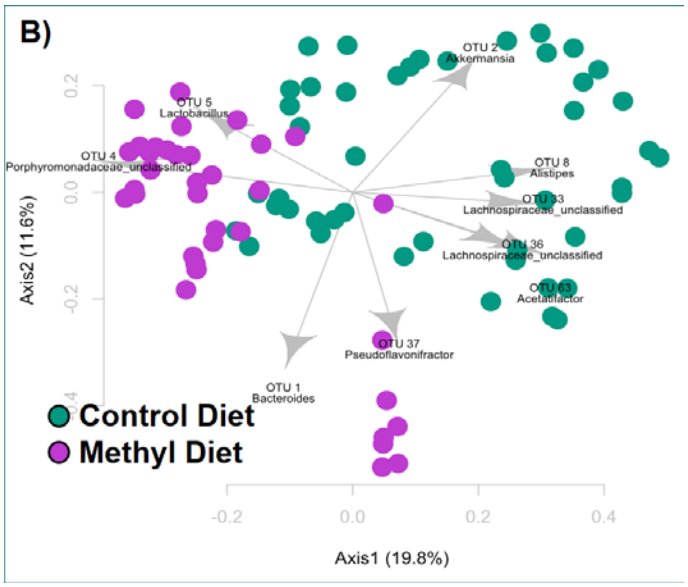

Figure 4-2 – Parental methyl donor diet intervention alters the gut microbiota in F1 mice. **A**) Relative abundances of the most abundant operational taxonomic units (OTUs) (>1% of all sequences) from fecal samples taken from F1 mice whose parents received the control diet (blue boxes) or methyl-supplementation (MS) donor diet (white boxes). Samples were clustered based on the Euclidian algorithm using the R package "pheatmap". **B**) Biplot representing community structure comparison of feces from control (teal) and MS diet (magenta) F1 mice. Principal coordinate analysis was based off of theta similarity (θ_{YC}). Arrows indicate OTUs that are significantly correlated with axes 1 and 2, and these were calculated using Spearman correlation (P<0.001). Data generated by Josie Libertucci from Young Lab.

Compared to control diet F1 mice, the MS diet F1 mice distinctly associate with different abundances of phyla in the fecal microbiota community structure (**Figure 4-2A**). We show that sequence similarity cluster F1 mice into distinct groups of control and MS diet, indicating that OTUs' abundances are distinctly different with the use of a MS diet. To identify similarities and dissimilarities associated with the pre- and peri-natal control diet versus methyl diet on F1 microbiota community, a biplot was generated via principal coordinate analysis based on theta similarity (θ_{YC}) (**Figure 4-2B**). The control diet is associated with enriched relative abundances of *Akkermansia*, *Alistipes*, *Lachnospiraceae*, and *Acetatifactor*. In contrast, the MS diet is associated with higher relative abundances of *Lactobacillus*, *Porphyromonadaceae*, and *Pseudoflavonifractor*.

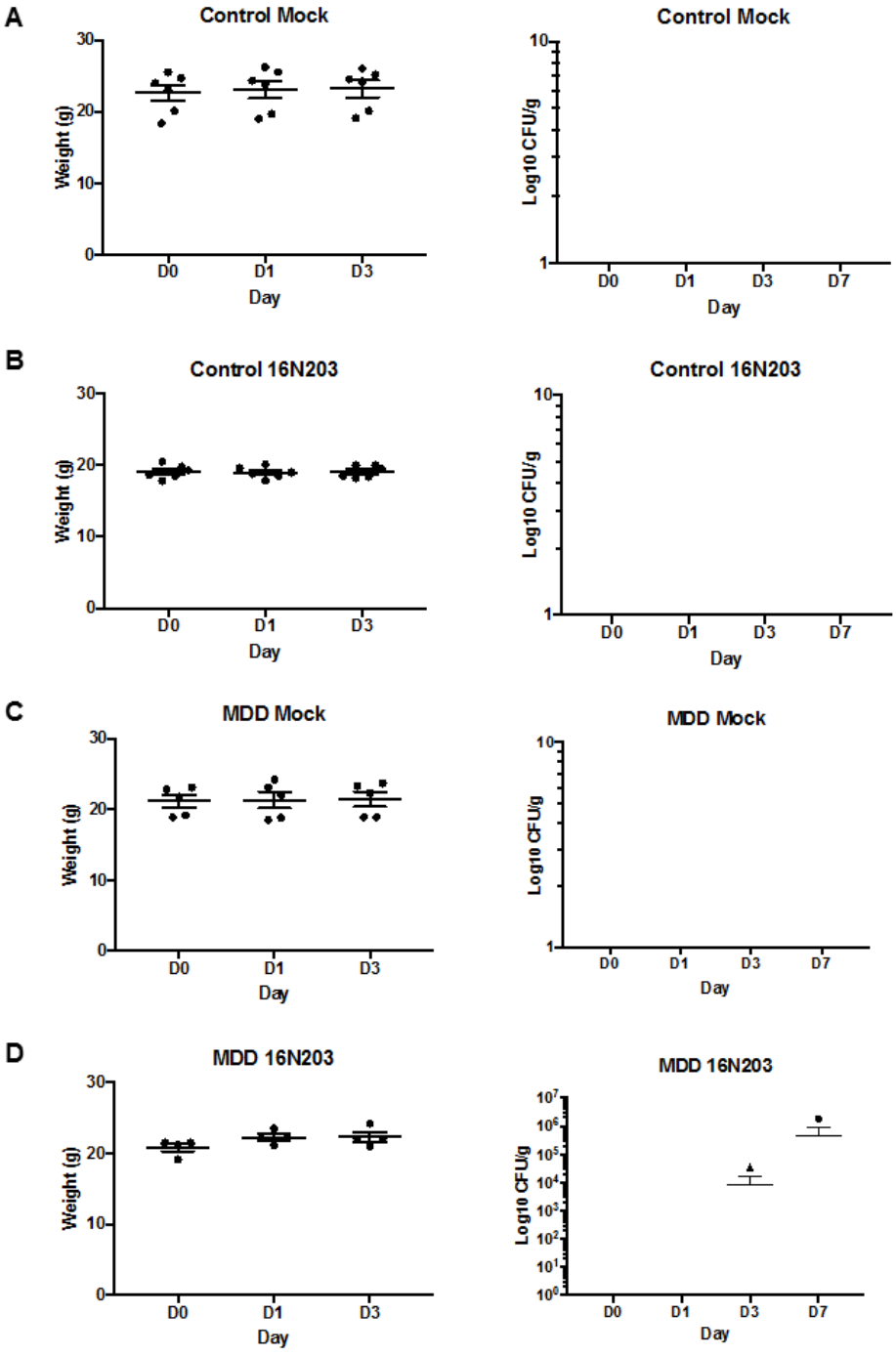

Figure 4-3 – Microbiota changes in MS diet F1 mice do not associate with changes to CDI susceptibility. Weight changes post-gavage with 10^4 spores or PBS in F1 mice and colonization detection in **A**) control diet mock-treated mice, **B**) control diet 16N203 *C. difficile* infected mice, **C**) methyl diet mock-treated mice, and **D**) methyl diet 16N203 *C. difficile* infected mice. The Kruskal-Wallis test was used to assess statistical significance, * $p<0.05$, ** $p<0.01$, *** $p<0.001$, **** $p<0.0001$. Data from this figure generated by Kim Vendrov and Josie Libertucci from Young Lab.

Interestingly, the microbiota community changes noted (**Figure 4-2**) in MS diet F1 mice (uninfected) do not associate with alterations to CDI susceptibility (**Figure 4-3**). When mice were challenged with 16N203 *C. difficile* with no pretreatment of antibiotics (**Figure 4-1B**), they do not become colonized nor develop observable symptom (weight loss) of CDI (**Figure 4-3A-C**). With exception, a single MS diet F1 mice mouse appear to become colonized by D3 and remain colonized on D7 (**Figure 4-3D**). However, this individual mouse does not lose body weight (**Figure 4-3D**) nor develop other clinical presentations (not shown) of CDI, it may have been an asymptomatic carrier.

In a separate cohort of mice, we use a standard dose of clindamycin pretreatment prior to a re-gavage with 16N203 spores (**Figure 4-1C**), we observe colonization and clinical presentation of CDI (**Figure 4-4**). On D11, fecal samples were collected and streaked on *C. difficile*-enrichment plates to determine colonization status of F1 mice. As expected, mock-treated control and MS diet F1 mice remain uncolonized, and 16N203 *C. difficile* exposed mice of both diets become highly colonized by D11 (**Figure 4-4A**). Interestingly, a subset of control diet F1 mice appears to have lower colonization than MS diet F1 mice. By D12, cecal contents are cultured to measure colonization, and both diet F1 groups were highly colonized (**Figure 4-4A**).

Clinical scores are assessed according to a previously established *C. difficile* infection (CDI) scoring system[196]. Briefly, the total clinical score of each animal is cumulative of 6 parameters including activity, posture, coat, diarrhea, eyes/nose, and weight loss scores. Mock-treated animals were free of colonization and exhibited no observable clinical phenotypes (**Figure 4-4B**). Whereas, 16N203 *C. difficile* infected mice of both diets are highly colonized, and control and MS diet mice both display CDI clinical phenotypes. Activity and posture scores are increased in MS diet mice ($p<0.001$ and $p<0.01$), total clinical scores between the two diet groups indicated no significant difference (**Figure 4-4B**).

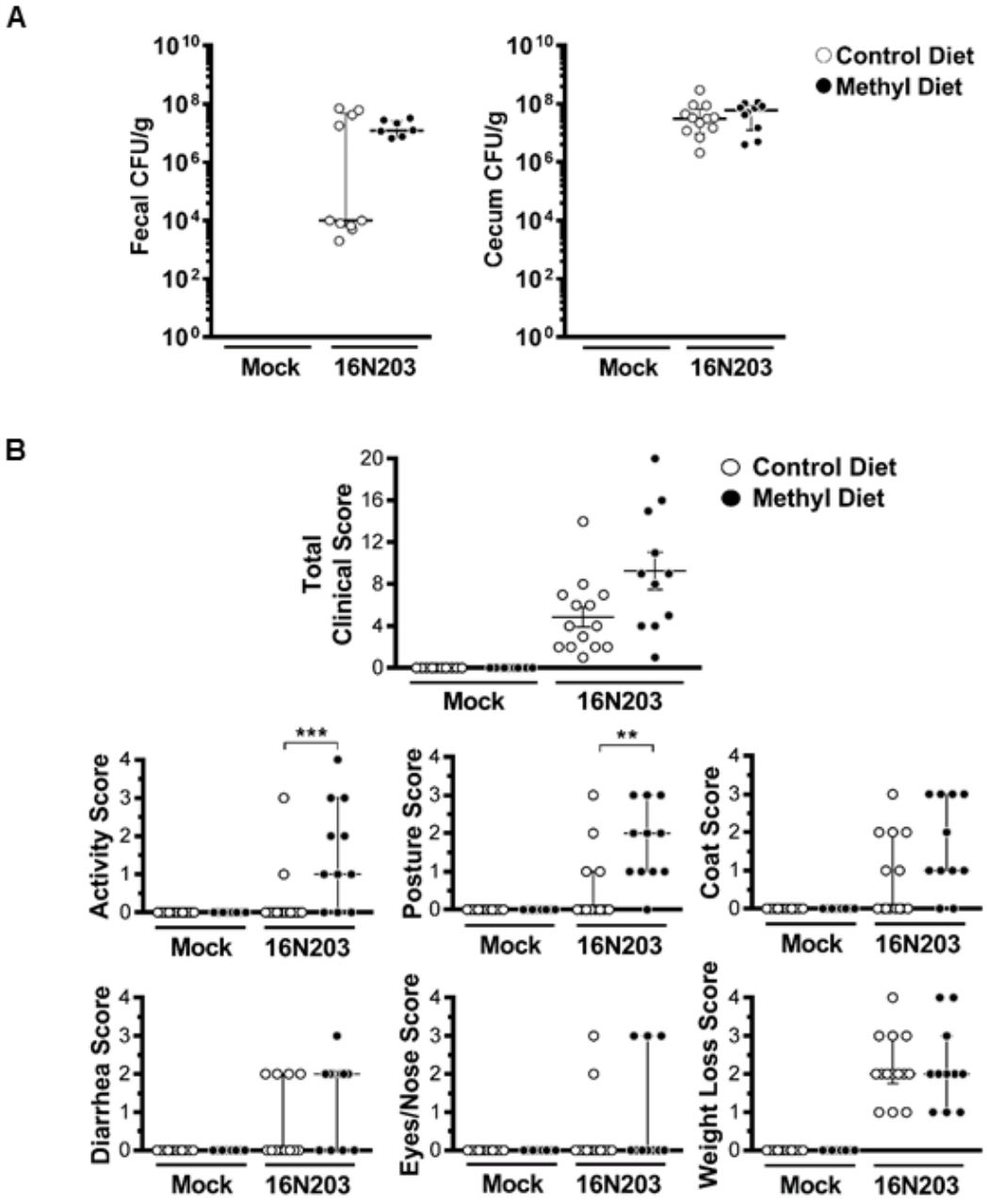

Figure 4-4 – 16N203 'outbreak' strain is pathogenic in both control and methyl F1 mice.
A) Colonization scores in pre- and peri-natal control (open circles) and MS diet (filled circles) F1 mice on day 11 in fecal samples and on day 12 from the cecum are shown on a logarithmic scale. **B**) Total clinical scores shown are cumulative of activity, posture, diarrhea, weight loss, coat, and eyes/nose scores on day 12. n=12-14 per diet/infection group. The Kruskal-Wallis test was used to assess statistical significance, * $p<0.05$, ** $p<0.01$, *** $p<0.001$, **** $p<0.0001$. Data from this figure generated by Kim Vendrov and Josie Libertucci from Young Lab.

At D12, animals were sacrificed and gastrointestinal (cecum and colon) tissues are collected for histological evaluation (**Figure 4-5**). Histological assessment of the cecum (**Figure 4-5A-D**) and colon (**Figure 4-6A-D**) indicate that 16N203 *C. difficile* led to evident submucosal edema and mucosal damage with sloughed epithelium and neutrophilic inflammation, consistent with other murine experimental *C. difficile* strains and similar to what was observed in the spontaneous outbreak from which the 16N203 strain was derived (Chapter 3). The cecum and colon summary scores were cumulative of edema, epithelial, and inflammation scores as previously described. Based on cecum and colon summary scores (**Figure 4-5E**), MS diet and control diet mice have similar CDI severity.

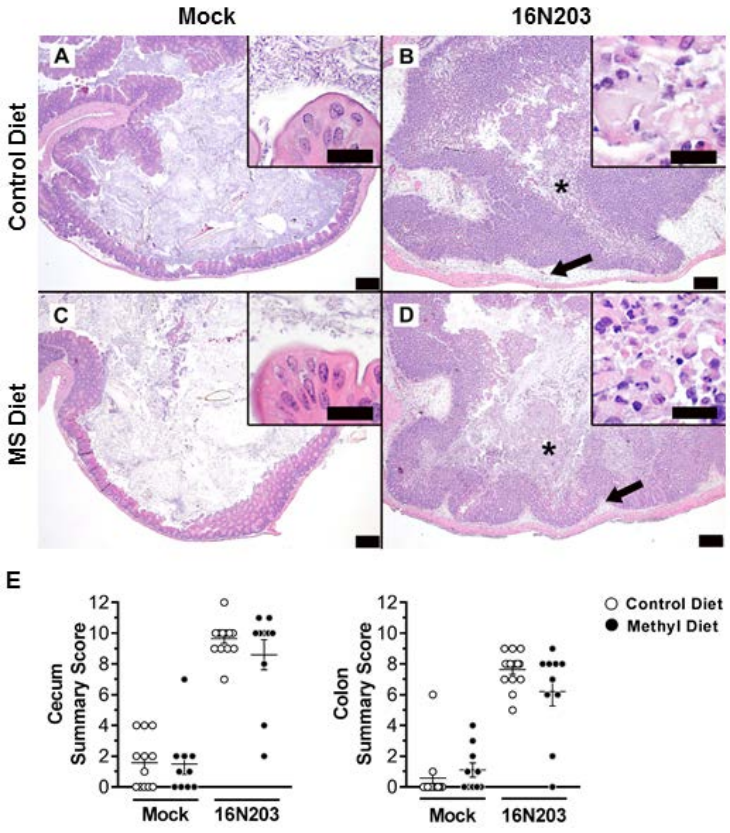

Figure 4-5 – Histopathology in the colon and cecum of 16N203 *C. difficile*-infected F1 mice. Representative histological images of cecum depict **A**) control diet/mock, **B**) control diet/16N203-infected, **C**) methyl diet/mock, and **D**) methyl diet/16N203-infected. Hematoxylin and eosin staining. Scale bars 200 µm (insets 20 µm). n=12-14 per diet/infection group. 16N203 *C. difficile* infected animals had submucosal edema (arrows) and mucosal damage (asterisks) consisting of sloughed epithelium and neutrophilic inflammation. **E**) Colon and cecum summary scores are cumulative of edema, inflammation, and epithelial scores, ranging from 0-4 per category, max=12. Ingrid Bergin, a board-certified histopathologist scored these. Kruskal-Wallis test, * $p<0.05$, ** $p<0.01$, *** $p<0.001$, **** $p<0.0001$.

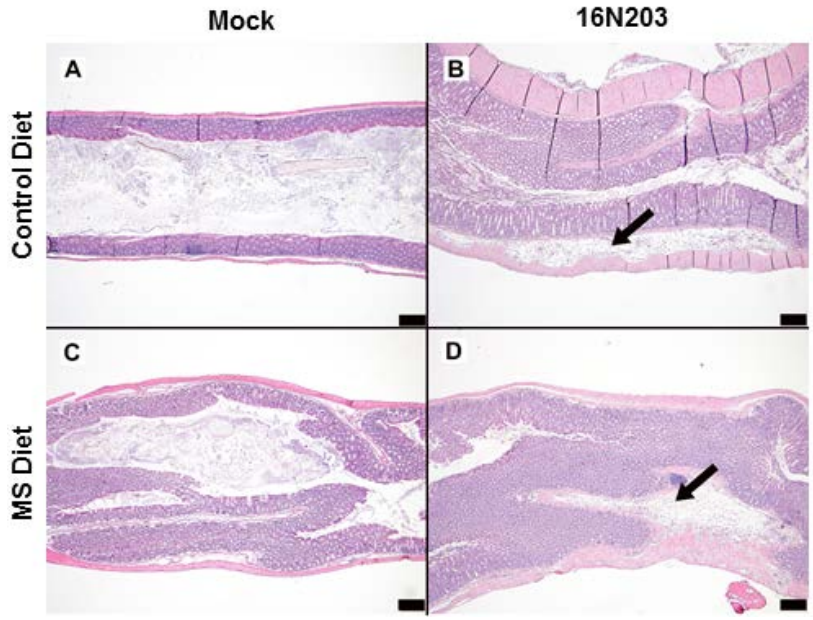

Figure 4-6 – Colon histopathology in MS diet and control diet F1 mice.
Representative histological images depict **A**) control diet/mock, **B**) control diet/16N203-infected, **C**) methyl diet/mock, and **D**) methyl diet/16N203-infected. 16N203 *C. difficile* infected animals had submucosal edema (arrows) and mucosal damage (asterisks) consisting of sloughed epithelium and neutrophilic inflammation. Insets depict higher magnification of mucosal surface. Hematoxylin and eosin staining. Scale bars 200 μm (insets 20 μm). Histopathology was assessed with n=12-14 per diet/infection group. Kruskal-Wallis test, * $p<0.05$, ** $p<0.01$, *** $p<0.001$, **** $p<0.0001$. Ingrid Bergin, a board-certified histopathologist scored these.

On D12, we also collect and perform flow cytometry analysis on total cells in the mesenteric lymph nodes (mes LN) and Peyer's patches (PP). We find that mock-treated MS diet F1 mice have higher total mes LN cells than control diet F1 mice ($p<0.05$) (**Figure 4-8A**). 16N203-infected MS diet F1 mice had higher total PP cells than controls ($p<0.05$) (not shown). We observe no differences in total CD3+ T cells in the mes LN, and there was a modest increase in the CD4:CD8 T cells in MS diet F1 mice when infected with 16N203 ($p<0.05$) (**Figure 4-8B**). Intracellular staining for CD4+ and CD8+ T cell cytokine expression of IL-10, IL-22, IL-17, and IFN-γ indicated no differences at D12, 36 hours post-infection within the mes LN (**Figure 4-8C**). We observe a small decrease in CD8+ Foxp3+ cells ($p<0.05$) with no changes in IL-10 expression (not shown). We find that mock controls and 16N203 animals had little difference—D12 (48 hours) may be too late of a timepoint for CDI immunological profiling in the mes LN.

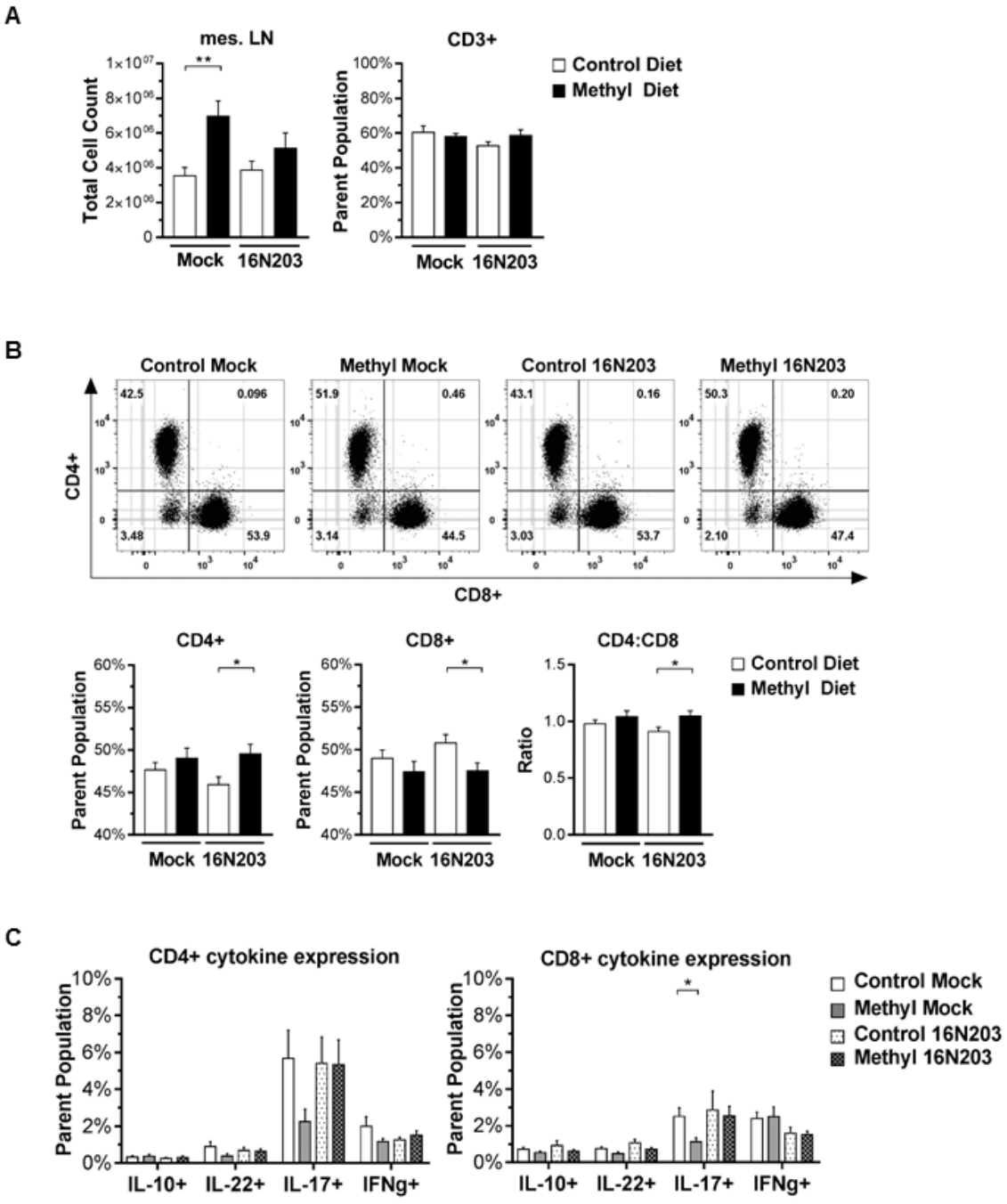

Figure 4-7 – MS diet F1 mice express higher CD4+:CD8+ T cell ratio during *C. difficile* infection. A) Total cell counts from mesenteric lymph nodes (mes LN) and total CD3+ T cells are shown between control diet and MS diet F1 mice that were either mock treated or infected with 16N203 *C. difficile*. **B**) Flow cytometry representative panel is gated on singlets > CD3+ > CD4+ (y-axis) and CD8+ (x-axis). Frequency of CD3+ cells are shown as a percentage of total singlets, CD4+ T and CD8+ T cells are shown as percentages of total CD3+ T cells. T cell ratio between CD4:CD8 is shown. **C**) Mesenteric lymph node cytokine expression of IL-10+, IL-22+, IL-17+, and IFN-γ+ were measured in CD3+CD4+ and CD3+CD8+ T cells. Error bars are SEM. Flow cytometry experiments contain n= 12-14 per diet/infection group.

A)

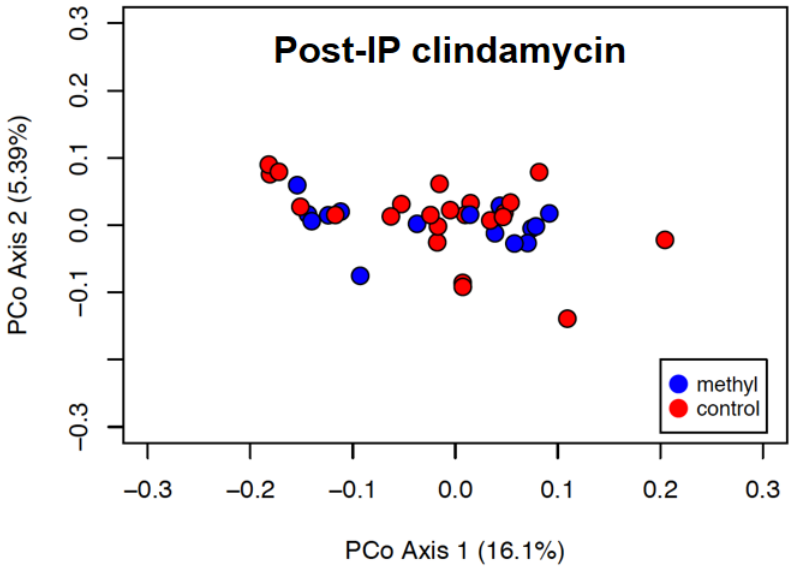

B)

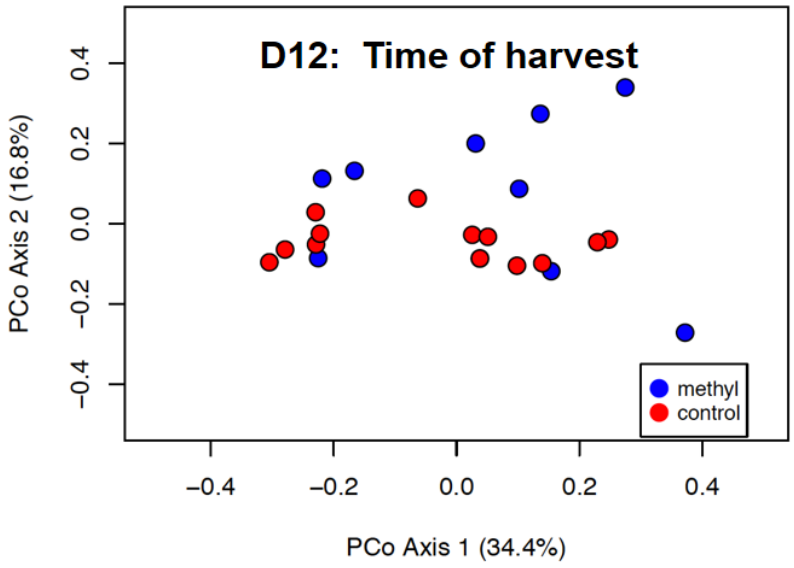

Figure 4-8 – Clindamycin flattens fecal and cecal microbiota community structure differences between control and MS diet F1 mice. Biplots representing community structure comparison of control (red) and MS diet (blue) F1 mice **A)** fecal contents on D10 post-IP clindamycin and **B)** cecal contents on D12 at the time of harvest. n=12-14 per diet/infection group. Principal coordinate analysis was based off of theta similarity (θ_{YC}). OTUs that are significantly correlated with axes 1 and 2 were calculated using Spearman correlation (P<0.001). Data generated by Josie Libertucci from Young Lab.

To determine how clindamycin may have altered fecal and cecal microbiota community structure in control and MS diet F1 mice, we compare the two diet groups on D10 (fecal) and D12 (cecal) (**Figure 4-7**). On D10, post-clindamycin injection and prior to re-gavage with 16N203 spores, a PCA indicates that clindamycin rendered both the fecal microbiota community structures in control and MS diet F1 mice to look similar. A second biplot was generated to compare cecal microbiota community structure between the two F1 diet groups on D12, showing that both F1 diet groups are not distinct from one another. Based on these data, we conclude the clindamycin pretreatment's effects on F1 diet mice fecal/cecal microbiota may contribute to the similarities observed in the CDI clinical, immunological, and histopathological outcomes between the two groups.

Discussion

Our data show the pre- and peri-natal methyl-supplementation donor (MS) diet administered to F0 C57BL/6 mice significantly alters F1 mice fecal microbiota community. The major changes we found in the MS diet F1 mice are the increases in *Lactobacillus* and *Porphyromonadaceae* and decreases in abundance of *Bacteroides*, *Akkermansia* and *Alistipes* compared to control mice. Interestingly, when challenged with the 16N203 *C. difficile* strain, MS diet F1 mice did not become colonized (with exception to 1 mouse that was asymptomatic). Additionally, our data indicate that the use of clindamycin erases the differences between control and methyl F1 diet mice, leading to similar susceptibility and severity towards 16N203 *C. difficile* as assessed by colonization and clinical scoring, gastrointestinal (cecum and colon) histopathology, and toxin quantification.

Alteration of the gut microbiota, leading to dysbiosis, is a major contributing factor to *Clostridium difficile* infection (CDI) susceptibility. As such, CDI typically occurs following multiple exposures to antibiotics, resulting in a disruption of the microbial community within the gut and therefore loss of colonization resistance[225,226]. Other environmental factors may also alter *C. difficile* susceptibility. Diet is among the environmental factors that influence CDI susceptibility. A recent report demonstrated that trehalose, a sugar present in many processed foods for humans and livestock, may have ignited the epidemic spread of *C. difficile* RT027 strains in North America[44]. In mice, excess zinc in diet alone can cause alterations to the microbiota and decrease the amount of antibiotic pretreatment to exacerbate experimental CDI[45].

Early nutrition in the form of pre- and peri- natal diet has been demonstrated to affect later life disease susceptibility in offspring[27], as such the potential impact of diet and CDI susceptibility is important to explore. For example, pre- and peri-natal methyl-supplementation (MS) diet use has been shown to alter F1 mice fecal microbiota community in such a way that exacerbates chemically-induced colitis [34,35]. This study concludes that the MS diet led to a pro-colitic microbiota, in particular, there was significantly higher abundance of *Clostridia* and *Firmicutes* accompanied by decreases in

Parabacteriodes and *Eubacterium*. In the same study, cage-swapping experiments for a fecal microbiome transfer (FMT) between MS diet, control diet, and germ-free mice was sufficient to worsen colitis in the mice that were exposed to MS diet fecal microbiota[34,35]. These studies did not venture into whether the microbial changes were associated with any immune responses.

The MS diet has been shown to affect immune responses (T cells) in an atherosclerosis mouse model[32,33]. In the current study, the modest increases to the CD4:CD8 T cell ratio in the mesenteric LNs of infected MS diet F1 mice were accompanied by no changes to CD4+ and CD8+ cytokine expression of IL-10, IL-22, IL-17, and IFN-γ. We postulate that two limitations may be the time point at which these immunological changes were assessed and the administration of clindamycin. At D12, 36-hours post-infection, mice infected with *C. difficile* had severe damage and alterations to gut structure and function as indicated by histopathology (and toxin levels). Given this context, mesenteric LNs and Peyer's patches T cells among other immune cells may be similarly aberrant and accurate measures of these cells difficult.

Our current study indicates that early-life diet intervention in the form of a pre- and peri-natal methyl-supplementation donor diet can alter the F1 microbial community structure. Changes in progeny microbiota is sustained rather than transient as community structure was evaluated in sexually mature adult mice. When challenged with 16N203 *C. difficile* prior to and following antibiotic administration, these changes in community structure did not result in altered colonization resistance nor clinical outcomes compared to control diet F1 mice. 16N203 is a ribotype 027 (RT027) *C. difficile* strain isolated from a spontaneous outbreak in a mouse colony that was associated with the administration of the MS pre- and peri-natal diet. During the outbreak, MS diet F1 mice succumbed to CDI at significantly higher numbers than control diet F1 mice (Chapter 3). Standard CDI mouse models rely on antibiotic disruption of the microbiota to enable colonization and disease. We postulated the MS diet alters F1 mice microbiota and possibly gut immune responses, and these changes, if true, may explain increased susceptibility in the outbreak.

In this current study, under experimental exposure of the 16N203 *C. difficile* strain to control and MS diet F1 mice, we found that parental diet does alter F1 microbiota. However, at the dosages we tested, 16N203 *C. difficile* did not colonize MS and control diet F1 mice until a dose of clindamycin was administered. The concentration of clindamycin that was used (10mg/ml) enabled CDI in this study but not a previous study[42]. In this study, clindamycin administration essentially led to a flattening of the microbiota diversity and erased differences between control and MS diet mice. Unsurprisingly, this led to very similar clinical outcomes in both diet groups. If a reduced concentration was used, this could have better tested microbial alterations that may have led to the differing CDI severity between control and MS diet F1 mice reported in the outbreak.

Our study was limited in that the clindamycin prescribed in infection model B was sufficient to enable colonization and disease which is not the case in a different study using the same strain. However, this parallels many recent studies[227–230] that show the microbiotas between colonies of the same strain of mice are different from various vendors can severely affect reproducibility. We postulate that it is also possible that the outbreak of 16N203 *C. difficile* in the mouse colony were mice from a different vendor-barrier, the microbiota of those mice may have interacted differently with the diet manipulation than the mice in this current study. These results provide support for continuing investigation of the relationship between parental diet intervention and susceptibility to *C. difficile* infection in offspring. Very little is known regarding the interactions between *C. difficile* and dietary alterations, microbiota composition, and host responses. Improved knowledge of how dietary factors influence gut microbiota structure and function could lead to a better understanding of *C. difficile* pathogenesis and may create potential for diet-based prevention strategies.

Chapter 5 – Methyl-donor supplementation diet does not protect C57BL/6J F1 mice from later-life diet-induced obesity

Abstract

Early-life nutritional programming influences late-life disease susceptibility across generations[1,2,19], in part through epigenetic mechanisms including DNA methylation. It has been shown that pre- and peri-natal diet rich in methyl-donor supplements (L-methionine, vitamin B-12, folic acid, choline, betaine, zinc) can protect the agouti viable yellow (A^{vy}) mouse from obesity[18] and cancer[24]. In other mouse models, this methyl-donor supplementation (MS) diet affect F1 host responses to disease in different ways[34,35,231]. We have previously shown the MS diet reduces T-cell mediated inflammation in a mouse model of spontaneous atherosclerosis[32,33]. In the same study, we noted that MS diet F1 C57BL/6J mice were born smaller and maintain these leaner body sizes into adulthood[33]. Here, we hypothesize the MS diet may resist the harmful effects of diet-induced obesity in F1 C57BL/6J mice through suppression and reduction of adipose tissue inflammation. Our results suggest that the MS diet does not alter obesity nor metabolic inflammation outcomes we measured in C57BL/6J F1 mice.

Introduction

The immune system develops extensively *in utero*[232–236], and maternal-fetal interactions are important for determination of immunity and tolerance[237,238]. As early as the 2nd trimester, the developing fetus gains a functional immune system that differs from adult immune system[239]. It has been shown that altering the developmental environment with maternal pre- and peri-natal methyl-donor diets can influence the establishment of epigenetic states during tissue differentiation in a developing fetus[20,23,25,240]. Methyl-donor diets influence the methylation process by enhancing the S-adenosylmethionine (SAM) pool which is an intermediate product of methionine metabolism[17].

In humans, folic acid supplementation has been used (since mid-1970s) to prevent fetal neural tube defects which are believed to partially occur due to insufficient methylation during development[241]. Methyl-donor supplements that have been used in mouse studies as a pre- or peri- natal diet typically include combinations of folate, choline, betaine, and vitamin B12[27]. The methyl-donor supplementation (MS) diet protects agouti viable yellow (A^{vy}) mouse offspring from developing obesity and tumors, thereby also extending their lifespan[18,23,24]. This is a classic demonstration of non-genomic inheritance of epigenetic marks and of early-diet's capacity to inflict later-life health outcomes. However, agouti viable yellow (A^{vy}) mice spontaneously develop obesity and tumors as a result of ectopically expressing *agouti* due to a retrotransposon insertion[25]. Therefore, it is important to determine whether these benefits of the MS diet are unique to the agouti viable yellow (A^{vy}) mice or useful beyond this model.

In our previous studies using the MS diet, we observed that compared to the control diet, MS diet F1 C57BL/6J mice were born smaller and maintain these leaner bodies into young adulthood[33]. C57BL/6J mice do not spontaneously develop obesity like the agouti viable yellow (A^{vy}) mice. Therefore, to test if the MS diet can protect C57BL/6J F1 mice from obesity, in this study, we challenged control and MS diet F1 mice with a normal diet (ND) or a 42% high fat diet (HFD). In order to determine if the MS diet protects F1 mice from obesity and diet-induced metabolic dysfunction, we assess adipose tissue inflammation in the gonadal white adipose tissue (WAT).

Inflammation in diet-induced obesity (DIO) is termed 'metaflammation.' It is a chronic, low-grade inflammation that has been attributed as the inflammatory pathogenesis of diet-induced metabolic dysfunction[242]. Adipose tissue inflammation is an especially crucial driver of metaflammation given the capacity and penchant of adipocyte and adipose tissue resident immune cells' secretion of pro-inflammatory mediators[51,59–61,63–66,69,70,75,77] during obesity. In particular, tumor necrosis factor-α (TNFα) produced by adipose tissue macrophages (ATMs) during metaflammation has been demonstrated to interfere and block insulin signaling, revealing part of the

molecular mechanism to insulin resistance[51]. ATMs in obese adipose tissue have been considered a major player in adipose tissue inflammation, as they are major constituents in the tissue and have shown to phenotypically 'switch' towards pro-inflammatory M1-polarized ATMs in DIO mouse models[60,61].

Materials and Methods

Animals and housing

C57BL/6J 8-week old mice were purchased from Jackson Laboratories (Jackson West RB08; Sacramento, CA). During the breeding and dietary intervention phase, all mice were housed under specific-pathogen free conditions in biosafety level 1 rooms maintained by the Unit for Laboratory Animal Medicine. During the experimental infection phase, mice were transferred to animal biosafety level 2 rooms where procedures were performed under a biosafety cabinet using a sporicidal disinfectant cleaner (Perisept, Triple S 48027). All procedures with animals and their care are approved by the University of Michigan Institutional Animal Care and Use Committee.

Dietary Study

In the initial dietary study, young adult (8 wk) C57Bl/6 mice were purchased from Jackson Laboratories. All custom diets "TD" are produced and distributed by Harlan-Teklad (Madison, WI). Mice were acclimated for 2 weeks before feeding either control (TD.06689) or methyl-donor supplementation (MS) diet (TD.110144). The MS diet contained 12g/kg methionine, 16.5 g/kg choline, 15 g/kg betaine, 16.5 mg/kg folic acid, 1.56 mg/kg vitamin B12, and 200 mg/kg Zn. Two weeks after starting diet, female and male mice were paired for mating. Mated F0 mice were fed the diet throughout pregnancy and lactation. F1 mice were weaned at 28 days. The F1 mice were then placed on a standard chow diet (PicoLab Laboratory Rodent Diet 5L0D, LabDiet, St. Louis, MO) or a 42% high-fat diet (HFD) (TD.88137).

Glucose tolerance test (GTT) and insulin tolerance test (ITT)

Mice were transferred to clean cages with water for a 6-hour fast. A 100mg/mL D-glucose solution was made in sterile -/- DPBS. Mice were weighed before experiment

to calculate and record the volume of 10% glucose solution required (0.7g/kg body mass of glucose) for IP injections. The volume of IP glucose injection (μl) =7 x body mass (g). The first drop of blood (approved, minimal tail snip) was discarded and a small drop of blood is placed on the test strip of an animal blood glucose meter (Abbott Alpha TRAK 2 Blood Glucose Monitoring System) to record the fasting glucose level (t=0). Mice were restrained with an approved and trained method of scruffing. Appropriate amounts of glucose were injected into the peritoneum as calculated. The blood glucose levels were measured at 0 (before),15, 30, 60, 90, and 120 minutes following glucose injections and recorded. At the end of the experimental session, mice were placed in former cages.

Insulin tolerance tests were similarly carried out but with insulin solution (Humulin R, functional concentration: 1 unit/kg of body mass). For smaller mice (mice on ND), a 1:1000 dilution of the insulin stock was used (100mU/mL), and for larger mice (mice on HFD), a 1:500 dilution of the insulin stock was used (200mU/mL). If glucose measure falls below 25 mg/dL and/or the animal had significant activity/mobility decrease (responsiveness to a gentle finger prod), assay was immediately aborted, and the animal was injected with a dose of glucose. GTT and ITT tests were carried out ≥7 days apart from one another to allow animals adequate recovery.

Tissue extraction: gWAT stromal vascular fraction

Gonadal white adipose tissue (gWAT) is removed with minimal cuts, weighed, and placed into a sterile petri-dish containing ice cold dye-free Dulbecco's Modified Eagle Medium (DMEM) containing 10% FBS (Gibco 21063-029) and 1% Penicillin Streptomycin (Gibco 15140-122). Collagenase (Sigma Life Science, #C6885-1G) is prepared in DMEM buffer with a final 10mg/mL concentration. gWAT fat pads were minced, gently passed through 100 μm filter, centrifuged (1500 RPM), and collagenase-digested in an 37° C incubator for 45 min with rotation. A second rinse-filter step follows. ACK lysis (Lonza, #10-548E) is mixed into cell pellets and neutralized at 5 minutes with ice cold PBS. A third rinse-filter step occurs with cold PBS. SVF cell fractions are resuspended in 1 mL of cold PBS and 10 μl is saved for trypan blue (Invitrogen) cell counting using the Cell Countess (Invitrogen).

Isolation of lymphocytes and cell counting

Lymph nodes (inguinal, brachial, axillary, and superficial cervicals) were excised, collected through a 70 µm filter, and washed with ice cold buffer (5% fetal bovine serum (FBS), 0.4% EDTA in PBS) prior to centrifugation (3000 RPM, 5 min.) to form a cell pellet. The supernatant was discarded and RBC depletion was performed with ACK (Lonza, #10-548E) and washed through a 70 µm filter to neutralize ACK. After rinse and resuspension in cold sterile PBS buffer, 10 µl aliquots of each sample was used for a cell count using Trypan blue paired with an automated cell counter (Invitrogen Countess 1754B).

Flow cytometry stains

SVF cells extracted from gWAT are washed and resuspended in sterile filtered FACs buffer (PBS, 0.5% BSA, 0.1% NaN3) and cells per sample are pooled together to form the control cells for Single Positive Controls (SPCs), Full-minus-one Controls (FMOs), and the negative cells. Samples are blocked with anti-mouse CD16/CD32 (eBioscienceaffymetrix #14-0161) for 1 hr on ice. After rinsing, cells are incubated with anti-mouse CD45 (eBioscienceaffymetrix #48-0451), CD64 (BD Pharmingen 558455), CD11c (eBioscienceaffymetrix #47-0114), and CD206 (eBioscienceaffymetrix #17-2061) for 1 hr on ice, in foil. Cells were fixed with 2% paraformaldehyde (PFA) for 20 min on ice prior to washing and storing in FACs buffer until analysis. Samples were run on a LSRFortessa (University of Michigan Flow Cytometry Core) and analyzed on FlowJo version 10.0.0.1.

mRNA isolation and RT-qPCR

Total RNA was isolated from whole adipose tissue (gonadal / inguinal depots), homogenized in Qiazol lysis reagent (Qiagen, #1023537), and processed through a QIAshredder (Qiagen, #79656) prior to using the RNeasy Lipid Tissue Mini Kit (Qiagen, #1023539) in conjunction with a RNase-Free DNase (Qiagen, #79254) digestion step. Reverse transcription and cDNA amplification was performed with QuantiTect SYBR

Green RT-PCR Kit (Qiagen, #1054498) on a real-time R6-6006 Corbett Thermalcycler. All primers were obtained from IDT and specific primer sequences are listed (Table 1.1).

Western blot

Briefly, whole gWAT protein lysates were mixed with 4x Laemmli (Biorad #161-0737), denatured, loaded at 40 μg per well into 15-well 4-20% gel casts (Biorad Mini-PROTEAN TGX Precast Gels, #456-1096) and ran at 90V in a Tris/Glycine/SDS buffer. It was transferred to a PVDF membrane (BioradImmun-Blot, #1620177) in a Tris/Glycine/20% MeOH buffer at 100V. Then, it is rinsed with TBS / 0.1% tween and blocked (Thermo Scientific Superblock T20, #37536) for 1 hr at RT on rotator. Primary antibody (CHOP (anti-DDIT3 Abcam ab179823), P62 (Abcam ab9691526), or IgG (goat anti-mouse IgG-HRP Santa Cruz sc-2031), a-tubulin (Abcam ab18251)) is administered overnight in a 4°C cold room. Blots were washed 3x 10 min with TBS / 0.1% tween prior to incubation with secondary antibody (in 5% non-fat milk powder in TBS/tween) for 30 min at RT on rotator. Chemiluminescence is captured via Pierce ECL Western Blotting Substrate (Thermo Scientific, #32106) on Image Quant LAS 4000 (GE Healthcare) machine. Densitometry is calculated with ImageJ software.

Results

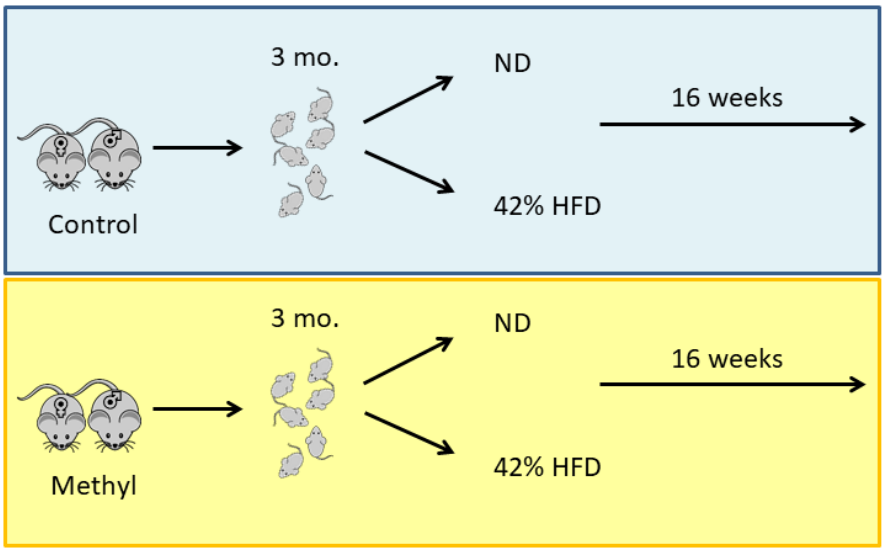

Figure 5-1 – Dietary and breeding protocol of methyl-donor supplementation diet study. F0 mice are placed on either a control or methyl-donor supplementation diet prior to and throughout breeding and lactation. Post-weaning, F1 mice are placed on normal chow diet until 3 months of age where they are either maintained on a normal chow diet (ND) or challenged with a 42% high fat diet (HFD) for 16 weeks. Following this, metabolic tests (glucose and insulin tolerance, and fasting insulin) commence and are spaced 1 week apart. Mice are sacrificed 1 week after at the age of 8-9 months old.

We placed C57BL/6J mice on either a control or methyl-donor supplementation (MS) diet prior to and throughout breeding (**Figure 5-1**). F1 mice generated from these two diet groups are then further separated into normal diet (ND) or a 42% high fat diet (HFD) challenge group three months post-weaning. After 16 weeks of HFD challenge, the metabolic assays including glucose and insulin tolerance tests begin. At ~8-9 months of age, F1 mice were sacrificed and the total body mass, gonadal white adipose tissue (gWAT) mass, and inguinal white adipose tissue (iWAT) mass were recorded (**Figure 5-2**). We found no differences between all adipose tissue masses recorded between the control and MS diet F1 mice from 3 sets of mice. After 16 weeks of HFD, MS and control diet F1 mice were challenged with glucose and insulin (7 days later) to assess glucose (**Figure 5-3**) and insulin (**Figure 5-4**) tolerance. Control and MS diet F1 mice of either gender do not have altered glucose tolerance test (GTT) nor insulin tolerance test (ITT) responses. There is a modest decrease in blood glucose during a GTT in MS diet F1 female mice compared to controls, though this trend does not reach significance.

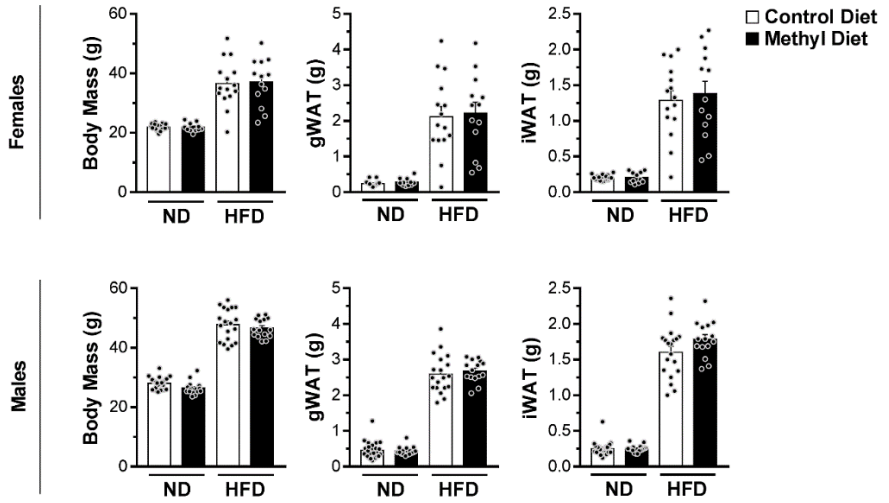

Figure 5-2 – Methyl-donor supplementation diet exposure does not alter F1 mice adiposity in response to diet-induced obesity challenge. Whole body mass, gonadal white adipose tissue (gWAT), and inguinal white adipose tissue (iWAT) were collected. For females, across 3 sets of mice, n=11-19 per group. For males, n=16-25. Open/white columns are F1 mice generated from control diet F0 and filled/black columns are F1 mice generated from MS diet F0. All values plotted as mean ± SEM.

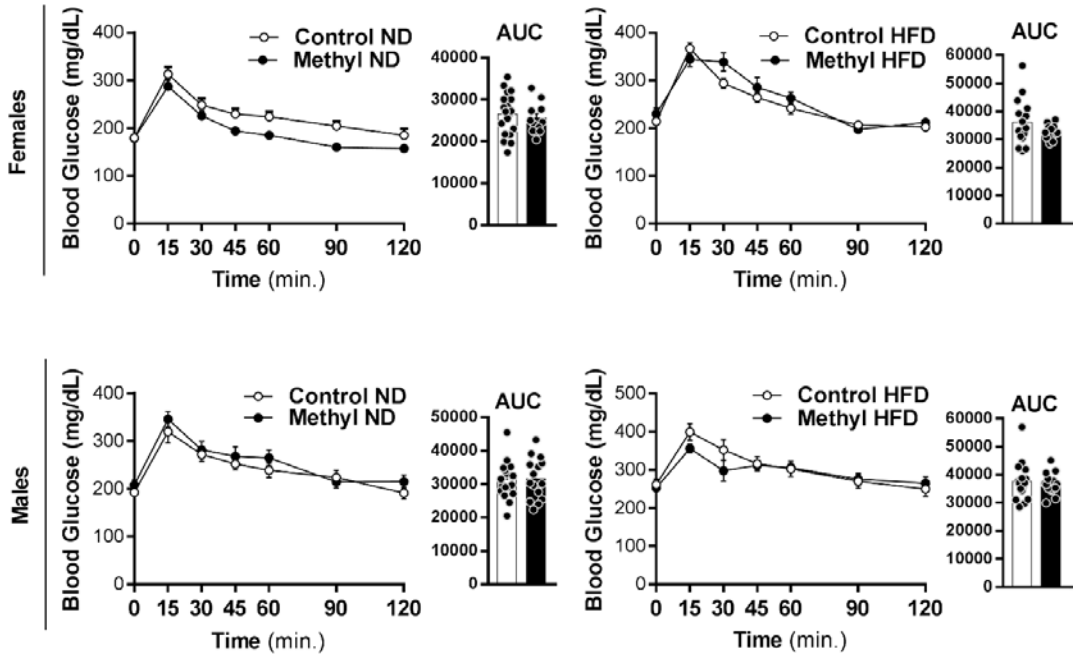

Figure 5-3 – MS diet does not alter glucose tolerance test in F1 mice. (Top row) Female C57BL/6J mice were assessed with a glucose tolerance test and blood glucose was tracked over the course of two hours. (Bottom row) Male C57BL/6J mice were assessed with a glucose tolerance test and blood glucose was tracked over the course of two hours. Area under the curve (AUC) calculations are adjacent to corresponding graphs plotted as mean ± SEM. For females, across 3 sets of mice, n=11-19 per group. For males, n=16-25. Open/white dots are F1 mice generated from control diet F0 and filled/black dots are F1 mice generated from MS diet F0.

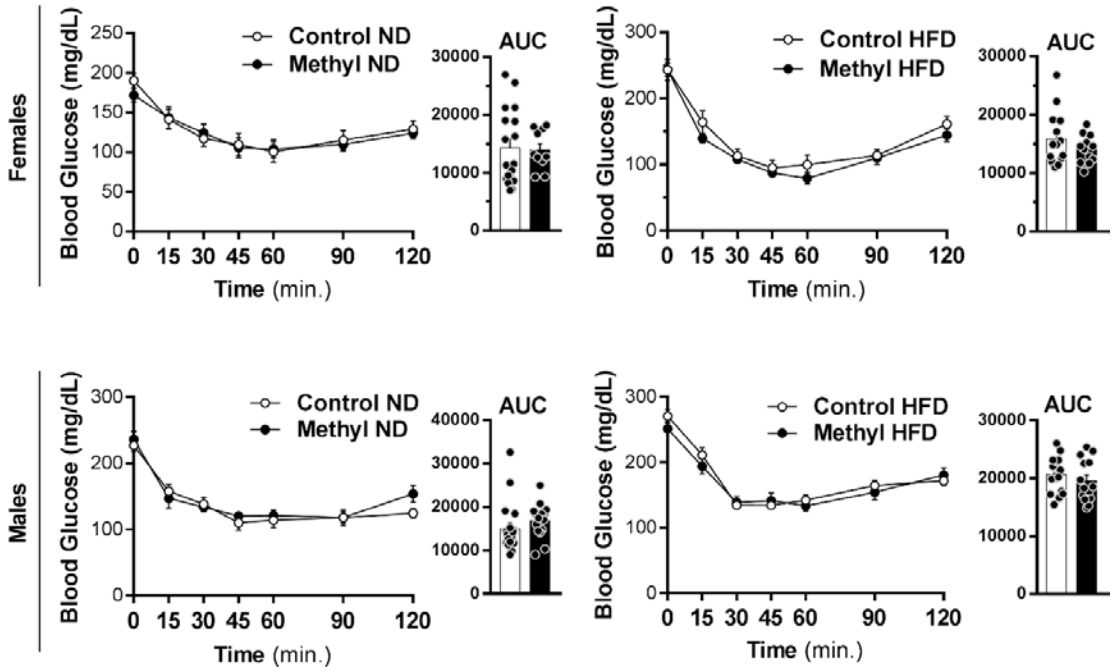

Figure 5-4 – MS diet does not alter insulin tolerance test in F1 mice. (Top) Female C57BL/6J mice were assessed with an insulin tolerance test and blood glucose was tracked over the course of two hours. (Bottom) Male C57BL/6J mice were assessed with an insulin tolerance test and blood glucose was tracked over the course of two hours. Area under the curve calculations plotted as mean ± SEM. For females, 3 sets of mice, n=11-19 per group. For males, n=16-25.

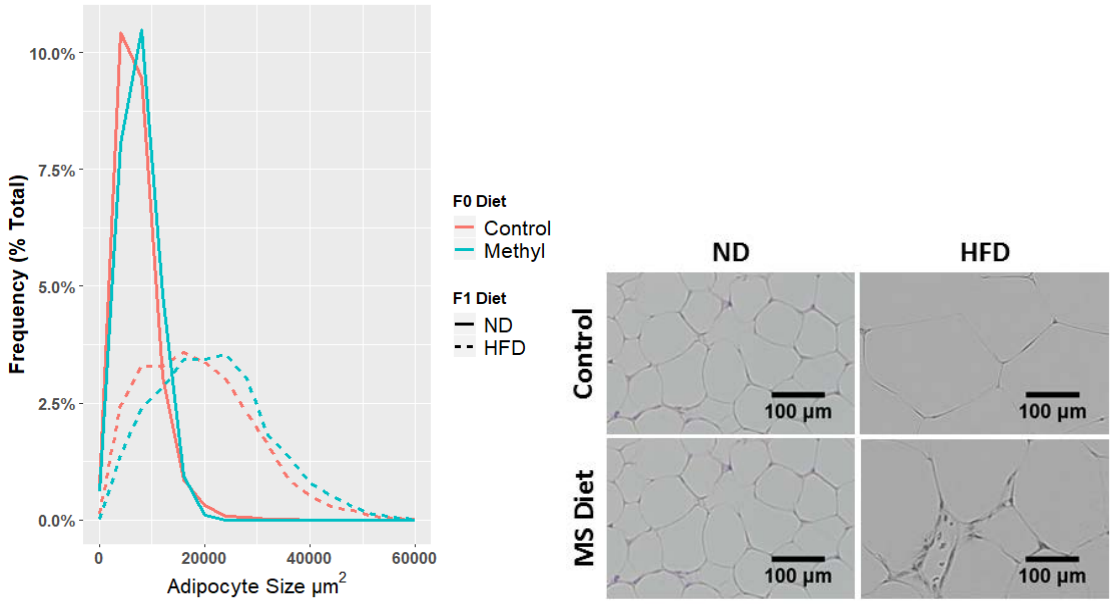

Figure 5-5 – Methyl-donor supplementation diet exposure does not alter F1 mice adipocyte size distribution. 8-9 month old C57BL6/J mice fed 42% HFD for 16 weeks were sacrificed and gWAT was fixed, sectioned and adipocytes were counted. Adipocyte distribution was graphed and visualized on R (left). H&E stained samples were used for counting and no sex difference was present. Representative images visualized on ImageJ (right). For females, across 3 sets of mice, n=7-18 per group. For males, n=15-19 per group. Figures generated by Martin O'Brien.

Adipocyte sizing analysis indicates that MS diet F1 mice do not have altered adipocyte size distribution (**Figure 5-5**). We collected stromal vascular fraction (SVF) cells from the gWAT to assess adipose tissue macrophage frequency by flow cytometry (**Figure 5-6**). MS diet appears to not affect leukocyte ($CD45^+$) frequency (**Figure 5-6A**). Similarly, adipose tissue macrophage subset (M1: $CD45^+CD64^+CD11c^+CD206^-$ and M2: $CD45^+CD64^+CD11c^-CD206^+$) frequencies in F1 mice are unaffected (**Figure 5-6A-B**). We next measured mRNA of *Il6, Tnfα,* and *Mcp1* in whole gWAT and also observe no significant differences between control and MS diet F1 mice (**Figure 5-7A-B**). We found in male mice, MS diet led to higher AKT expression in F1 mice on normal diet compared to control diet ($p<0.01$), and we did not find any significant differences in AKT protein expression in female mice (**Figure 5-8**).

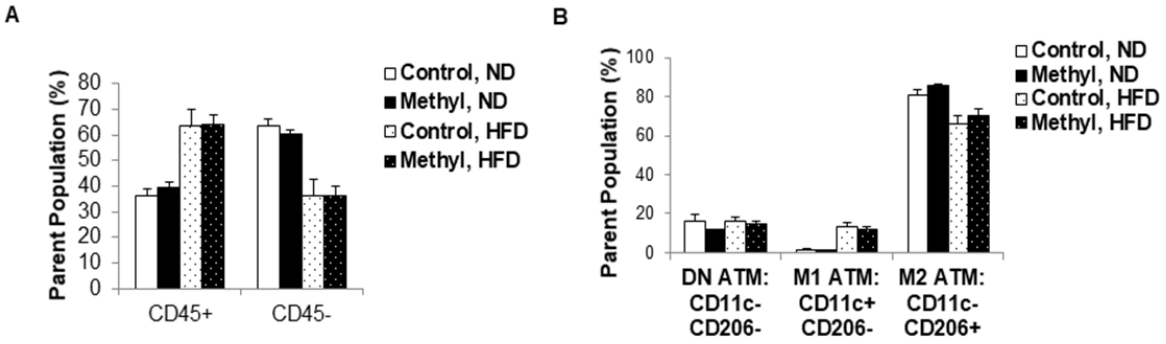

Figure 5-6 – MS diet does not alter adipose tissue macrophage composition in F1 mice. Gonadal WAT stromal vascular fraction cells were extracted and stained for adipose tissue macrophages. A) CD45+ and CD45- cells reported as a percentage of parent population. B) Adipose tissue macrophages (CD45+CD64+) were reported in either CD11c+CD206- "M1" or CD11c-CD206+ "M2" as a percentage of parent population. All values are graphed as mean ± SEM. Flow cytometry data shown is 1 experiment with female mice n=4-6 per group and reflects trends in 3 other repeat-experiments with male and female mice.

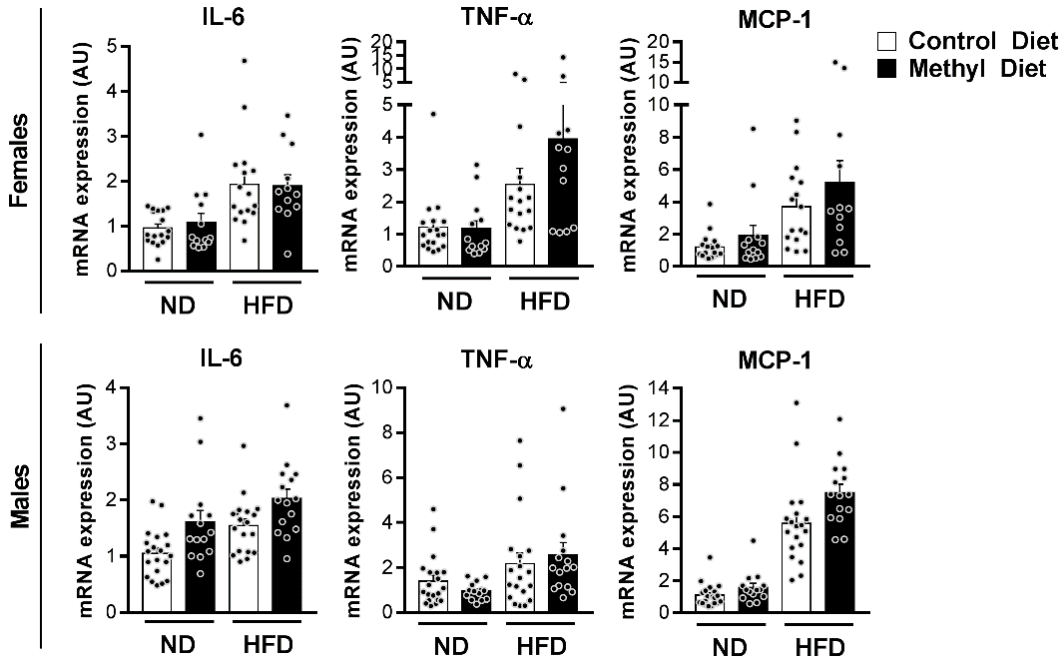

Figure 5-7 – Expression of pro-inflammatory cyto- and chemo-kines in gWAT. mRNA expression of *Il6*, *Tnfα*, and *Mcp1* were assessed in gonadal WAT of **A**) female and **B**) male F1 mice on either normal (ND) or high fat diet (HFD) with either an F0-diet background of control or methyl-donor supplementation (MS) diet. For females, across 3 sets of mice, n=11-19 per group. For males, n=16-25. Open/white bars are F1 mice generated from control diet F0 and filled/black bars are F1 mice generated from MS diet F0. All values reported as mean ± SEM.

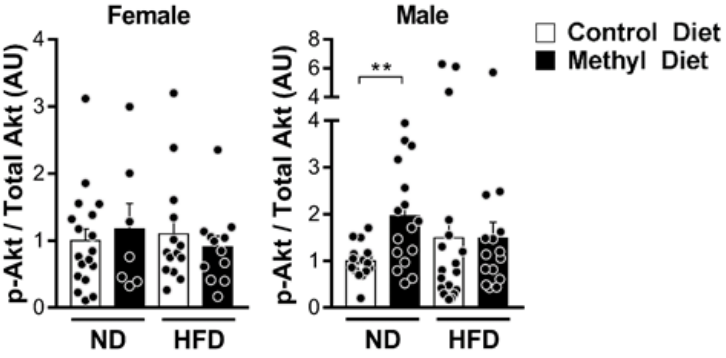

Figure 5-8 – MS diet male F1 mice on normal diet have increased p-Akt. Whole gonadal white adipose tissue protein lysates were used to measure phosphorylated-Akt in control and MS diet F1 mice. For females, across 3 sets of mice, n=7-18 per group. For males, n=15-19 per group. Open/white bars are F1 mice generated from control diet F0 and filled/black bars are F1 mice generated from MS diet F0. All values reported as mean ± SEM.

Discussion

In the classic agouti viable yellow (A^{vy}) mouse, the methyl-donor supplementation (MS) diet protects F1 mice from obesity and tumor development. In another *agouti* mouse study, it was reported that the MS diet can protect from bisphenol A (BPA)-induced hypomethylation in F1 mice. This study is considered an important demonstration of an environmental-stress biosensor mouse model[21], but it should be noted that a different study could not repeat these findings[26]. We have previously reported that the MS diet in C57BL/6J mice are born smaller and maintain smaller bodies into adulthood[33]. In this study, we tested if the MS diet can protect F1 mice from diet-induced obesity (DIO) and found that the MS diet does not protect F1 mice from DIO nor obesity-associated metabolic function and adipose tissue inflammation.

We observe that the MS diet F1 mice of both sexes had similar body and fat pad (gonadal and inguinal) masses to that of control diet F1 mice. Glucose and insulin tolerance tests indicate that both diet F1 mice were similarly affected by the 42% high fat diet. There was some indication that the MS diet could be protective in female mice, but the modest decrease of glucose tolerance response in MS diet F1 mice fed the normal diet (ND) was absent in MS diet F1 mice fed the 42% high fat diet (HFD). Our GTT and ITT experiments indicate that the metabolic function between MS and control diet F1 mice were similar under both ND and HFD feeding conditions. We analyzed the adipose tissue and found that the macrophage subset proportions were also similar between the two pre- and peri-natal diet F1 mice. Interestingly, we saw a moderate increase in AKT protein expression in MS diet male mice fed the ND, but without changes in other measured parameters, we are unable to make a conclusive interpretation of this difference.

Previous studies have shown that a similar methyl-donor diet (with an addition of genistein and lower methionine) can be protective in the context of gestational diabetes or HFD intake during pregnancy[243,244]. One study showed some evidence that C57BL/6J pregnant dams fed a 60% HFD during gestation leads to obesity and obesity-associated adverse effects in F1 mice that could be mildly reversed if the HFD had methyl-donor

supplementation[243]. They also report that a control diet infused with MS diet led to smaller C57BL/6J pups being born[243], similar to what we have reported[33]. However, the study did not yield many useful conclusions as the data analyses seemed inappropriately executed (they compared F1 mice from dams fed control + MS to F1 mice from dams fed HFD + MS rendering it impossible to interpret if MS diet protects F1 from HFD intake during gestation—but they claim that it does). A subsequent study performed by another group aimed to repeat and clarify these experiments using an identical MS diet as the first study, but they also elected to use a 45% HFD instead[244]. Their rationale behind the HFD switch was primarily because 60% HFD is abnormally high and may be testing an extreme form of overnutrition. This study reported highly significant and beneficial differences between F1 mice derived from HFD dams and the F1 mice from HFD + MS diet dams. F1 mice from the latter are born with similar body masses but do not gain weight like their HFD F1 mice and have improved metabolic parameters in comparison (e.g. increased *pparγ, leptin, adiponectin, fas* expression, decreased plasma glucose, HDL, FFA, and increased plasma insulin).

In this current study, we asked a different question by challenging MS diet F1 mice (instead of the dams) with HFD consumption. In the agouti viable yellow (A^{vy}) mice, the MS diet strongly prevents a genetically-predisposed type of obesity[18], and this elicited the question of how effective this would be in a non-agouti model. Our data suggests that the MS diet's protective effect of obesity in F1 mice are limited to the *agouti* mouse model, where the *agouti* gene is highly sensitized to methylation[18,21,23–25]. Furthermore, methylation directly affects the primary culprit (ectopic *agouti* expression). It is therefore reasonable that using the MS diet in a wild-type, common laboratory mouse strain with no unique retrotransposon insertion in its *agouti* gene promoter yielded no beneficial protection. It remains possible that a different mouse strain from agouti or C57BL/6J could also have different responses to the MS diet. Agouti mice are known for their exemplary modeling of diet, epigenetics, and later-life obesity/tumors, but it seems this model, based on our data, could be an idiosyncratic feature of the *agouti* mice.

Table 3 – Sequences for RT-PCR primers used in this chapter

Gene of Interest	Forward 5' → 3'	Reverse 5' → 3'
Il6	CTTCCATCCAGTTGCCTTCT	CTCCGACTTGTGAAGTGGTATAG
Tnfα	TTGTCTACTCCCAGGTTCTCT	GAGGTTGACTTTCTCCTGGTATG
Mcp1	CTCACCTGCTGCTACTCATTC	ACTACAGCTTCTTTGGGACAC
Gapdh	AACAGCAACTCCCACTCTTC	CCTGTTGCTGTAGCCGTATT

Chapter 6 – Conclusions and Future Directions

Final Notes (Chapter 2)

In Chapter 2, early-life pharmaceutical lifespan interventions were administered to HET3 mice, and we measured adipose tissue biology parameters at the 22-month time point to determine if these drugs prevented or mitigated age-associated effects in the adipose tissue. As discussed in Chapter 2, the high variation and range in old control data demonstrates that aging experiments and working with a heterogeneous mouse strain may require more attention to experimental design for optimization. In these final notes, I wish to highlight thoughts that our lab and I have discussed that are useful to improve future work related to (aging) adipose tissue biology and its relation to lifespan.

In Chapter 2, we noted in the discussion that the old control HET3 mice had a large variation. The separation of the old control mice into distinct groups is not limited to the use of heterogeneous mice. Our lab has previously noted within homogenous, in-bred strains of mice, old mice similarly separate, with age, into different groups. In murine studies where a measured variable in homogenous and young mice have a small standard error of mean, the analysis is straightforward—the average of the young control mice is representative of the cohort. However, in this case (Chapter 2) where the variable (aging biomarker) is affected by age and heterogeneous animals are used, the standard error of mean is large. There could either be a wide-range of values or clustering of data groups. In either of these scenarios, the analysis is complicated in a few ways. Variation in an aging variable tested in HET3 mice or another heterogeneous mouse strain may signify that this is a strain-specific aging biomarker (or idiosyncrasy) and therefore is different (or absent) in heterogeneous mice.

However, the variation of an aging biomarker could also represent a natural phenomenon associated with differential aging outcomes and may be cumulative of genetic predisposition or unknown environmental-epigenetic interactions throughout their

lives. Future work will benefit from anticipating these outcomes and would justify using larger control groups. If the data and numbers allow (is sufficient for separate analysis), it would be useful to consider separating the controls into at least 2 groups to analyze and discuss. What is lacking is a clearer understanding behind the separation of these control points. I believe that setting up operational definitions (where we can distinguish old mice based on criteria for categorization) for these groups could both prevent difficult interpretation of data and better model the differential aging outcomes we see in humans in these heterogeneous mouse models.

The 22-month time point we selected for the adipose tissue biology evaluation posed a few lessons. An important phenomenon we had not taken into account prior to these experiments was that at the 22-month time point, HET3 male mice in particular begin to undergo age-associated body mass decline. Old-age adipose tissue inflammation is typically associated and studied in conjunction with age-related adiposity. However, the more advanced stages of aging preceding death can also be accompanied by body mass decline. Based on previous studies[143,145,169] that recorded HET3 mice body masses at several additional time points (at 6-, 12-, 18-, 20-) during lifespan measurements, we observe that males have had substantial body mass reduction between 18 and 22 months of age. Female HET3 mice also appear to obtain peak body mass around 18 months of age, but compared to their male counterparts, it appears they lose smaller quantities of body mass and/or have delayed body weight decline. Given that female HET3 mice live longer than males, as previously discussed in Chapter 2, the decline in body mass we observed in the males is a later-stage of aging than females. Therefore, the 22-month time point may be beyond the stage at which it is most appropriate to study old-age adipose tissue inflammation, at least in HET3 mice. This, imaginably, could be important for other strains of mice where the time and duration of the stages of aging and body mass fluctuations are different, but they could similarly be present.

A limitation for interpretation of our senescent-marker expression in inguinal white adipose tissue (iWAT) is the data on *p16* expression. There is a recent report that found p16-positive macrophages surround senescent cells in an *ex vivo* synthetic model

with glass beads[245,246]. This study's data suggest that p16-positive 'senescent cells' extracted from various tissues may be a mixture of p16-positive senesced cells along with the recruited p16-positive macrophages that may be attempting to clear the senescent cells. This indicates that it is possible that studies that have reported the inflammatory nature of the so-called senescence-associated secretory phenotype (SASP) is documenting macrophage inflammation and not senescent cells' inflammation. Another possibility is that macrophages are prone to senescence in old age, and therefore p16 may be marking primarily senescence of macrophages which are already equipped to secrete pro-inflammatory mediators.

The significant increase in M1 macrophages in Rapa-treated HET3 mice, as discussed is also interesting in that it was associated to a previous study showing that they have compromised glucose tolerance but intact insulin tolerance[142,143]. An interesting future direction could be to assess the chemo-/cytokine profile of these adipose tissue macrophages and determine if these macrophages are enhanced regionally or systemically. For future work involving aging adipose tissue biology and ITP drugs, it may be important to also assess other immune cells that have been attributed as metabolic health influencers such as regulatory T cells (Tregs) in the fat pad. The work presented in Chapter 2 primarily showed that 1 of 3 ITP drugs we tested (Rapa) could be affecting adipose tissue inflammation as a means of lifespan extension. An important question would be what function these M1 macrophages serve in Rapa-treatment and whether they are a negative, neutral, or positive contributor to the lifespan extension benefits in HET3 mice.

Final Notes (Chapter 3 & 4)

In Chapter 3, a spontaneous outbreak of C. difficile in our mouse colony was presented and in Chapter 4, we used the outbreak strain ('16N203') derived from Chapter 3 to test our hypothesis that the methyl-donor supplement (MS) diet leads to a microbiota that loses colonization resistance against *C. difficile* infection (CDI). In these final notes, I discuss the challenges we faced during the outbreak investigation and the subsequent

study that tried to recapitulate the observations we had during the outbreak under experimental conditions.

We observed during the outbreak that MS diet F1 mice had higher total mortality than control mice. Three of the biggest variables we were unable to include or grasp in our subsequent experimental design was 1) barrier from which animals were ordered, 2) uncontrolled outbreak conditions (spores, continuous husbandry handling, etc.) and 3) age of animals. These discussions will also be broadly useful to reproducibility issues bound to model-based biomedical research in mice.

Within the data in Chapter 4, we discussed the possible conditions that could explain why the F1 diet mice did not lose colonization resistance with the MS diet alone. One of our primary concerns was that the Jackson Laboratory barrier from which the mice were ordered differed between the 'outbreak' mice and the batch of mice we raised in the new mouse colony. Surmounting literature and studies indicate that even a horizontal transfer between mouse rooms in the same institution could result in different microbiota[247]. Recently, studies on vendor and vendor-barrier effects on microbiota were shown to be significantly different[228,248]. In the future, even if the same barrier from which the outbreak mice were sourced was used for experiments, the microbiota could have already shifted. However, this emphasizes that barriers are crucial for reproducibility and consistency in microbiota studies—though it could be argued that any biological animal model system would be plagued by these variables as well.

Our second set of concerns for the outbreak investigation and the subsequent use of the outbreak strain in an experimental model was the number of conditions we cannot account for that occurred in the outbreak. In our experimental testing of 16N203-CDI (Chapter 4), we used a standard quantity of spores (10^4) to infect the animals, and we retain control over how many exposures this will be. However, during the outbreak, the spore quantity was unknown, and the lengthy outbreak period (over 8 months) ensures that multiple exposures of spores and cycles of re-infection may have affected the acuity of the outbreak. Thinking back to the experimental data we collected in Chapter 4, we suspect that these unaccounted conditions may explain why a microbiota shift in experimental conditions did not lead to colonization resistance loss. Along this point, a

microbiota shift in the context of multiple re-infection and varying quantities of spores in the mouse colony outbreak could be how the F1 diet mice suffered higher mortality than controls without antibiotics.

In the outbreak (Chapter 3), mice of all ages were present in the colony. Many of our older mice (13-16 months old) were lost in comparison to the younger mice, but this could not be a reportable observation given the associations drawn would be based on numerous age groups. However, C57BL/6J mice typically do not die from age-related causes in their middle ages. Therefore, it is rational to consider that in the experimental-infection (Chapter 4), using 3-4-months old adult F1 mice may be another important limitation-factor. The age-associated risk of CDI is known and one of beliefs is that there is age-associated decline in microbial diversity in the gut. Knowledge on age-related shifts in gut microbiota is still in its infancy[249], and this factor, in conjunction with MS diet, may have also synergistically enabled an advantageous environment for 16N203 CDI during the outbreak that could not be recapitulated in our younger-infection model.

In Chapter 4, I also test, alternative to the microbiota, if the MS diet led to different host immune responses that could have contributed to the increased mortality in MS diet F1 mice in the outbreak. However, the use of a dose of clindamycin to encourage CDI manifestation in the study also led to flattening of the microbiota in both control and MS diet F1 mice. This prevents a true assessment of my original question. Furthermore, an important lesson and limitation from isolating mesenteric lymph nodes and Peyer's patches in mice infected with CDI is that the selected immunological time point at 48-hours post-colonization was difficult. At 48 hours, mice were extremely sick, and the isolated immune cells may be similarly dysfunction and yield misleading results. For example, we did not observe any difference in T cell numbers nor subset differences between mock and *C. difficile*-infected animals. During *C. difficile* colitis, extensive damage of the gastrointestinal tissues has already occurred (as noted in histopathology) and the immune cells isolated at this time point in the mesenteric LN and PP likely do not accurately represent a host immune response to CDI. Instead, it may reflect an acute, pre-mortem phase. Discussions with other colleagues who work on gut inflammation have confirmed these points of concern. The better time points may be at 12 or 24 hours

(depending on strain and dosages), but the location of immunological assessment should also include the lamina propria to measure mucosal-regional responses.

Final Notes (Chapter 5)

In Chapter 5, the MS diet used in a C57BL/6J F0 mice do not generate F1 mice that are protected from diet-induced obesity (DIO) as we had hypothesized and have seen in previous reports on the agouti mice. Based on the data presented in this dissertation and the HFD consumption-during-gestation studies in literature[243,244], the MS diet may be uniquely protective in the agouti mouse model or as a counterbalance to HFD consumption during murine gestation. The limitation to these conclusions is that the gestational studies were done with a similar but different MS diet where there was an addition of genistein and a 37.5% reduction in methionine supplementation levels per kg of diet[243,244]. In our MS diet, which is modeled after the agouti mice obesity study, we use 12g/kg methionine whereas the gestational studies used 7.5g/kg methionine and an additional 0.3g/kg genistein.

Another important lesson from Chapter 5 is that we used F1 mice from different litters prior to realizing that the metabolic outcomes in each litter may vary. We observe variation between the GTT and ITT outcomes between each litter in both MS and control diet mice. When the data is pooled across the 3 litters, the data was flattened. Due to the limitation of time and loss of time from the outbreak that occurred in our mouse colony, we decided against repeating the experiment in another set of mice and looking at whether litter truly affected metabolic outcomes. However, in the future, these observations (though unconfirmed at this point) may be useful for explaining the difficulty behind repeating biological models, in addition to the microbiota obstacles discussed in Chapter 3's and 4's final notes.

The MS diet study originated from our observation that MS diet F1 mice are born smaller and maintain smaller body masses into adulthood at various ages[33]. The smaller body mass does not appear to affect lifespan (unpublished) and appear to diminish with age, but on average, it was still a significant percent of body mass difference (~5-15%). I also noted that MS diet F1 mice either had smaller numbers per litter born or fewer F1 newborn pups survive to weaning stages. This may be due to smaller F1 may be deemed

unfit by parents and killed. We attempted to carefully count newborns immediately and found that MS diet F1 mice seem to be born in similar numbers as control diet F1 mice. Therefore, another possibility is MS diet F1 mice have decreased viability during early childhood, but without further and more exact experiments, this question remains unanswered. Necessary improvements to the MS diet and metabolic-outcomes related studies would be to clearly document its effect on litter viability and sizes. Addressing these variables could better inform the applicability and optimal dosages of the MS diet. The methyl-donor composition and proportions may be appropriate for the *agouti* mice model but may be too high for C57BL/6J mice—given that hypomethylation at the agouti promoter leads to obesity and tumors, but in C57BL/6J mice, the level of methyl-donors deficiency could be different.

Summary

Chapters 2-5 are of separate questions but converge on the note that they explore the effect of either a diet or drug early in life and its impact on later life disease. In Chapter 2, the project tested the effects of 3 Interventions Testing Program (ITP) drugs, acarbose (ACA), 17α-estradiol (17aE2), and rapamycin (Rapa), on adipose tissue inflammation. We found that ACA and 17aE2 do not significantly affect any aspect of adipose tissue biology we tested while Rapa significantly increased pro-inflammatory adipose tissue macrophages. The subsequent chapters (3-5) all stem from the use of the methyl-donor supplementation (MS) diet mouse model. While investigating a spontaneous *C. difficile* outbreak (Chapter 3), we observed higher mortality in MS diet F1 mice during the outbreak, and after successful identification and isolation of the outbreak strain '16N203' we attempted to test our observation under experimental conditions. We infected MS diet F1 mice with the 16N203 *C. difficile*. Interestingly, we found that the MS diet significantly alters the F1 microbiota, and these changes alone did not allow for *C. difficile* colonization and infection. In Chapter 5, I present data from the original thesis project that explored whether MS diet protects F1 mice from diet-induced obesity and aspects of the DIO-associated metabolic syndrome. Important to note, the original project challenges F1 mice at 1 month of age (nearly immediately after weaning). However, due to the interruption of the outbreak, this time point was shifted to 3 months of age in all three sets of mice reported in Chapter 5. We find that the MS diet does not alter DIO nor metabolic responses in F1 C57BL/6J mice which suggests that the protective effects of the MS diet may be limited to preventing the adverse effects of maternal HFD intake during gestational phase of the fetus as previously reported by others[243,244] and/or unique to the agouti viable yellow (A^{vy}) mouse model.

The data in this dissertation supports and emphasizes the importance of diet, adipose tissue biology, and inflammation in the intersection of early-life diet and later-life disease. Moreover, the dissertation demonstrates that early interventions can affect an organism's disease susceptibility and health outcomes later in its own life (Chapter 2) as well as in the subsequent generation (Chapter 3-5).

REFERENCES

1. Bygren, L. O., Kaati, G. & Edvinsson, S. Longevity determined by paternal ancestors' nutrition during their slow growth period. *Acta Biotheor.* **49,** 53–59 (2001).

2. Kaati, G., Bygren, L. O. & Edvinsson, S. Cardiovascular and diabetes mortality determined by nutrition during parents' and grandparents' slow growth period. *Eur. J. Hum. Genet.* **10,** 682–688 (2002).

3. Lumey, L. H. Decreased birthweights in infants after maternal in utero exposure to the Dutch famine of 1944–1945. *Paediatr. Perinat. Epidemiol.* **6,** 240–253 (1992).

4. Martyn, C. N., Barker, D. J. P. & Osmond, C. Mothers' pelvic size, fetal growth, and death from stroke and coronary heart disease in men in the UK. *Lancet* **348,** 1264–1268 (1996).

5. Barker, D. J. P. Maternal nutrition, fetal nutrition, and disease in later life. *Nutrition* **13,** 807–813 (1997).

6. Hales, C. N. Fetal and infant growth and impaired glucose tolerance in adulthood: the 'thrifty phenotype' hypothesis revisited. *Acta Paediatr. Suppl.* **422,** 73–77 (1997).

7. Hales, C. N. & Barker, D. J. P. Type 2 (non-insulin-dependent) diabetes mellitus: the thrifty phenotype hypothesis. *Int. J. Epidemiol.* **42,** 1215–1222 (2013).

8. Barker, D. J. P. & Osmond, C. INFANT MORTALITY, CHILDHOOD NUTRITION, AND ISCHAEMIC HEART DISEASE IN ENGLAND AND WALES. *Lancet* **327,** 1077–1081 (1986).

9. Ozanne, S. E. Programming of hepatic and peripheral tissue insulin sensitivity by maternal protein restriction. *Biochem Soc Trans* **27,** 94–97 (1999).

10. Ozanne, S. E. & Hales, C. N. The long-term consequences of intra-uterine protein malnutrition for glucose metabolism. in *Proceedings of the Nutrition Society* **58,** 615–619 (1999).

11. Ozanne, S. E. & Hales, C. N. Early programming of glucose-insulin metabolism. *Trends in Endocrinology and Metabolism* **13,** 368–373 (2002).

12. Ozanne, S. E. *et al.* Early growth restriction leads to down regulation of protein kinase C zeta and insulin resistance in skeletal muscle. *J. Endocrinol.* **177,** 235–241 (2003).

13. Waterland, R. A. Assessing the Effects of High Methionine Intake on DNA Methylation. *J. Nutr.* **136,** 16365–16405 (2006).

14. Sato, F., Tsuchiya, S., Meltzer, S. J. & Shimizu, K. MicroRNAs and epigenetics. *FEBS J.* **278,** 1598–1609 (2011).

15. Fan, G. & Hutnick, L. Methyl-CpG binding proteins in the nervous system. *Cell Research* **15,** 255–261 (2005).

16. Klose, R. J. & Bird, A. P. Genomic DNA methylation: The mark and its mediators. *Trends in Biochemical Sciences* **31,** 89–97 (2006).

17. Barrows, L. R. & Magee, P. N. Nonenzymatic methylation of dna by s-adenosylmethionine in vitro. *Carcinogenesis* **3,** 349–351 (1982).

18. Dolinoy, D. C., Weidman, J. R., Waterland, R. A. & Jirtle, R. L. Maternal genistein alters coat color and protects Avy mouse offspring from obesity by modifying the fetal epigenome. *Environ. Health Perspect.* **114,** 567–572 (2006).

19. Rakyan, V. K. *et al.* Transgenerational inheritance of epigenetic states at the murine AxinFu allele occurs after maternal and paternal transmission. *Proc. Natl. Acad. Sci.* **100,** 2538–2543 (2003).

20. Obeid, R. The metabolic burden of methyl donor deficiency with focus on the betaine homocysteine methyltransferase pathway. *Nutrients* **5,** 3481–3495 (2013).

21. Dolinoy, D. C. The agouti mouse model: An epigenetic biosensor for nutritional and environmental alterations on the fetal epigenome. in *Nutrition Reviews* **66,** (2008).

22. Waterland, R. a & Jirtle, R. L. Transposable Elements : Targets for Early Nutritional Effects on Epigenetic Gene Regulation Transposable Elements : Targets for Early Nutritional Effects on Epigenetic Gene Regulation. *Mol. Cell. Biol.* **23,** 5293–5300 (2003).

23. Wolff, G. L., Kodell, R. L., Moore, S. R. & Cooney, C. A. Maternal epigenetics and methyl supplements affect agouti gene expression in Avy/a mice. *Faseb J.* **12,** 949–957 (1998).

24. Wolff, G. L. Variability in gene expression and tumor formation within genetically homogeneous animal populations in bioassays. *Fundamental and Applied Toxicology* **29,** 176–184 (1996).

25. Dolinoy, D. C., Huang, D. & Jirtle, R. L. Maternal nutrient supplementation counteracts bisphenol A-induced DNA hypomethylation in early development. *Proc. Natl. Acad. Sci.* **104,** 13056–13061 (2007).

26. Rosenfeld, C. S. *et al.* Maternal exposure to bisphenol A and genistein has minimal effect on Avy/a offspring coat color but favors birth of agouti over nonagouti mice. *Proc. Natl. Acad. Sci.* **110,** 537–542 (2013).

27. O'Neill, R. J., Vrana, P. B. & Rosenfeld, C. S. Maternal methyl supplemented diets and effects on offspring health. *Front. Genet.* **5,** 1–10 (2014).

28. Huang, Y. *et al.* Maternal high folic acid supplement promotes glucose intolerance and insulin resistance in male mouse offspring fed a high-fat diet. *Int. J. Mol. Sci.* **15,** 6298–6313 (2014).

29. Downing, C. *et al.* Subtle decreases in DNA methylation and gene expression at the mouse Igf2 locus following prenatal alcohol exposure: Effects of a methyl-supplemented diet. *Alcohol* **45,** 65–71 (2011).

30. Barua, S. *et al.* Increasing maternal or post-weaning folic acid alters gene expression and moderately changes behavior in the offspring. *PLoS One* **9,** (2014).

31. Giudicelli, F., Brabant, A. L., Grit, I., Parnet, P. & Amarger, V. Excess of Methyl Donor in the Perinatal Period Reduces Postnatal Leptin Secretion in Rat and Interacts with the Effect of Protein Content in Diet. *PLoS One* **8,** (2013).

32. Delaney, C. *et al.* Maternal Diet Supplemented with Methyl-Donors Protects against Atherosclerosis in F1 ApoE-/- Mice. *PLoS One* **8,** (2013).

33. Delaney, C. *et al.* Maternal Micronutrient Supplementation Suppresses T Cell Chemokine Receptor Expression and Function in F1 Mice. *J. Nutr.* **142,** 1329–1335 (2012).

34. Schaible, T. D., Harris, R. A., Dowd, S. E., Smith, C. W. & Kellermayer, R. Maternal methyl-donor supplementation induces prolonged murine offspring colitis susceptibility in association with mucosal epigenetic and microbiomic changes. *Hum. Mol. Genet.* **20,** 1687–1696 (2011).

35. Mir, S. A. *et al.* Prenatal methyl-donor supplementation augments colitis in young adult mice. *PLoS One* **8,** e73162 (2013).

36. Buffie, C. G. & Pamer, E. G. Microbiota-mediated colonization resistance against intestinal pathogens. *Nature Reviews Immunology* **13,** 790–801 (2013).

37. Britton, R. A. & Young, V. B. Role of the intestinal microbiota in resistance to colonization by Clostridium difficile. *Gastroenterology* **146,** 1547–1553 (2014).

38. Kim, D., Zeng, M. Y. & Núñez, G. The interplay between host immune cells and gut microbiota in chronic inflammatory diseases. *Exp. Mol. Med.* **49,** e339 (2017).

39. Dethlefsen, L., Huse, S., Sogin, M. L. & Relman, D. A. The pervasive effects of an antibiotic on the human gut microbiota, as revealed by deep 16s rRNA sequencing. *PLoS Biol.* **6,** 2383–2400 (2008).

40. Kyne, L., Sougioultzis, S., McFarland, L. V. & Kelly, C. P. Underlying Disease Severity as a Major Risk Factor for Nosocomial Clostridium difficile Diarrhea. *Infect. Control Hosp. Epidemiol.* **23,** 653–659 (2002).

41. Peterfreund, G. L. *et al.* Succession in the Gut Microbiome following Antibiotic and Antibody Therapies for Clostridium difficile. *PLoS One* **7,** (2012).

42. Theriot, C. M. *et al.* Antibiotic-induced shifts in the mouse gut microbiome and metabolome increase susceptibility to Clostridium difficile infection. *Nat. Commun.* **5,** (2014).

43. Rupnik, M., Wilcox, M. H. & Gerding, D. N. Clostridium difficile infection: New developments in epidemiology and pathogenesis. *Nature Reviews Microbiology* **7,** 526–536 (2009).

44. Collins, J. *et al.* Dietary trehalose enhances virulence of epidemic Clostridium difficile. *Nature* (2018). doi:10.1038/nature25178

45. Zackular, J. P. *et al.* Dietary zinc alters the microbiota and decreases resistance to Clostridium difficile infection. *Nat. Med.* **22,** 1330–1334 (2016).

46. Ahima, R. S. Connecting obesity, aging and diabetes. *Nat. Med.* **15,** 996–997 (2009).

47. Tchkonia, T. *et al.* Fat tissue, aging, and cellular senescence. *Aging Cell* **9,** 667–684 (2010).

48. Palmer, A. K. & Kirkland, J. L. Aging and adipose tissue: potential interventions for diabetes and regenerative medicine. *Exp. Gerontol.* **86,** 97–105 (2016).

49. Kuk, J. L., Saunders, T. J., Davidson, L. E. & Ross, R. Age-related changes in total and regional fat distribution. *Ageing Research Reviews* **8,** 339–348 (2009).

50. Stout, M. B., Tchkonia, T. & Kirkland, J. L. The aging adipose organ: Lipid redistribution, inflammation, and cellular senescence. in *Adipose Tissue and Adipokines in Health and Disease: Second Edition* 69–80 (2014). doi:10.1007/978-1-62703-770-9_5

51. Hotamisligil, G. S., Shargill, N. S. & Spiegelman, B. M. Adipose expression of tumor necrosis factor-alpha: direct role in obesity-linked insulin resistance. *Science* **259,** 87–91 (1993).

52. Bluher, M., Kahn, B. & Kahn, C. Extended Longevity in Mice Lacking the Insulin Receptor in Adipose Tissue. *Science (80-.).* **299,** 572–574 (2003).

53. Giannakou, M. *et al.* Long-Lived Drosophila with Overexpressed dFOXO in Adult Fat Body. *Science (80-.).* **307,** 361 (2005).

54. Bluher, M. Adipose tissue inflammation: a cause or consequence of obesity-related insulin resistance? *Clin. Sci.* **130,** 1603–1614 (2016).

55. Hainer, V. & Aldhoon-Hainerová, I. Obesity paradox does exist. *Diabetes Care* **36,** (2013).

56. Lavie, C. J., De Schutter, A. & Milani, R. V. Healthy obese versus unhealthy lean:

the obesity paradox. *Nat. Rev. Endocrinol.* **11,** 55–62 (2014).

57. Yaghootkar, H. *et al.* Genetic evidence for a normal-weight 'metabolically obese' phenotype linking insulin resistance, hypertension, coronary artery disease, and type 2 diabetes. *Diabetes* **63,** 4369–4377 (2014).

58. Abizanda, P. *et al.* Energetics of Aging and Frailty: The FRADEA Study. *Journals Gerontol. - Ser. A Biol. Sci. Med. Sci.* **71,** 787–796 (2016).

59. Gökhan S . Hotamisligil, N. S. . S. and B. M. . S. Adipose Expression of Tumor Necrosis Factor-α : Direct Role in Obesity-Linked Insulin Resistance. **259,** 87–91 (2016).

60. Lumeng, C. N., Delproposto, J. B., Westcott, D. J. & Saltiel, A. R. Phenotypic switching of adipose tissue macrophages with obesity is generated by spatiotemporal differences in macrophage subtypes. *Diabetes* **57,** 3239–3246 (2008).

61. Lumeng, C. N., Bodzin, J. L. & Saltiel, A. R. Obesity induces a phenotipic switch in adipose tissue macrophage polarization. *J Clin Invest* **117,** 175–184 (2007).

62. Martinez, F. O. & Gordon, S. The M1 and M2 paradigm of macrophage activation: time for reassessment. *F1000Prime Rep.* **6,** 1–13 (2014).

63. Weisberg, S. P. *et al.* Obesity is associated with macrophage accumulation in adipose tissue. *J. Clin. Invest.* **112,** 1796–1808 (2003).

64. Murano, I. *et al.* Dead adipocytes, detected as crown-like structures, are prevalent in visceral fat depots of genetically obese mice. *J. Lipid Res.* **49,** 1562–1568 (2008).

65. Zamarron, B. F. *et al.* Macrophage proliferation sustains adipose tissue inflammation in formerly obese mice. *Diabetes* **66,** 392–406 (2017).

66. Kawasaki, N., Asada, R., Saito, A., Kanemoto, S. & Imaizumi, K. Obesity-induced endoplasmic reticulum stress causes chronic inflammation in adipose tissue. *Sci. Rep.* **2,** 1–7 (2012).

67. Ozcan, U. *et al.* Endoplasmic Reticulum Stress Links Obesity, Insulin Action, and Type 2 Diabetes. *Distribution* 457–461 (2004).

68. Suzuki, T. *et al.* ER Stress Protein CHOP Mediates Insulin Resistance by Modulating Adipose Tissue Macrophage Polarity. *Cell Rep.* **18,** 2045–2057 (2017).

69. Shan, B. *et al.* The metabolic ER stress sensor IRE1α suppresses alternative activation of macrophages and impairs energy expenditure in obesity. *Nat. Immunol.* **18,** (2017).

70. Nishimura, S. *et al.* CD8+ effector T cells contribute to macrophage recruitment

and adipose tissue inflammation in obesity. *Nat. Med.* **15,** 914–920 (2009).

71. Feuerer, M. *et al.* Lean, but not obese, fat is enriched for a unique population of regulatory T cells that affect metabolic parameters. *Nat. Med.* **15,** 930–939 (2009).

72. Wu, D. *et al.* Aging Up-Regulates Expression of Inflammatory Mediators in Mouse Adipose Tissue. *J. Immunol.* **179,** 4829–4839 (2007).

73. Winer, D. A. *et al.* B Lymphocytes Promote Insulin Resistance through Modulation of T Lymphocytes and Production of Pathogenic IgG Antibody. *Nat Med* **17,** 610–617 (2011).

74. Liu, J. *et al.* Genetric deficiency and pharmacological stabilization of mast cells reduce diet-induced obesity and diabetes in mice. *Nat Med.* **15,** 940–945 (2010).

75. Ouchi, N., Parker, J. L., Lugus, J. J. & Walsh, K. Adipokines in inflammation and metabolic disease. *Nat. Rev. Immunol.* **11,** 85–97 (2011).

76. Iyer, A., Fairlie, D. P., Prins, J. B., Hammock, B. D. & Brown, L. Inflammatory lipid mediators in adipocyte function and obesity. *Nat. Rev. Endocrinol.* **6,** 71–82 (2010).

77. Scherer, P. E. The multifaceted roles of adipose tissue - Therapeutic targets for diabetes and beyond: The 2015 banting lecture. *Diabetes* **65,** 1452–1461 (2016).

78. Nguyen, M. T. A. *et al.* A subpopulation of macrophages infiltrates hypertrophic adipose tissue and is activated by free fatty acids via toll-like receptors 2 and 4 and JNK-dependent pathways. *J. Biol. Chem.* **282,** 35279–35292 (2007).

79. Nguyen, M. T. A. *et al.* JNK and tumor necrosis factor-α mediate free fatty acid-induced insulin resistance in 3T3-L1 adipocytes. *J. Biol. Chem.* **280,** 35361–35371 (2005).

80. Yu, C. *et al.* Mechanism by which fatty acids inhibit insulin activation of insulin receptor substrate-1 (IRS-1)-associated phosphatidylinositol 3-kinase activity in muscle. *J. Biol. Chem.* **277,** 50230–50236 (2002).

81. Hwang, D. & Rhee, S. H. Receptor-mediated signaling pathways : potential targets of modulation by dietary fatty acids 1 – 4. (1999).

82. Summers, S. A. Ceramides in insulin resistance and lipotoxicity. *Prog. Lipid Res.* **45,** 42–72 (2006).

83. Park, E., Wong, V., Guan, X., Oprescu, A. I. & Giacca, A. Resveratrol prevents insulin resistance caused by short-term elevation of free fatty acids in vivo. *J. Endocrinol.* **195,** 323–31 (2007).

84. Glass, C. K. & Olefsky, J. M. Inflammation and lipid signaling in the etiology of insulin resistance. *Cell Metab.* **15,** 635–645 (2012).

85. Pal, D. *et al.* Fetuin-A acts as an endogenous ligand of TLR4 to promote lipid-

induced insulin resistance. *Nat. Med.* **18,** 1279–1285 (2012).

86. Mathews, S. T. *et al.* Fetuin-null mice are protected against obesity and insulin resistance associated with aging. *Biochem. Biophys. Res. Commun.* **350,** 437–443 (2006).

87. Ghosh, A. K., Brien, M. O., Mau, T. & Yung, R. Toll - like receptor 4 (TLR4) deficient mice are protected from adipose tissue inflammation in aging. **9,** 1–12 (2017).

88. Carr, A. *et al.* A syndrome of peripheral lipodystrophy, hyperlipidaemia and insulin resistance in patients receiving HIV protease inhibitors. *Aids* **12,** F51–F58 (1998).

89. Lumeng, C. N. *et al.* Aging Is Associated with an Increase in T Cells and Inflammatory Macrophages in Visceral Adipose Tissue. *J. Immunol.* **187,** 6208–6216 (2011).

90. Ghosh, A. K. *et al.* Elevated Endoplasmic Reticulum Stress Response Contributes to Adipose Tissue Inflammation in Aging. *Journals Gerontol. Ser. A Biol. Sci. Med. Sci.* **70,** 1320–1329 (2015).

91. Chen, Y., Wu, Z., Zhao, S. & Xiang, R. Chemical chaperones reduce ER stress and adipose tissue inflammation in high fat diet-induced mouse model of obesity. *Sci. Rep.* **6,** 27486 (2016).

92. Ghosh, A. K., Mau, T., O'Brien, M., Garg, S. & Yung, R. Impaired autophagy activity is linked to elevated ER-stress and inflammation in aging adipose tissue. *Aging (Albany. NY).* **8,** 2525–2537 (2016).

93. Garg, S. K. *et al.* Aging is associated with increased regulatory T-cell function. *Aging Cell* **13,** 441–448 (2014).

94. Richardson, B. & Yung, R. Role of DNA methylation in the regulation of cell function. *Journal of Laboratory and Clinical Medicine* **134,** 333–340 (1999).

95. Mendez, S., Reckling, S. K., Piccirillo, C. A., Sacks, D. & Belkaid, Y. Role for $CD4^+$ $CD25^+$ Regulatory T Cells in Reactivation of Persistent Leishmaniasis and Control of Concomitant Immunity. *J. Exp. Med.* **200,** 201–210 (2004).

96. Sharma, S., Dominguez, A. L. & Lustgarten, J. High accumulation of T regulatory cells prevents the activation of immune responses in aged animals. *J. Immunol. (Baltimore, Md 1950)* **177,** 8348–8355 (2006).

97. Yang, H. *et al.* Obesity Increases the Production of Proinflammatory Mediators from Adipose Tissue T Cells and Compromises TCR Repertoire Diversity: Implications for Systemic Inflammation and Insulin Resistance. *J. Immunol.* **185,** 1836–1845 (2010).

98. Bapat, S. P. *et al.* Depletion of fat-resident Treg cells prevents age-associated

insulin resistance. *Nature* (2015). doi:10.1038/nature16151

99. FRANCESCHI, C. *et al.* Inflamm-aging: An Evolutionary Perspective on Immunosenescence. *Ann. N. Y. Acad. Sci.* **908,** 244–254 (2006).

100. Franceschi, C. & Campisi, J. Chronic inflammation (Inflammaging) and its potential contribution to age-associated diseases. *Journals Gerontol. - Ser. A Biol. Sci. Med. Sci.* **69,** S4–S9 (2014).

101. Arai, Y. *et al.* Inflammation, But Not Telomere Length, Predicts Successful Ageing at Extreme Old Age: A Longitudinal Study of Semi-supercentenarians. *EBioMedicine* **2,** 1549–1558 (2015).

102. Krabbe, K. S., Pedersen, M. & Bruunsgaard, H. Inflammatory mediators in the elderly. *Exp. Gerontol.* **39,** 687–699 (2004).

103. Kevin Howcroft, T. *et al.* The role of inflammation in age-related disease. *Aging (Albany. NY).* **5,** 84–93 (2013).

104. Bauer, M. E. & De la Fuente, M. Oxidative Stress, Inflammaging, and Immunosenescence. *Inflammation, Adv. Age Nutr. Res. Clin. Interv.* **74,** 39–47 (2013).

105. Furman, D. *et al.* Expression of specific inflammasome gene modules stratifies older individuals into two extreme clinical and immunological states. *Nat. Med.* **23,** 174–184 (2017).

106. Tchkonia, T., Zhu, Y., Deursen, J. Van, Campisi, J. & Kirkland, J. L. Cellular senescence and the senescent secretory phenotype: therapeutic opportunities. *J. Clin. Invest.* **123,** 966–972 (2013).

107. De Felice, F. G. & Ferreira, S. T. Inflammation, defective insulin signaling, and mitochondrial dysfunction as common molecular denominators connecting type 2 diabetes to Alzheimer Disease. *Diabetes* **63,** 2262–2272 (2014).

108. Wiley, C. D. *et al.* Mitochondrial dysfunction induces senescence with a distinct secretory phenotype. *Cell Metab.* **23,** 303–314 (2016).

109. Biagi, E., Candela, M., Franceschi, C. & Brigidi, P. The aging gut microbiota: New perspectives. *Ageing Res. Rev.* **10,** 428–429 (2011).

110. Salvioli, S. *et al.* Immune System, Cell Senescence, Aging and Longevity - Inflamm-Aging Reappraised. *Curr. Pharm. Des.* **19,** 1675–1679 (2013).

111. Barzilai, N. & Gupta, G. Revisiting the role of fat mass in the life extension induced by caloric restriction. *J. Gerontol. A. Biol. Sci. Med. Sci.* **54,** B89–B96 (1999).

112. Mau, T. & Yung, R. Adipose tissue inflammation in aging. *Exp. Gerontol.* (2017). doi:10.1016/j.exger.2017.10.014

113. Park, S. E. *et al.* Depot-specific changes in fat metabolism with aging in a type 2 diabetic animal model. *PLoS One* **11,** 1–14 (2016).

114. Barzilai, N. & Rossetti, L. Relationship between changes in body composition and insulin responsiveness in models of the aging rat. *Am. J. Physiol.* **269,** E591–E597 (1995).

115. Guo, S. S., Zeller, C., Chumlea, W. C. & Siervogel, R. M. Aging, body composition, and lifestyle: The Fels Longitudinal Study. *Am. J. Clin. Nutr.* **70,** 405–411 (1999).

116. Kyle, U., Genton, L. & Hans, D. Original Communications-Age-related differences in fat-free mass, skeletal muscle, body cell mass and fat mass between 18 and 94 years. *Eur. J. Clin. Nutr.* 663–672 (2001).

117. Marcus, R. L., Addison, O., Kidde, J. P., Dibble, L. E. & Lastayo, P. C. Skeletal muscle fat infiltration: Impact of age, inactivity, and exercise. *J. Nutr. Heal. Aging* **14,** 362–366 (2010).

118. Campisi, J. Senescent cells, tumor suppression, and organismal aging: Good citizens, bad neighbors. *Cell* **120,** 513–522 (2005).

119. Adams, P. D. Healing and Hurting: Molecular Mechanisms, Functions, and Pathologies of Cellular Senescence. *Mol. Cell* **36,** 2–14 (2009).

120. Gire, V. & Wynford-Thomas, D. Reinitiation of DNA synthesis and cell division in senescent human fibroblasts by microinjection of anti-p53 antibodies. *Mol. Cell. Biol.* **18,** 1611–21 (1998).

121. Brown, J. P. Bypass of Senescence After Disruption of p21CIP1/WAF1 Gene in Normal Diploid Human Fibroblasts. *Science (80-.).* **277,** 831–834 (1997).

122. Deursen, J. M. The role of senescent cells in ageing. *Nature* **509,** 439–446 (2014).

123. Baker, D. J. *et al.* Clearance of p16Ink4a-positive senescent cells delays ageing-associated disorders. *Nature* **479,** 232–236 (2011).

124. Baker, D. J. *et al.* Naturally occurring p16Ink4a-positive cells shorten healthy lifespan. *Nature* **530,** 184–189 (2016).

125. Miller, R. A., Burke, D. & Nadon, N. Announcement : Four-Way Cross Mouse Stocks: A New, Genetically Heterogeneous Resource for Aging Research. *J. Gerontol. Biol. Sci.* **54,** 1999–2001 (1999).

126. Nadon, N. L. *et al.* Design of aging intervention studies: The NIA interventions testing program. *Age* **30,** 187–199 (2008).

127. Nadon, N. L., Strong, R., Miller, R. A. & Harrison, D. E. NIA Interventions Testing Program: Investigating Putative Aging Intervention Agents in a Genetically Heterogeneous Mouse Model. *EBioMedicine* **21,** 3–4 (2017).

128. Fagiolo, U. *et al.* Increased cytokine production in mononuclear cells of healthy elderly people. *Eur. J. Immunol.* **23,** 2375–2378 (1993).

129. Baggio, G. *et al.* Lipoprotein(a) and lipoprotein profile in healthy centenarians: a reappraisal of vascular risk factors. *FASEB J.* **12,** 433–437 (1998).

130. Bonafè, M. *et al.* A gender-dependent genetic predisposition to produce high levels of IL-6 is detrimental for longevity. *Eur. J. Immunol.* **31,** 2357–2361 (2001).

131. Coppola, R., Mari, D., Lattuada, A. & Franceschi, C. Von Willebrand factor in Italian centenarians. *Haematologica* **88,** 39–43 (2003).

132. Zanni, F. *et al.* Marked increase with age of type 1 cytokines within memory and effector/cytotoxic CD8+T cells in humans: A contribution to understand the relationship between inflammation and immunosenescence. *Exp. Gerontol.* **38,** 981–987 (2003).

133. Franceschi, C. *et al.* Genes involved in immune response/inflammation, IGF1/insulin pathway and response to oxidative stress play a major role in the genetics of human longevity: The lesson of centenarians. in *Mechanisms of Ageing and Development* **126,** 351–361 (2005).

134. Wikby, A. *et al.* The immune risk phenotype is associated with IL-6 in the terminal decline stage: Findings from the Swedish NONA immune longitudinal study of very late life functioning. *Mech. Ageing Dev.* **127,** 695–704 (2006).

135. Krabbe, K. S., Pedersen, M. & Bruunsgaard, H. Inflammatory mediators in the elderly. *Experimental Gerontology* **39,** 687–699 (2004).

136. Franceschi, C. & Campisi, J. Chronic inflammation (Inflammaging) and its potential contribution to age-associated diseases. *Journals of Gerontology - Series A Biological Sciences and Medical Sciences* **69,** S4–S9 (2014).

137. Shimomura, I. *et al.* Insulin resistance and diabetes mellitus in transgenic mice expressing nuclear SREBP-1c in adipose tissue: model for congenital generalized lipodystrophy. *Genes Dev.* **12,** 3182–94 (1998).

138. Hamrick, M. W. *et al.* Age-related loss of muscle mass and bone strength in mice is associated with a decline in physical activity and serum leptin. *Bone* **39,** 845–853 (2006).

139. Périè, L., Parenté, A., Baraige, F., Magnol, L. & Blanquet, V. Alterations in Adiposity and Glucose Homeostasis in Adult Gasp-1 Overexpressing Mice. *Cell. Physiol. Biochem.* **44,** 1896–1911 (2018).

140. Harrison, D. E. *et al.* Rapamycin fed late in life extends lifespan in genetically heterogeneous mice. *Nature* **460,** 392–395 (2009).

141. Wilkinson, J. E. *et al.* Rapamycin slows aging in mice. *Aging Cell* **11,** 675–682 (2012).

142. Lamming, D. W. *et al.* Young and old genetically heterogeneous HET3 mice on a rapamycin diet are glucose intolerant but insulin sensitive. *Aging Cell* **12,** 712–718 (2013).

143. Miller, R. A. *et al.* Rapamycin-mediated lifespan increase in mice is dose and sex dependent and metabolically distinct from dietary restriction. *Aging Cell* **13,** 468–477 (2014).

144. Miller, R. A. *et al.* An aging Interventions Testing Program: Study design and interim report. *Aging Cell* **6,** 565–575 (2007).

145. Harrison, D. E. *et al.* Acarbose, 17-α-estradiol, and nordihydroguaiaretic acid extend mouse lifespan preferentially in males. *Aging Cell* **13,** 273–282 (2014).

146. Zaseck, L. W., Miller, R. A. & Brooks, S. V. Rapamycin attenuates age-associated changes in tibialis anterior tendon viscoelastic properties. *Journals Gerontol. - Ser. A Biol. Sci. Med. Sci.* **71,** 858–865 (2016).

147. Flurkey, K., Astle, C. M. & Harrison, D. E. Life extension by diet restriction and N-acetyl-L-cysteine in genetically heterogeneous mice. *Journals Gerontol. - Ser. A Biol. Sci. Med. Sci.* **65 A,** 1275–1284 (2010).

148. Miller, R. A. *et al.* Rapamycin, but not resveratrol or simvastatin, extends life span of genetically heterogeneous mice. *Journals Gerontol. - Ser. A Biol. Sci. Med. Sci.* **66 A,** 191–201 (2011).

149. Huffman, D. M. & Barzilai, N. Contribution of adipose tissue to health span and longevity. in *Body Composition and Aging* **37,** 1–19 (2010).

150. Gabriely, I. *et al.* Removal of visceral fat prevents insulin resistance and glucose intolerance of aging: An adipokine-mediated process? *Diabetes* **51,** 2951–2958 (2002).

151. Stout, M. B. *et al.* Growth hormone action predicts age-related white adipose tissue dysfunction and senescent cell burden in mice. *Aging (Albany. NY).* **6,** 575–586 (2014).

152. Giannakou, M. E. *et al.* Long-lived Drosophila with over-expressed dFOXO in adult fat body. *Science (80-.).* **305,** 361 (2004).

153. Libina, N., Berman, J. R. & Kenyon, C. Tissue-Specific Activities of C. elegans DAF-16 in the Regulation of Lifespan. *Cell* **115,** 489–502 (2003).

154. Blüher, M., Kahn, B. B. & Kahn, C. R. Extended longevity in mice lacking the insulin receptor in adipose tissue. *Science (80-.).* **299,** 572–574 (2003).

155. Sun, L., Sadighi Akha, A. A., Miller, R. A. & Harper, J. M. Life-span extension in mice by preweaning food restriction and by methionine restriction in middle age. *Journals Gerontol. - Ser. A Biol. Sci. Med. Sci.* **64,** 711–722 (2009).

156. Pascot, A. *et al.* Age-related increase in visceral adipose tissue and the metabolic risk profile of premenopausal women. *Diabetes Care* **22,** 1471–1478 (1999).

157. Tardif, N. *et al.* Muscle ectopic fat deposition contributes to anabolic resistance in obese sarcopenic old rats through eIF2α activation. *Aging Cell* **13,** 1001–1011 (2014).

158. Gautiar, E. L. *et al.* Gene-expression profiles and transcriptional regulatory pathways that underlie the identity and diversity of mouse tissue macrophages. *Nat. Immunol.* **13,** 1118–1128 (2012).

159. Cho, K. W. *et al.* Adipose Tissue Dendritic Cells Are Independent Contributors to Obesity-Induced Inflammation and Insulin Resistance. *J. Immunol.* **197,** 3650–3661 (2016).

160. Yoneshiro, T. *et al.* Age-related decrease in cold-activated brown adipose tissue and accumulation of body fat in healthy humans. *Obesity* **19,** 1755–1760 (2011).

161. Rogers, N. H., Landa, A., Park, S. & Smith, R. G. Aging leads to a programmed loss of brown adipocytes in murine subcutaneous white adipose tissue. *Aging Cell* **11,** 1074–1083 (2012).

162. Wu, J. *et al.* Beige adipocytes are a distinct type of thermogenic fat cell in mouse and human. *Cell* **150,** 366–376 (2012).

163. Seale, P. *et al.* Prdm16 determines the thermogenic program of subcutaneous white adipose tissue in mice. *J. Clin. Invest.* **121,** 96–105 (2011).

164. Di Micco, R. *et al.* Oncogene-induced senescence is a DNA damage response triggered by DNA hyper-replication. *Nature* **444,** 638–642 (2006).

165. Krishnamurthy, J. *et al.* Ink4a/Arf. *J. Clin. Invest.* **114,** 1299–1307 (2004).

166. Strong, R. *et al.* Longer lifespan in male mice treated with a weakly estrogenic agonist, an antioxidant, an α-glucosidase inhibitor or a Nrf2-inducer. *Aging Cell* **15,** 872–884 (2016).

167. Strong, R. *et al.* Nordihydroguaiaretic acid and aspirin increase lifespan of genetically heterogeneous male mice. *Aging Cell* **7,** 641–650 (2008).

168. Garratt, M., Nakagawa, S. & Simons, M. J. P. Comparative idiosyncrasies in life extension by reduced mTOR signalling and its distinctiveness from dietary restriction. *Aging Cell* **15,** 737–743 (2016).

169. Garratt, M., Bower, B., Garcia, G. G. & Miller, R. A. Sex differences in lifespan extension with acarbose and 17-α estradiol: gonadal hormones underlie male-specific improvements in glucose tolerance and mTORC2 signaling. *Aging Cell* **16,** 1256–1266 (2017).

170. Han, M. S. *et al.* JNK expression by macrophages promotes obesity-induced

insulin resistance and inflammation. *Science (80-.).* **339,** 218–222 (2013).

171. Mercalli, A. *et al.* Rapamycin unbalances the polarization of human macrophages to M1. *Immunology* **140,** 179–190 (2013).

172. Lessa, F. C. *et al.* Burden of *Clostridium difficile* Infection in the United States. *N. Engl. J. Med.* **372,** 825–834 (2015).

173. Kuehne, S. A. *et al.* The role of toxin A and toxin B in Clostridium difficile infection. *Nature* **467,** 711–713 (2010).

174. Just, I. *et al.* Glucosylation of Rho proteins by Clostridium difficile toxin B. *Nature* **375,** 500–503 (1995).

175. Just, I. *et al.* The enterotoxin from Clostridium difficile (ToxA) monoglucosylates the Rho proteins. *J. Biol. Chem.* **270,** 13932–13936 (1995).

176. Brito, G. A. *et al.* Mechanism of Clostridium difficile toxin A-induced apoptosis in T84 cells. *J. Infect. Dis.* **186,** 1438–1447 (2002).

177. Gerding, D. N., Johnson, S., Rupnik, M. & Aktories, K. Clostridium difficile binary toxin CDT: mechanism, epidemiology, and potential clinical importance. *Gut microbes* **5,** 15–27 (2014).

178. Gerhard, R. *et al.* Glucosylation of Rho GTPases by Clostridium difficile toxin A triggers apoptosis in intestinal epithelial cells. *J. Med. Microbiol.* **57,** 765–770 (2008).

179. Redelings, M. D., Sorvillo, F. & Mascola, L. Increase in Clostridium difficile-related mortality rates, United States, 1999-2004. *Emerg. Infect. Dis.* **13,** 1417–1419 (2007).

180. Warny, M. *et al.* Toxin production by an emerging strain of Clostridium difficile associated with outbreaks of severe disease in North America and Europe. *Lancet* **366,** 1079–1084 (2005).

181. Stiles, B. G., Wigelsworth, D. J., Popoff, M. R. & Barth, H. Clostridial Binary Toxins: Iota and C2 Family Portraits. *Front. Cell. Infect. Microbiol.* **1,** (2011).

182. Schwan, C. *et al.* Clostridium difficile toxin CDT induces formation of microtubule-based protrusions and increases adherence of bacteria. *PLoS Pathog.* **5,** (2009).

183. Carman, R. J. *et al.* Clostridium difficile binary toxin (CDT) and diarrhea. *Anaerobe* **17,** 161–165 (2011).

184. Stewart, D. B., Berg, A. & Hegarty, J. Predicting Recurrence of C. difficile Colitis Using Bacterial Virulence Factors: Binary Toxin Is the Key. *J. Gastrointest. Surg.* **17,** 118–125 (2013).

185. Chen, X. *et al.* A Mouse Model of Clostridium difficile-Associated Disease.

Gastroenterology **135,** 1984–1992 (2008).

186. Buffie, C. G. *et al.* Profound alterations of intestinal microbiota following a single dose of clindamycin results in sustained susceptibility to Clostridium difficile-induced colitis. *Infect. Immun.* **80,** 62–73 (2012).

187. Lawley, T. D. *et al.* Antibiotic treatment of Clostridium difficile carrier mice triggers a supershedder state, spore-mediated transmission, and severe disease in immunocompromised hosts. *Infect. Immun.* **77,** 3661–3669 (2009).

188. Reeves, A. E., Koenigsknecht, M. J., Bergin, I. L. & Young, V. B. Suppression of Clostridium difficile in the gastrointestinal tracts of germfree mice inoculated with a murine isolate from the family Lachnospiraceae. *Infect. Immun.* **80,** 3786–3794 (2012).

189. Theriot, C. M. *et al.* Cefoperazone-treated mice as an experimental platform to assess differential virulence of Clostridium difficile strains. *Gut Microbes* **2,** 326–334 (2011).

190. Rinttilä, T., Kassinen, A., Malinen, E., Krogius, L. & Palva, A. Development of an extensive set of 16S rDNA-targeted primers for quantification of pathogenic and indigenous bacteria in faecal samples by real-time PCR. *J. Appl. Microbiol.* **97,** 1166–1177 (2004).

191. Persson, S., Torpdahl, M. & Olsen, K. E. P. New multiplex PCR method for the detection of Clostridium difficile toxin. A (tcdA) and toxin. B (tcdB) and the binary toxin (cdtA/cdtB) genes applied to a Danish strain collection. *Clin. Microbiol. Infect.* **14,** 1057–1064 (2008).

192. Andrews, S. FastQC: A quality control tool for high throughput sequence data. *Http://Www.Bioinformatics.Babraham.Ac.Uk/Projects/Fastqc/* http://www.bioinformatics.babraham.ac.uk/projects/ (2010). doi:citeulike-article-id:11583827

193. Bolger, A. M., Lohse, M. & Usadel, B. Trimmomatic: A flexible trimmer for Illumina sequence data. *Bioinformatics* **30,** 2114–2120 (2014).

194. Bankevich, A. *et al.* SPAdes: A New Genome Assembly Algorithm and Its Applications to Single-Cell Sequencing. *J. Comput. Biol.* **19,** 455–477 (2012).

195. Price, M. N., Dehal, P. S. & Arkin, A. P. FastTree 2 - Approximately maximum-likelihood trees for large alignments. *PLoS One* **5,** (2010).

196. Warren, C. A. *et al.* Amixicile, a novel inhibitor of pyruvate:Ferredoxin oxidoreductase, shows efficacy against Clostridium difficile in a mouse infection model. *Antimicrob. Agents Chemother.* **56,** 4103–4111 (2012).

197. Perez, J., Susan Springthorpe, V. & Sattar, S. A. Clospore: A liquid medium for producing high titers of semi-purified spores of Clostridium difficile. *J. AOAC Int.* **94,** 618–626 (2011).

198. Dingle, K. E. *et al.* Effects of control interventions on Clostridium difficile infection in England: an observational study. *Lancet Infect. Dis.* **17,** 411–421 (2017).

199. Dingle, K. E. *et al.* Clinical clostridium difficile: Clonality and pathogenicity locus diversity. *PLoS One* **6,** (2011).

200. Griffiths, D. *et al.* Multilocus sequence typing of Clostridium difficile. *J. Clin. Microbiol.* **48,** 770–778 (2010).

201. Wellcome Sanger Institute. 027 sequencing projects (https://www.ebi.ac.uk/ena/data/view/PRJEB2318). *European Nucleotide Archive* Available at: https://www.ebi.ac.uk/ena/data/view/PRJEB2318.

202. Wellcome Sanger Institute. 027 sequencing projects (https://www.ebi.ac.uk/ena/data/view/PRJEB2958). *European Nucleotide Archive* Available at: https://www.ebi.ac.uk/ena/data/view/PRJEB2958.

203. Etienne-Mesmin, L. *et al.* Toxin-positive Clostridium difficile latently infect mouse colonies and protect against highly pathogenic C. difficile. *Gut* **67,** 860–871 (2018).

204. Rao, K. *et al.* Clostridium difficile Ribotype 027: Relationship to Age, Detectability of Toxins A or B in Stool with Rapid Testing, Severe Infection, and Mortality. *Clin. Infect. Dis.* **61,** 233–241 (2015).

205. Lawley, T. D. & Young, V. B. Murine models to study Clostridium difficile infection and transmission. *Anaerobe* **24,** 94–97 (2013).

206. de Oliveira, C. A. *et al.* Rodents are carriers of Clostridioides difficile strains similar to those isolated from piglets. *Anaerobe* **51,** 61–63 (2018).

207. Theriot, C. M. & Young, V. B. Interactions Between the Gastrointestinal Microbiome and *Clostridium difficile*. *Annu. Rev. Microbiol.* **69,** 445–461 (2015).

208. Hryckowian, A. J., Pruss, K. M. & Sonnenburg, J. L. The emerging metabolic view of Clostridium difficile pathogenesis. *Current Opinion in Microbiology* **35,** 42–47 (2017).

209. Bliss, D. Z. *et al.* Acquisition of Clostridium difficile and Clostridium difficile-associated diarrhea in hospitalized patients receiving tube feeding. *Ann. Intern. Med.* **129,** 1012–9 (1998).

210. O'Keefe, S. J. D. Tube feeding, the microbiota, and Clostridium difficile infection. *World J. Gastroenterol.* **16,** 139–42 (2010).

211. Hryckowian, A. J. *et al.* Microbiota-Accessible carbohydrates suppress Clostridium difficile infection in a murine model. *Nat. Microbiol.* **3,** 662–669 (2018).

212. Moore, J. H. *et al.* Defined nutrient diets alter susceptibility to clostridium difficile associated disease in a murine model. *PLoS One* **10,** (2015).

213. Blankenship-Paris, T. L., Walton, B. J., Hayes, Y. O. & Chang, J. Clostridium difficile infection in hamsters fed an atherogenic diet. *Vet. Pathol.* **32,** 269–273 (1995).

214. Kawano, A. *et al.* Colitis associated with Clostridium difficile in specific-pathogen-free C3H-scid mice. *J Vet Med Sci* **69,** 973–975 (2007).

215. Koya, V. *et al.* Outbreak of Abdominal Distension and Obstipation in a C57BL/6J Experimental Autoimmune Encephalomyelitis Study. *Vet. Pathol.* **49,** 528–531 (2012).

216. Mir, S. A. *et al.* Prenatal methyl-donor supplementation augments colitis in young adult mice. *PLoS One* **8,** (2013).

217. Leffler, D. A. & Lamont, J. T. *Clostridium difficile* Infection. *N. Engl. J. Med.* **372,** 1539–1548 (2015).

218. Vindigni, S. M. & Surawicz, C. M. C. Difficile infection: Changing epidemiology and management paradigms. *Clinical and Translational Gastroenterology* **6,** (2015).

219. Kozich, J. J., Westcott, S. L., Baxter, N. T., Highlander, S. K. & Schloss, P. D. Development of a dual-index sequencing strategy and curation pipeline for analyzing amplicon sequence data on the miseq illumina sequencing platform. *Appl. Environ. Microbiol.* **79,** 5112–5120 (2013).

220. Seekatz, A. M. *et al.* Fecal microbiota transplantation eliminates Clostridium difficile in a murine model of relapsing disease. *Infect. Immun.* **83,** 3838–3846 (2015).

221. Schloss, P. D. *et al.* Introducing mothur: Open-source, platform-independent, community-supported software for describing and comparing microbial communities. *Appl. Environ. Microbiol.* **75,** 7537–7541 (2009).

222. Schloss, P. D. A high-throughput DNA sequence aligner for microbial ecology studies. *PLoS One* **4,** (2009).

223. Pruesse, E. *et al.* SILVA: a comprehensive online resource for quality checked and aligned ribosomal RNA sequence data compatible with ARB. *Nucleic Acids Res.* **35,** 7188–96 (2007).

224. Westcott, S. L. & Schloss, P. D. OptiClust, an Improved Method for Assigning Amplicon-Based Sequence Data to Operational Taxonomic Units. *mSphere* **2,** e00073-17 (2017).

225. Koenigsknecht, M. J. *et al.* Dynamics and establishment of Clostridium difficile infection in the murine gastrointestinal tract. *Infect. Immun.* **83,** 934–941 (2015).

226. Rao, K. & Safdar, N. Fecal microbiota transplantation for the treatment of Clostridium difficile infection. *Journal of Hospital Medicine* **11,** 56–61 (2016).

227. Hufeldt, M. R., Nielsen, D. S., Vogensen, F. K., Midtvedt, T. & Hansen, A. K. Variation in the gut microbiota of laboratory mice is related to both genetic and environmental factors. *Comp. Med.* **60,** 336–342 (2010).

228. Ericsson, A. C. *et al.* Effects of vendor and genetic background on the composition of the fecal microbiota of inbred mice. *PLoS One* **10,** (2015).

229. Franklin, C. L. & Ericsson, A. C. Microbiota and reproducibility of rodent models. *Lab Animal* **46,** 114–122 (2017).

230. Hugenholtz, F. & de Vos, W. M. Mouse models for human intestinal microbiota research: a critical evaluation. *Cellular and Molecular Life Sciences* **75,** 149–160 (2018).

231. Hollingsworth, J. W. *et al.* In utero supplementation with methyl donors enhances allergic airway disease in mice. *J. Clin. Invest.* **118,** 3462–3469 (2008).

232. S., H. *et al.* A subset of monocytic cells derived from human embryonic stem cells can give rise to mesenchymal stromal cells. *Blood* **118,** (2011).

233. Hoeffel, G. *et al.* Adult Langerhans cells derive predominantly from embryonic fetal liver monocytes with a minor contribution of yolk sac–derived macrophages. *J. Exp. Med.* **209,** 1167–1181 (2012).

234. Gomez Perdiguero, E. *et al.* Tissue-resident macrophages originate from yolk-sac-derived erythro-myeloid progenitors. *Nature* **518,** 547–551 (2015).

235. Hoeffel, G. *et al.* C-Myb+Erythro-Myeloid Progenitor-Derived Fetal Monocytes Give Rise to Adult Tissue-Resident Macrophages. *Immunity* **42,** 665–678 (2015).

236. Hoeffel, G. & Ginhoux, F. Fetal monocytes and the origins of tissue-resident macrophages. *Cell. Immunol.* **330,** 5–15 (2018).

237. Gill, T. J. MATERNAL/FETAL INTERACTIONS AND THE IMMUNE RESPONSE. *Lancet* **301,** 133–135 (1973).

238. Thornton, C. A., MacFarlane, T. V. & Holt, P. G. The hygiene hypothesis revisited: Role of materno-fetal interactions. *Current Allergy and Asthma Reports* **10,** 444–452 (2010).

239. McGovern, N. *et al.* Human fetal dendritic cells promote prenatal T-cell immune suppression through arginase-2. *Nature* **546,** 662–666 (2017).

240. Li, E., Beard, C. & Jaenisch, R. Role for DNA methylation in genomic imprinting. *Nature* **366,** 362–365 (1993).

241. Blom, H. J. Folic acid, methylation and neural tube closure in humans. *Birth Defects Res. Part A - Clin. Mol. Teratol.* **85,** 295–302 (2009).

242. Hotamisligil, G. S. Inflammation, metaflammation and immunometabolic disorders. *Nature* **542,** 177–185 (2017).

243. Carlin, J. L., George, R. & Reyes, T. M. Methyl Donor Supplementation Blocks the Adverse Effects of Maternal High Fat Diet on Offspring Physiology. *PLoS One* **8,** (2013).

244. Jiao, F. *et al.* Protective effects of maternal methyl donor supplementation on adult offspring of high fat diet-fed dams. *J. Nutr. Biochem.* **34,** 42–51 (2016).

245. Hall, B. M. *et al.* p16(Ink4a) and senescence-associated β-galactosidase can be induced in macrophages as part of a reversible response to physiological stimuli. *Aging (Albany. NY).* **9,** 1867–1884 (2017).

246. Hall, B. M. *et al.* Aging of mice is associated with p16(Ink4a)- and β-galactosidasepositive macrophage accumulation that can be induced in young mice by senescent cells. *Aging (Albany. NY).* **8,** 1294–1315 (2016).

247. Franklin, C. L. & Ericsson, A. C. Microbiota and reproducibility of rodent models. *Lab Anim. (NY).* **46,** 114–122 (2017).

248. Rausch, P. *et al.* Analysis of factors contributing to variation in the C57BL/6J fecal microbiota across German animal facilities. *Int. J. Med. Microbiol.* **306,** 343–355 (2016).

249. A., P. Effect of age on clostridium difficile infection in a murine model of infection. *FASEB J.* **29,** (2015).